Marie Skłodowska-Curie Actions

This project has received funding from the European Union's Horizon 2020 research and innovation programme under the Marie Skłodowska-Curie grant agreement No. 642453

Training in Reducing Uncertainty in Structural Safety

D5.2 Final Report

WP5 - Rail and Road Infrastructure

Revision [final version]

Deliverable Number	Deliverable Title	Lead Beneficiary	Type	Dissemination Level	Due date
D5.2	Final Report	The University of Nottingham	Report	Public	31-Dec-2018

Start Date of the Project: 01-Jan-2015 Duration: 48 months

List of Contributors

The order below is by alphabetical order of the authoring organizations, and has nothing to do with the extent or importance of the contributions. The main contributors to a specific research topic are provided at the start of each chapter.

COTCA SL, Barcelona, Spain
Sergi Villalba

Full Scale Dynamics Ltd (FSDL), Exeter, UK
Farhad Huseynov (ESR7)
James M.W. Brownjohn

Microlise Ltd, Nottingham, UK
Mohammad Mesgarpour

Phimeca Engineering, Cournon-d'Auvergne, France
Barbara Heitner (ESR8)
Thierry Yalamas

Queen's University Belfast, Belfast, UK
David Hester

Technical University of Catalonia (UPC), Barcelona, Spain
António Barrias (ESR11)
Joan R. Casas
John J. Moughty (ESR10)

TRL Ltd, Wokingham, UK
Emma Benbow
Helen Viner

Université de Nantes, Nantes, France
Franck Schoefs

University College Dublin (UCD), Dublin, Ireland
Arturo González (Project Coordinator)
Daniel Martínez Otero (ESR12)
Debra Laefer
Eleni Mangina
Eugene J. OBrien
Siyuan Chen (ESR14)

University of Exeter, Exeter, UK
Karen Faulkner

University of Nottingham (UNOTT), Nottingham, UK
Federico Perrotta (ESR13)
John Andrews
Luis C. Neves
Matteo Vagnoli (ESR9)
Rasa Remenyte-Prescott (WP5 leader)
Tony Parry

Edited by Arturo González, Rasa Remenyte-Prescott and Parisa Beizaei

Table of Contents

Executive Summary

This deliverable reports on the outputs of eight Early Stage Researchers (ESR7-ESR14) in work package, WP5 (Rail and Road Infrastructure), under the supervision of academic and industrial experts during the three years of their projects within the EU TRUSS (Training in Reducing Uncertainty in Structural Safety, 2015-2018) Innovative Training Network (ITN) programme (http://trussitn.eu/). Two types of infrastructure are analysed in WP5: **bridges** (ESR7-ESR12) and **pavements** (ESR13-ESR14). The first six projects aim to reduce uncertainty in bridge safety. They address areas of work such as bridge condition assessment (ESR7), probabilistic modelling of bridge damage using damage indicators (ESR8), railway bridge condition monitoring and fault diagnostics (ESR9), condition assessment based on measured vibration level (ESR10), the use of optical fibre distributed sensing for monitoring (ESR11), and the use of displacement and velocity measurements for damage localisation (ESR12). The last two projects are on uncertainty in pavement safety, where ESR13 considers the use of truck sensors for road pavement performance and asset management and ESR14 investigates the possibility of using unmanned aerial vehicles and photogrammetry method for road and bridge inspections. Generally, the areas of work developed in this work package are vehicle-infrastructure interaction, traffic load modelling, road materials, uncertainty modelling, reliability analysis, field measurement and Structural Health Monitoring (SHM) of bridges.

Assessment of infrastructure asset condition is one of the key areas of work, and a number of projects are focussed on methods for defining, measuring and predicting **bridge** condition. Other projects, such as ESR7 and ESR11, place their efforts in developing monitoring solutions. For example, Farhad Huseynov (ESR7), in *Chapter 1*, proposes a number of accurate and cost-effective monitoring methods for assessing the condition of bridge infrastructure. Such methods should help to move away from visual and tactile inspections which are prone to human error and insufficiently frequent. Three in-field studies on UK bridges are carried out and their outcomes analysed. The first case study is conducted on a three-span composite simply supported bridge structure, and it is used to obtain the transverse load distribution factors of the deck structure. The second case study is focussed on a historical railway bridge. Crack movement on the abutment wall is monitored using an Imetrum camera system, and it is demonstrated that tiny deformations on the masonry wall can be detected in three dimensions. A novel method is proposed to measure rotations from recorded accelerations, and then use these rotations to calculate deflections. In the third case study on a simply supported steel railway bridge, a newly axle detection system is tested. The system is based on the second derivative of the strain signal, and it is demonstrated that peaks of this derivative relate to the presence of an axle.

The project by Barbara Heitner (ESR8), described in *Chapter 2*, investigates the integration of the proposed monitoring and damage detection methods into a bridge safety model or bridge maintenance decision making process. Three contributions are achieved. The first is a Bayesian framework for better estimation of the implications for safety, of corrosion in reinforced concrete bridges. Six different damage indicators are proposed and compared based on different sensor measurements, such as strain, deflection, and rotation. The second contribution is about the use of in-field data, recorded in ambient traffic conditions, for the proposed damage indicators. The effectiveness is investigated using simultaneously recorded temperature data from a highway culvert near Ljubljana, in Slovenia. As both temperature and corrosion cause small reductions in stiffness, temperature was used here as a proxy for damage. The third contribution is in the area of finding the influence line of a structure based on in-field data, without the usage of pre-weighed trucks or a Finite Element (FE) model of the structure. An iterative approach is used to obtain the influence line and relative axle weights of passing trucks. This is a highly significant development as it greatly reduces the cost of installation. An influence line is a key measure of bridge behaviour and responds significantly to damage such as bearing seizure. It is shown that the mean inferred Gross Vehicle Weight of the passing trucks also has good potential for damage detection, and, as above, the method is validated against temperature data (i.e., the method can detect the effect of a change in temperature which is strong evidence that it can detect damage).

In *Chapter 3*, Matteo Vagnoli (ESR9) proposes five bridge condition monitoring and diagnostics methods for railway bridges. Firstly, a Bayesian Belief Network (BBN) is developed and verified using two FE models of bridges. A part of the network, known as the Conditional Probability Tables (CPTs), are defined using an expert knowledge elicitation process. The BBN method can be used to take account of interdependencies between different elements and uncertainty in bridge behaviour due to deterioration. Secondly, a data analysis method for defining Health Indicators of bridge elements is proposed. The methodology is tested on two in-field bridges: a steel truss bridge, and a post-tensioned concrete bridge, which were undergoing a progressive damage test. Thirdly, a machine learning method is used to assess the health state of a post-tensioned concrete bridge automatically. A Neuro-Fuzzy Classifier is adopted in this method. Fourthly, a method for updating the CPTs of the BBN continuously is proposed, where information about the actual health state and the knowledge of bridge engineers are merged. Finally, an ensemble-based change-point detection method is developed and applied to a tunnel structure. The method is used to analyse a database of historical and unknown infrastructure behaviour and to identify the most critical change of the health state. The in-field data is based on tunnel movements due to renewal activities. As in ESR7, it is envisaged that such condition detection and diagnostics methods would replace time-consuming, expensive and subjective visual inspections of bridges.

John James Moughty (ESR10) is also concerned with bridge deterioration, the influence of environmental and operational effects and the measurement of that deterioration. The

researchers in this project believe that the common modal-based damage sensitive analysis needs an alternative. Their proposed option in *Chapter 4* is to use vibration-based damage sensitive features which do not require external input loading or bridge closures and can be continuously recorded. A number of vibration parameters are proposed and investigated, and the analysis is carried out on two progressively damaged bridges, subjected to ambient and operational loading, respectively. The first bridge is the S101 bridge, a pre-stressed flyover near Vienna in Austria, and the second bridge is a simply supported steel truss bridge in Japan. It is demonstrated that many of the novel empirical vibration parameters are suitable for damage detection, localisation, and quantification. To achieve this, a suitably applicable vibration signal type is needed, and a suitable outlier detection method has to be chosen (which is based on the distribution type of the extracted vibration parameter).

Similarly to the project by ESR7, António Barrias (ESR11) moves forward modern sensor technology for bridge condition assessment. In this case, Distributed Optical Fibre Sensing (DOFS), and more specifically, the Optical Backscattered Reflectometry (OBR) based system, is the subject of *Chapter 5*. Different laboratory experimental campaigns are carried out to assess multiple aspects of the instrumentation of the DOFS technology. The latter include the study of new implementation methods, comparison and performance analysis of different bonding adhesives and spatial resolution, and also the long-term performance. The technology is applied to two concrete structures in Barcelona, in Spain. The first application is at the historical and UNESCO world heritage site, Sant Pau Hospital. Due to the implementation of DOFS technology in this historic structure, it is possible to follow the developed strains due to the rehabilitation works, to ensure safety and to maintain the structure in operation. The second case is the Sarajevo bridge, and similar benefits are gained. The long-term effect of temperature variation and its compensation are also considered.

Chapter 6 provides the outcomes of the project by Daniel Martínez Otero (ESR12), which deal with damage detection and localisation using deflection and velocity measurements from an instrumented vehicle, as opposed to direct measurements on the bridge employed in previous chapters. In his first contribution, curvature (the second spatial derivative of deflection) is proposed as a damage indicator, which is assumed to be measurable using drive-by measurements and Laser Doppler Vibrometers (LDV). Instantaneous Curvature is investigated as a means of finding a local loss of stiffness in a bridge using drive-by measurements. The use of LDVs is established in the Traffic Speed Deflectometer (TSD), a specialist truck instrumented with several LDVs, which is used for road pavement monitoring. In this project, this concept is explored for bridge damage detection. The Rate of Instantaneous Curvature (RIC) is introduced as a bridge damage indicator. It is shown that bridge damage is detectable by comparing the RIC measurements from healthy and damaged bridges, although the levels of accuracy needed suggest that it may not be commercially exploitable until the next generation of LDVs are installed. The second contribution relates to the direct calculation of bridge stiffness from deflection measurements. The bridge stiffness profile is obtained from drive-by measurements of deflection. However, a filtering method based on the Blackman window is proposed to remove noise, and a numerical case study is used to demonstrate the effectiveness of the method. The main novelty of this approach is that there is no need to measure random traffic axle weights to detect damage. This stiffness profile calculation qualifies for level 3 damage detection.

The project of Federico Perrotta (ESR13) addresses in *Chapter 7* how to reduce uncertainty in **road** pavement performance, through assessment of the impact of road surface characteristics, such as unevenness and macro-texture, on the fuel consumption of trucks. A Big Data approach is proposed, combining advanced statistics, data mining, and regression techniques. The method provides reliable estimates about the impact of road roughness and macro-texture that can support pavement engineers and road asset managers in their decisions. In-field data is provided by Microlise and TRL Ltd, containing records of thousands of trucks driving across the Strategic Road Network in England. The analysis of results shows that machine learning algorithms outperforms linear regression. Performing a parametric analysis is demonstrated to be a good way to partially interpret the results of machine learning algorithms, as its output graphs are easily readable and allow the identification of how fuel consumption varies in different situations.

Finally, the project by Siyuan Chen (ESR14) applies Unmanned Aerial Vehicles (UAVs) and the photogrammetry method to road pavement and bridge inspections in *Chapter 8*. The aim of this project is to develop methods for associated data processing, quality evaluation, and damage extraction. It is shown that low price commercial UAVs have the capability to collect high-quality images, which can then be used for 3D documentation and damage detection. The Structure From Motion (SFM) method is proposed for the images, based on 3D point cloud generation. For the post-processing stage, automatic noise reduction and a damage segmentation method are also developed. The method is demonstrated on a number of in-field surveys, such as Wicklow road, Wicklow Bridge and the Boyne viaduct in Ireland. The proposed UAV inspection method offers a suitable alternative to visual inspections due to significant reductions in surveying costs.

The ESRs also propose future research direction for their projects. Examples of these include: population of influence lines should be studied in addition to instantaneous lines, followed by spatial variation in deterioration and its detection (ESR8); vehicle induced excitation should be investigated so that the variability of loads can be adjusted (ESR10); the work of damage localisation using displacement and velocity measurements needs to be further tested on real highway bridges (ESR12); the method of on-road performance monitoring could be extended to the analysis of urban drive cycles and other vehicle types (ESR13). Overall, this report illustrates that the research carried over the three years of the TRUSS project is in line with the original objective of WP5 - to reduce uncertainty, improve structural assessments and management of transport infrastructure via the development of:

- New monitoring (ESR13 and ESR14) /sensor (ESR11 and ESR12) technologies that will allow more efficient data collection, and

- new algorithms (ESR7, ESR9 and ESR10) that will process the data collected from a structure to estimate its safety (ESR8) more accurately than current approaches.

Chapter 1: Development of innovative bridge field testing techniques - case studies

Farhad Huseynov[1,2], James M.W. Brownjohn[1], Eugene J. OBrien[2], David Hester[4], Karen Faulkner[3]
[1]Full Scale Dynamics LTD, Kay Building North Park Road, Exeter EX4 4QF, UK
[2]School of Civil Engineering, University College Dublin, Richview Newstead Block B, Belfield, Dublin 4, Ireland
[3]Vibration Engineering Section, College of Engineering, Mathematics and Physical Sciences, University of Exeter, North Park Road, Exeter EX4 4QF, UK
[4]School of Natural and Built Environment, Queen's University Belfast, Stranmillis Road, Belfast, Northern Ireland BT9 5AG, UK
email: f.huseynov@fullscaledynamics.com, j.brownjohn@ fullscaledynamics.com, eugene.obrien@ucd.ie, d.hester@qub.ac.uk, kf312@exeter.ac.uk

ABSTRACT: Bridges, connecting communities and serving as regional lifelines, are vital components of transport infrastructure. In most of the developed countries, the majority of bridges are nearing the end of their designed service life. Current bridge evaluation techniques are mainly based on visual and tactile inspections, which are qualitative and prone to errors due to the human factor. Therefore, bridge owners are particularly interested in accurate and innovative methods for assessing their aging structures, which is the main motivation behind this research project. In order to overcome the existing shortfalls in the bridge monitoring field, this project carries out extensive numerical analyses to develop cost-effective bridge monitoring solutions that will benefit the stakeholders. Subsequently, the developed methodologies are tested on real bridges through field testing campaigns. The results obtained from these testing campaigns are summarised within the scope of this chapter.

KEY WORDS: Deflection monitoring; Rotation measurements; Field testing; Railway.

1 INTRODUCTION

Almost half of the UK's bridges are built during the post-war period, hence, they are nearing the end of their design lives. Over time they are exposed to many degradation processes due to environmental factors and changing loading conditions. According to a recent investigation by the Royal Automobile Club (RAC) Foundation, the number of substandard council-maintained road bridges in the UK has risen 35% in just two years [1]. The resulting cost of clearing the backlog of work associated with the deterioration of the country's bridge stock is estimated to be £5 billion. These substandard bridges do not only have a significant impact on the UK's economy, but are also a threat to public safety. In the last five years alone, there have been several incidents. In December 2015, Forth Road Bridge, one of the busiest and most iconic bridges in Scotland, was closed to traffic after a crack was found in the steel support. The cause of the crack was identified as a pin that had corroded and seized at the end of the truss link, which over time led to overload and eventual failure of the link. A report to the Scottish Parliament stated that "only a high-tech structural health monitoring system could potentially have revealed the problem" [2]. The final bill for repairs was established at £16 million, and the cost to the economy is estimated at £1 million/day for the duration of the closure. Identifying possible structural defects on a bridge at an early stage is crucial in preventing such events and is the main motivation behind this research.

This chapter presents the results of three bridge field testing campaigns. The first case study is conducted on a healthy but aging composite I-girder roadway bridge structure in Exeter, UK. The bridge is instrumented with strain sensors and loaded with a four-axle 32-tonne truck. The second field testing campaign is conducted on a historical railway bridge structure that experiences a vertical crack on its abutment wall. The third field testing campaign is performed on a new simply supported bridge structure in an attempt to validate the robustness of a novel axle detection system.

2 CASE STUDY 1 – EXE NORTH BRIDGE FIELD TESTING

Current bridge evaluation techniques are mainly based on visual and tactile inspections which are qualitative and fail to identify strength reserve capacity of a bridge. One of the main sources of strength reserve capacities in a bridge is associated with unexpected transverse load distribution factors of a bridge [3]. The purpose of this field testing is to obtain transverse load distribution factors of the Exe North Bridge from the measured strains. The test structure is a three-span simply supported bridge consisting of 12 main girders and carrying four traffic lanes. Figure 1 shows the elevations view of the bridge and the sketch of deck cross-section.

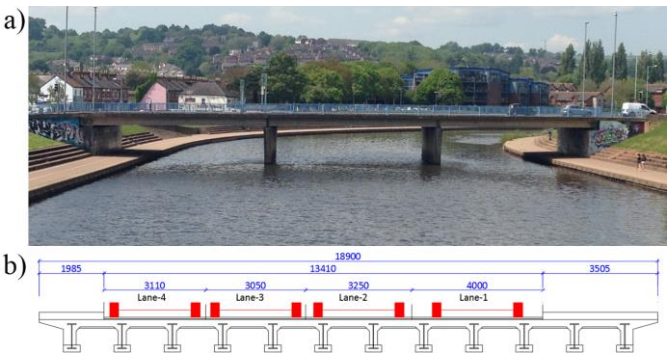

Figure 1. Exe North Bridge: (a) Elevation view, (b) sketch of deck cross-section.

ST350 model strain transducers are used to measure strains during the field testing. The sensors are attached on the soffit of the main girder. Due to the water constraints, the strain sensors are attached at quarter-span location. Figure 2 shows the sensor installation on the soffit of the main girder.

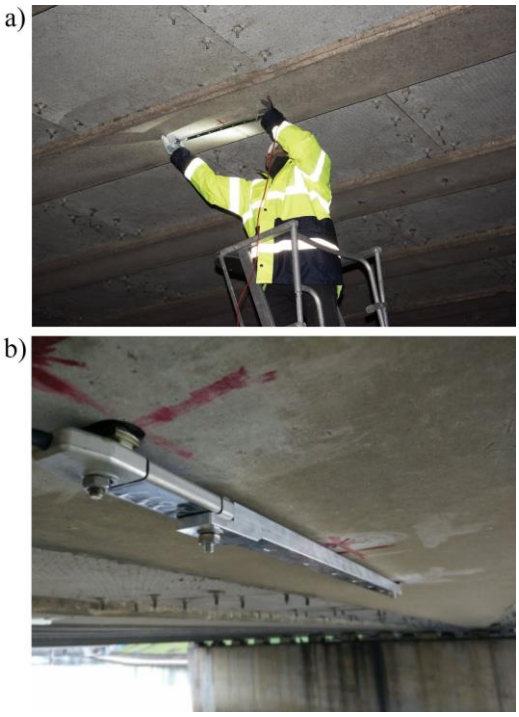

Figure 2. Sensor installation: (a) ESR installing sensors on the soffit of the main girder, (b) close view of the installed sensor.

The test is carried out overnight to avoid public traffic disruption. During the testing, the bridge is loaded with a 32 tonnes four-axle truck that remains stationary for approximately 45 seconds at each lane. In total, the bridge is loaded 16 times; 4 times at each lane. Figure 3 shows the test vehicle while it is stationary positioned on Lane 4.

Figure 3. Four-axle 32 tonnes test vehicle.

Figure 4 presents a typical strain time history recorded for the different sensors during the test. Obtaining transverse load distribution factors of a bridge is vital information in bridge assessment activities. It is a measure of the transverse distribution of load through the structure. Bridges are typically designed in such a way that traffic load is distributed between girders as fairly as possible so as not to overstress any particular load carrying member. Therefore, the transverse load distribution factors play a very important role in the load carrying assessment of a beam-and-slab bridge.

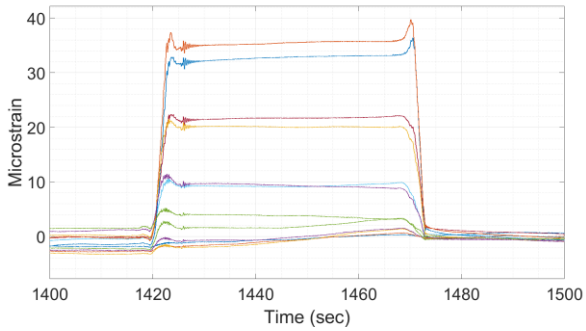

Figure 4. Typical strain time history

In this investigation, transverse load distribution factors are calculated dividing the average strain measured on the soffit of a girder by the total sum of the average measured strains of all girders. Figures 5(a) and (b) show the average strains recorded at each girder for each lane loading and the corresponding calculated transverse load distribution factors, respectively.

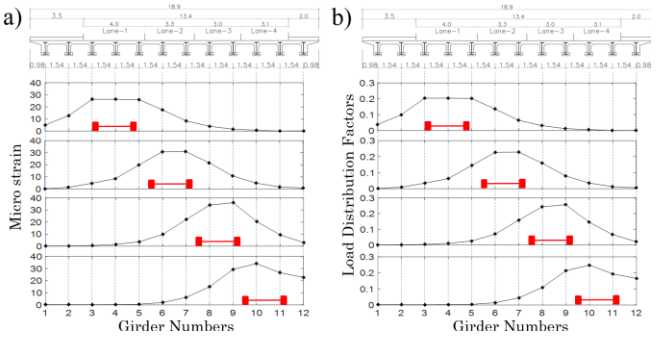

Figure 5. Results of the field testing: (a) Average strains recorded on the soffit of girder at quarter-span location while the truck remained stationary at each lane, (b) calculated transverse load distribution factors.

3 CASE STUDY 2 – FIELD TESTING ON A HISTORICAL RAILWAY BRIDGE

The test structure investigated in this section is a historical railway bridge built in the 1870s and located in Somerset, UK. The bridge is a 14.8 m long single span simply supported steel bridge. The deck consists of two cast iron main girders carrying a single railway track, and the route is predominantly serviced by steam-powered locomotives. The heaviest locomotive running on the line weighs 76.4 tonnes with a single axle load of 17 tonnes. Figure 6 shows the elevation view of the test structure.

Figure 6. Elevation view of the test structure.

The bridge is supported by two masonry type abutments skewed by 60 degrees. The abutments consist of the main wall and two integrated wing walls. The height of the main and wing walls above the ground surface is approximately 5 m and 3.8 m, respectively.

During the latest visual inspection, the structural condition of the bridge is deemed to be sufficient to carry the normal daily traffic however, some defects are found on the abutment structure. Although it does not pose a danger to normal traffic, the wing wall of the abutment structure exhibit some vertical cracks running the full height of the wing wall approximately 2 m from the face of the abutment. Figure 7 shows the vertical crack on the abutment wing wall.

Figure 7. Vertical crack on the abutment wing wall.

The main objective of this research is threefold. The first objective is to monitor the crack movement on the abutment wing wall under train loading. The second objective is to measure rotations on the deck structure using accelerometers for academic purposes. Finally, the last objective is to determine deck deflections using measured rotation responses.

3.1 Monitoring abutment wall crack movement

The crack movement on the wing wall structure is monitored using three Imetrum camera systems, which use image processing to accurately measure structural deformations. Two of the Imetrum cameras are used to monitor the crack movement of the wing wall in three dimensions. One camera is placed pointing perpendicular to the wing wall (Y direction) whereas another camera is set up parallel to the wing wall (X direction). Two L-shaped (X-Z and Y-Z planes) optical targets are mounted on the abutment structure on both sides of the crack line (being Test Point 1 (TP1) and Test Point 2 (TP2) in Figure 8) to track X, Y, Z movement for each of the two targets using two cameras pointing from both directions. The targets installed on the wing wall are 150 x 150 x 5 mm steel angles and have optical targets attached to them. The angles are attached to the wing wall using epoxy glue. The third camera is pointed to deck midspan to measure the midspan deflection. The results for the deck structure are presented in the following section. Figure 8 shows the wide-angle view of the test setup at the bridge site.

Figure 8. View of the test layout.

Figure 9 shows the recorded X, Y and Z movements on both sides of the crack while a steam locomotive crossed the bridge site. The left-hand column of Figure 9 shows the X, Y and Z movement of Test Point 1 and the right-hand column shows the corresponding results for Test Point 2.

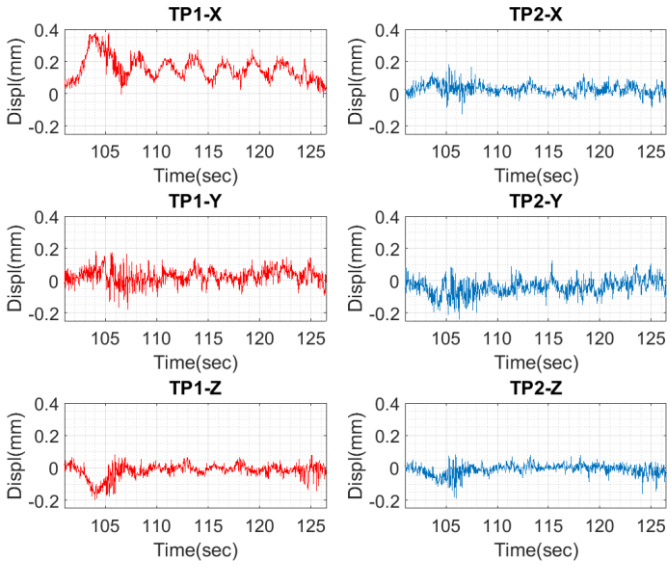

Figure 9. 3-D movement on both sides of the crack due to the passage of a steam locomotive.

From Figure 9, it is clearly visible that the abutment wall is moving under train loading with the dominant direction of movement being in the bridge longitudinal direction (X). The maximum magnitudes of deformations recorded during the field testing are 0.4 mm and 0.15 mm in longitudinal (X) and vertical (Z) directions, respectively. It is observed that the left side of the crack (TP1) moves significantly more than the opposite side of the crack. The wall movement is cyclic, and the magnitude of the movements appears to be approximately in proportion to the magnitude of the load.

3.2 *Rotation measurements using accelerometers and deflection calculations*

Inclinometers are the most common sensors used to measure the angle of rotation of an object, but can only be used to measure the rotation with respect to gravity. For this investigation, a single axis of acceleration is used to determine the angle of rotation instead of inclinometers. The rotation is determined by projecting the gravity vector on the axes of acceleration. Figure 10 shows five accelerometers placed in the horizontal direction at two supports, quarter-, mid- and three-quarter span locations.

Figure 10. Accelerometers placed on the top flange of the main girder.

A novel methodology is developed for measuring rotation from the recorded accelerations. Figure 11(a) shows the measured acceleration response due to a passage of a steam locomotive. Rotations obtained from the measured acceleration response are presented in Figure 11(b). The first peak in the plot, which also has the maximum amplitude, represents the passage of the locomotive. The following 8 peaks, that are smaller in magnitude, correspond with the passage of 8 carriages.

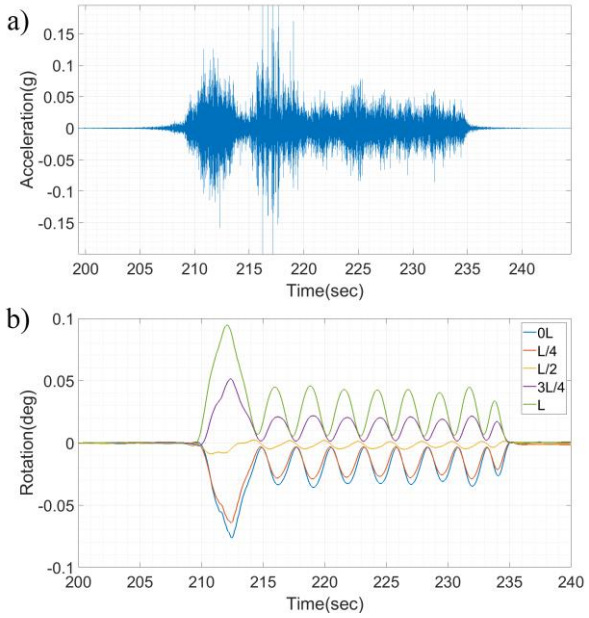

Figure 11. Results from accelerometers: (a) Recorded acceleration time history at the support location, (b) calculated rotations from measured accelerations.

Deflection is a damage sensitive parameter, hence, any change in bridge structural condition results in a change in deflection measurements. Therefore, measuring deflection on a bridge could provide useful information regarding the performance of the structure. Here, the methodology developed by Helmi et al [4] is applied to calculate the deflection of the bridge from its rotation response. Figure 12 presents the deflection-time history recorded during the field testing. The red plot with circular data markers is obtained using the rotation response measured by accelerometers. The blue plot is recorded using the Imetrum camera system pointed to the optical target at the bridge midspan location. It is clearly visible from Figure 12 that measured deflection using accelerometers matches very well with the corresponding results obtained from the Imetrum system.

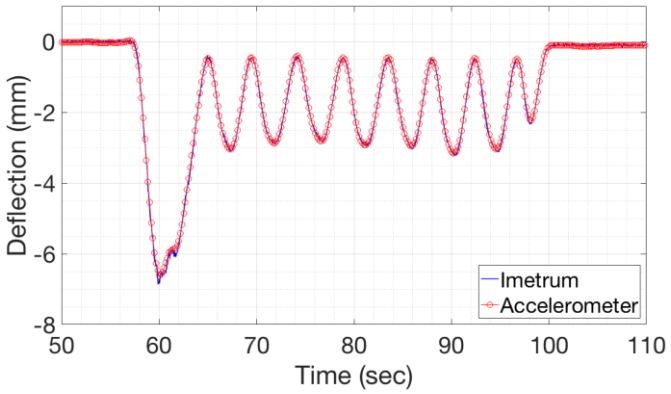

Figure 12. Deflection time history obtained from accelerometers and Imetrum camera system.

4 WILLITON BRIDGE FIELD TESTING

This section explains the outcomes of a field testing carried out on a simply supported steel railway bridge in an attempt to validate the robustness of a novel axle detection system developed within the scope of this project. Section 4.1 describes the theoretical basis of the proposed methodology and Section 4.2 presents the results of the field testing.

4.1 *Theoretical basis*

This section develops the theoretical basis for the proposed axle detection concept. Initially, numerical analyses are carried out on a 1-D simply supported bridge structure to obtain a strain response of the bridge model due to a moving 2-axle vehicle. The hypothetical structure is modelled as a 5.1 m long simply supported steel bridge. The elastic modulus and second moment of area are as assumed to be 210 GPa and 1.23×10^9 mm^4, respectively. The axle weights of the moving vehicle are taken as 3.5 tonnes, spaced by 2.6 m. The vehicle travels over the bridge at a speed of 4 m/s. Approach spans, 4 m long, are located at the entrance and exit of the bridge. A hypothetical sensor is placed at 1.1 m from the left-hand support location to 'record' the strain response of the bridge due to the moving vehicle loading. Figure 13 shows a sketch of the 1-D bridge model, axle configuration of the moving vehicle and the location of the strain sensor.

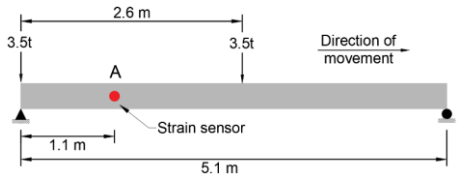

Figure 13. Sketch of the 1-D simply supported bridge model.

Figure 14(a) presents the strain-time history obtained from the numerical model due to the two-axle moving vehicle loading. The black curve shows the total response of the structure, while the red and blue dashed curves represent the contributions of the individual axles.

The proposed axle detection concept is based on the second derivative of the strain time history signal with respect to time. The strain time history function due to the moving multi-axle loading is a first order conditional polynomial. The first derivative of the first order conditional polynomial with respect to time becomes discontinuous at the points where axles arrive or depart from the bridge or pass the sensor location. The red plot in Figure 14(b) depicts the corresponding results obtained from the first derivative of the strain time history. Discontinuous functions are not differentiable at locations where there is a lack of continuity so the first derivative of the strain signal with respect to time is taken as continuous. The dashed blue lines in Figure 14(b) represent the corrections to re-establish the continuity of the signal.

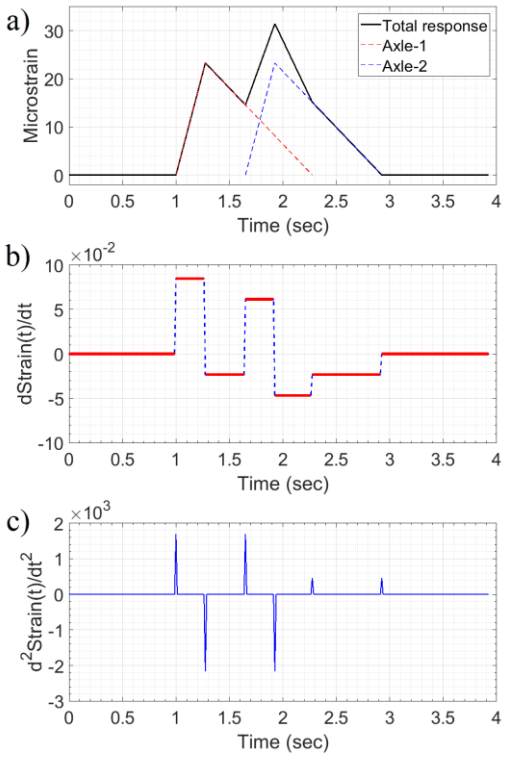

Figure 14. (a) Moment-time history obtained at the hypothetical sensor location, (b) first derivative of moment with respect to time, (c) second derivative of moment with respect to time.

Having observed the discontinuity feature in the first derivative of the strain response with respect to time, it is proposed that the second derivative of the strain signal with respect to time, will smooth out the constant part of the function. At locations where the first derivative of the function would normally become discontinuous, this will result in peaks that will identify axle locations.

The corresponding results obtained by differentiating the strain signal twice are presented in Figure 14(c). There are four positive and two negative peaks observed in this plot. The positive peaks correspond to the time when an axle enters or exits the bridge, whereas negative peaks occur when each axle passes the sensor location. Since the hypothetical sensor is placed on the left-hand side of the bridge, the magnitude of peaks when an axle arrives on the bridge is greater than the magnitude when it leaves the structure.

4.2 Field testing

The test structure is a single span simply supported steel railway bridge located in South West England, UK. The bridge is 5.1 m long and consists of two main girders placed 1505 mm apart. The connection between the bridge deck and abutments consists of laminated elastomeric bearings designed to allow free span movement in the bridge longitudinal direction. The bridge is located approximately 50 m away from a train station and carries a single track which rests on top of the main girders. Figure 15 shows a photograph of the test site.

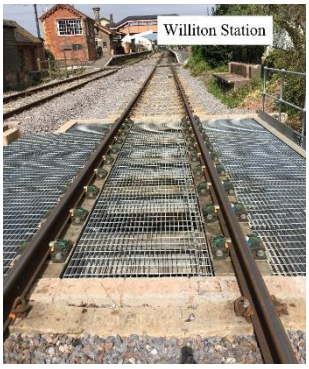

Figure 15. Photograph of the test site (in foreground).

The test structure is instrumented with a strain transducer at 1.1 m from the support location on the train station side of the bridge to record strains under train loading. Figure 16(a) shows the location of the test point and Figure 16(b) shows a photograph of the strain sensor installed on the bridge.

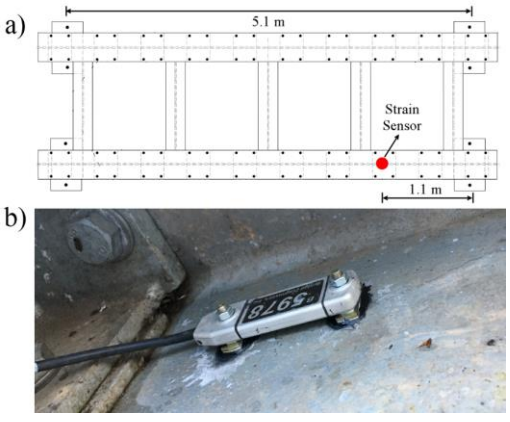

Figure 16. (a) Sketch of the test structure depicting sensor location, (b) strain transducer installed on the bridge.

The strain data are recorded while a British Class 115 Diesel Multiple Units (DMU) type train crosses the bridge. The train consists of three sets: Two Driving Motor Brake Second (DMBS) cars which are located at the front and rear and a Trailer Composite with Lavatory (TCL) type carriage located in the centre. Each set consists of 2 bogies, and each bogie has 2 axles spaced at 2.6 m, adding up to 12 axles in total for the full set of cars. Figure 17 shows a sketch of the DMBS and TCL cars and the British Class 115 type train crossing the test structure.

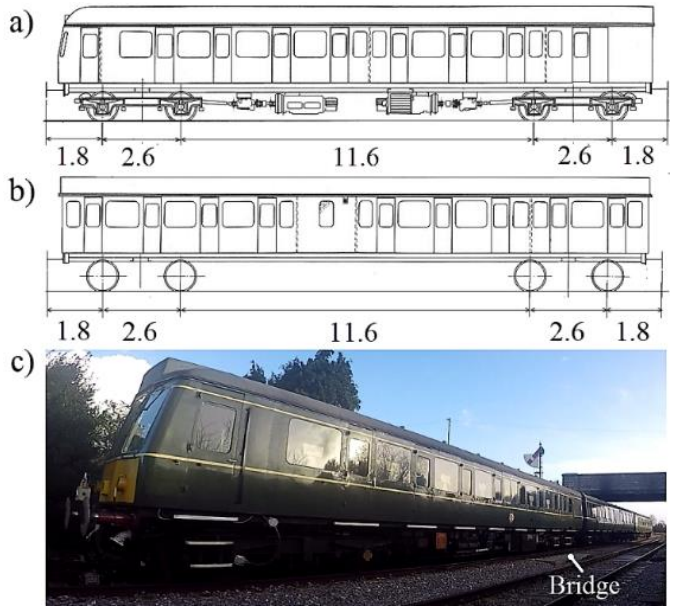

Figure 17. (a) Sketch of the DMBS car, (b) sketch of the TCL car, (c) British class 115 train crossing the test structure.

The strain-time history obtained in response to the British Class 115 type train loading is presented in Figure 18(a). There are 6 peaks in the strain signal, which correspond to the passage of the 6 bogies across the length of the test structure. The strain signal obtained under train loading is differentiated twice to identify the presence of axles, and the corresponding results are presented in Figure 18(b). As described in the previous section, positive peaks show the time when an axle enters or leaves the bridge, whereas negative peaks correspond with times when an axle passes the sensor location. Looking at the negative peaks first, there are twelve in total, which identify the time instants when axles are at the sensor locations.

Among the positive peaks, the ones with higher amplitude show the time instants when axles enter the bridge. There are 12 peaks identified in Figure 18(b) which are marked with solid black circle markers. The remained positive peaks (blue solid circle markers in Figure 18(b)) correspond with time instants when an axle leaves the bridge structure. Since the magnitudes of negative peaks when axles are leaving the structure are much less than the corresponding peaks when axles enter the bridge, for some axles, such as axles 3-10, it is not possible to accurately identify the time when they are leaving the structure.

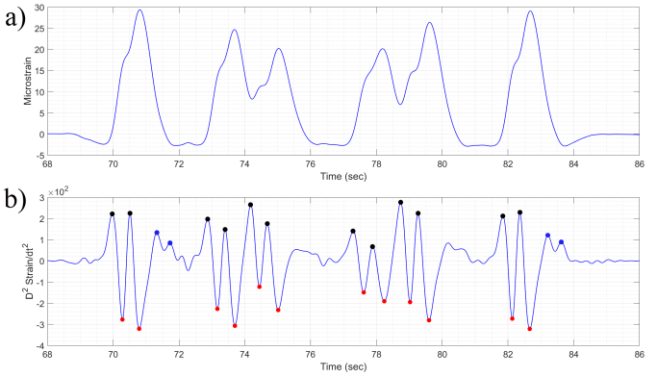

Figure 18. (a) Strain time history recorded under train loading, (b) second derivative of strain measurements with respect to time.

5 CONCLUSIONS

This chapter has presented the results from three field testing campaigns. The first case study has been conducted on a three-span composite simply supported bridge structure to obtain the transverse load distribution factors of the deck structure. The second case study has investigated the structural behaviour of a historical railway bridge loaded with steam locomotives. Within the scope of the field testing, the crack movement has been monitored on the abutment wall of the structure using an Imetrum camera system. The results have showed that by using image processing techniques, it is possible to obtain tiny deformations on the masonry wall in three dimensions. Besides, accelerometers have been placed on the deck structure to measure rotations and eventually obtain deck deflections at midspan location. Also, by using the methodology described in this chapter, it has been possible to calculate deflections accurately. The last field experiment has tested the robustness of a novel axle detection system, which is based on the second derivative of the strain signal. It has been demonstrated that the second derivative of strain signal results in peaks related to the presence of an axle.

ACKNOWLEDGMENTS

This project has received funding from the European Union's Horizon 2020 research and innovation programme under the Marie Skłodowska-Curie grant agreement No. 642453.

REFERENCES

[1] RAC Foundation, *RAC Foundation Report: Bridge Maintenance in Great Britain 2016-2017*, London, UK, 2018.

[2] *Inquiry into the circumstances surrounding the closure of the Forth Road Bridge*, 2016, accessed 2 December 2018, <http://www.parliament.scot/parliamentarybusiness/CurrentCommittees/94916.aspx>.

[3] Huseynov, F., Brownjohn, J.M.W., OBrien, E.J. and Hester, D. (2017), 'Analysis of load test on composite I-girder bridge', *Journal of Civil Structural Health Monitoring*, Springer, 7, 163-173.

[4] Helmi, K., Taylor, T., Zarafshan, A. and Ansari, F. (2015), 'Reference free method for real time monitoring of bridge deflections', *Engineering Structures*, Elsevier, 125, 116-124.

Chapter 2: Probabilistic modelling of bridge safety using damage indicators

Barbara Heitner[1,2], Eugene J. OBrien[1], Thierry Yalamas[2], Franck Schoefs[3]
[1]School of Civil Engineering, University College Dublin, Dublin, Ireland
[2]Phimeca Engineering, Cournon-d'Auvergne, France
[3]Research Institute of Civil Engineering and Mechanics, Université de Nantes, Nantes, France
email: heitner@phimeca.com, eugene.obrien@ucd.ie, yalamas@phimeca.com, franck.schoefs@univ-nantes.fr

ABSTRACT: This research project is motivated by the actual challenges in bridge inspection and maintenance planning and in estimating the actual and future safety level of bridges. It is searching for alternative ways of bridge health monitoring and damage detection and how these methods can be integrated into a bridge safety model or in bridge maintenance strategies. In a first contribution, a Bayesian framework is presented for better estimation of the corrosion loss in reinforced concrete bridges with the use of damage indicators based on different sensor measurements. In a second contribution, field data recorded in ambient traffic conditions are used for the proposed damage indicators. The effectiveness of these damage indicators is validated with simultaneously recorded temperature data. A third contribution is about finding the influence line of a structure based on field data recorded in ambient traffic conditions and without the need of pre-weighed trucks and/or a finite element model of the structure.

KEY WORDS: Bridge; Reliability; Damage indicator; Bayesian; Structural Health Monitoring (SHM); Deterioration; Maintenance.

1 INTRODUCTION

Bridges are particularly important assets of transport infrastructure due to their functionality, economic value as well as for their contribution to the landscape. Owners and managers are urged to find the best solution for deploying available sources efficiently, with the least possible social and environmental impact. On the other hand, the serviceability of assets and the safety of users have to be ensured. Bridge management is, therefore, an important and complex subject. One of the key issues is to estimate the current and future health state of bridges as accurately as possible, taking into account all relevant uncertainties.

Traditionally visual inspections, sometimes combined with non-destructive tests (NDT), are used in order to have a better understanding of the health state of bridges and thus to determine the optimal timing for more detailed and instrumented inspections, maintenance actions or, in extreme cases, replacement. Various NDT methods exist [1]. These often focus on the material properties of the structure, such as the strength of concrete [2] or the chloride ingress in concrete [3]. However, these NDT methods are not practical and not reliable enough for long-term monitoring of structures exposed to loading and deterioration with a high level of uncertainties.

In a small but increasing number of cases, health monitoring systems are installed on bridges, which seek to identify any anomalous behaviour of the structures. Among these, vibration-based health monitoring systems are particularly preferred for bridges [4]. There is a significant amount of research going on, that focuses on processing the measurement data, extracting the relevant information and building an appropriate framework in which the obtained data can effectively be used for damage detection or for determining the global health state of the bridge. However, there is a gap between research and industrial application in this field, mainly due to the high associated costs of Structural Health Monitoring (SHM) systems (installation, road closure, maintenance, etc.) and the small number of validated and working real-life examples. This issue is targeted by an on-going COST Action [5], which strives for quantifying and evaluating the value of SHM systems for improving the decision basis for design and maintenance of structures.

This research project aims at proposing and comparing damage indicators based on different sensor measurements while introducing a Bayesian framework to better estimate bridge deterioration (Section 2). It also aims at proposing an alternative validation for such damage indicators using the temperature sensitivity of reinforced concrete structures (Section 3). Finally, it aims at demonstrating an innovative method for finding the influence line of the bridge based on sensor measurement under ambient traffic conditions, which can also be used for damage detection (Section 4).

2 UPDATING PROBABILITIES OF BRIDGE REINFORCEMENT CORROSION USING HEALTH MONITORING DATA

2.1 Damage indicators

Six Damage Indicators (DIs), based on various SHM systems, are considered in this contribution. The damage indicators are established within a probabilistic context, assuming ambient traffic conditions during the measurement and therefore assuming no (or minimal) restrictions during the times of measurement. The damage indicators considered are based on (a) strain measurement, (b) deflection measurement, or (c) rotation measurement. For each sensing type, two measures are investigated here, that can be defined as follows:

- Average value of the area under the response signals corresponding to single truck crossing events:

$$DI_a = \frac{\sum_{i=1}^{n} \int_0^{s_i} f_i(x)dx}{n} \quad (1)$$

where $f_i(x)$ is the signal of the i^{th} truck, s_i is the length of this signal in [m], and n is the number of trucks/signals considered.

- Average value of the maximum of the response signals corresponding to crossing events:

$$DI_p = \frac{\sum_{i=1}^{n} \max_{j=0...s_i} (f_i(x))}{n} \quad (2)$$

The averaging can be done based on the number of trucks or based on a time period. For example, average over 100 trucks or average over 2 hours of (daytime) traffic.

2.2 Updating the information of corrosion

Corrosion is the principal deterioration process for Reinforced Concrete (RC) structures. Corrosion modelling, however, involves a great deal of uncertainty and depends on different variables, which are particularly hard to obtain with a high level of confidence and which vary with time. At the time of bridge inspection, it is assumed that the age of the bridge is known and therefore, applying the stochastic corrosion model, some estimate of the prior knowledge on actual reinforcing bar area loss can be obtained. In this project, Monte Carlo simulation is used to obtain the empirical distribution of residual reinforcing bar area at a given time instant. Afterwards, using well-established distribution fitting techniques (e.g. moments method or maximum likelihood method), one can find the distribution and parameters that best fit the simulated data at a time instant. This fitted distribution can be then used as the prior distribution for the updating process.

Applying Bayes' theorem, it is possible to improve the prior model by incorporating newly obtained health monitoring data. The prior distribution, in this case, is the probability density function of reinforcing bar area loss due to corrosion and the new data comes from damage indicators.

2.3 The methodology and the example application

The proposed methodology for estimating bridge safety and plan the maintenance regime can be seen in Figure 1. In the example application, different corrosion levels are taken into account in order to link the calculated DI values with the level of corrosion. To obtain this correlation between DI and Reinforcement Area Loss (RAL) due to corrosion, simulations on a simply supported beam model are conducted (see Figure 2).

In this example application, the time of inspection is fixed at year 40, which is used for the stochastic corrosion modelling to obtain the a priori distribution of the reinforcement area loss. The true value of reinforcement area loss has to be determined as well. This value is used to simulate the 'measured' signals and hence to obtain the DI values. It is also used as a reference for comparing the final results with.

The measured signals under ambient traffic conditions are obtained through simulations using a Weigh-In-Motion (WIM) database of truck properties and a simply supported RC beam model. The quality of the measurements may vary for the different cases and therefore measurement-dependent uncertainty is introduced in the model by adding white noise to the calculated signals. Based on these signals, 6 different DIs are defined (see Table 1). The objective for all DIs is to provide a means of updating the safety evaluation of the bridge, i.e., in this case, the estimation of the reinforcement area loss.

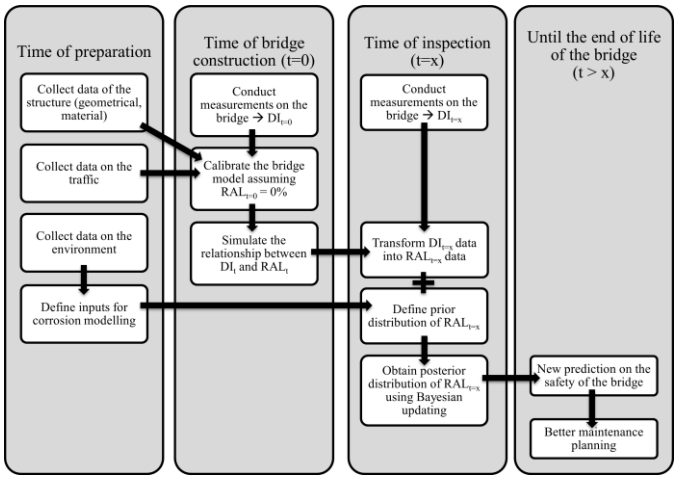

Figure 1. Flowchart of the proposed methodology.

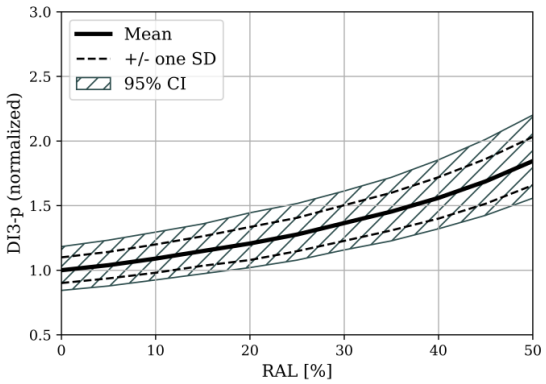

Figure 2. Trends in DI3-p for reinforcement area loss (RAL) between 0 and 50%.

Table 1. Damage indicators investigated

Damage Indicator	Measurement	Signal attribute
DI1-a	Strain	Area under signal
DI1-p	Strain	Peak value of signal
DI2-a	Deflection	Area under signal
DI2-p	Deflection	Peak value of signal
DI3-a	Rotation	Area under signal
DI3-p	Rotation	Peak value of signal

The updated and prior estimates of reinforcement area loss can be compared, for example, based on the obtained mean value of RAL, as per Figure 3. It can already be seen from this figure that rotation measurements show particular promise (i.e., DI3-p). This conclusion is strengthened based on the further examination that can be found in [6]. It must be noted that using the presented Bayesian framework, it is possible to compare and evaluate different SHM systems.

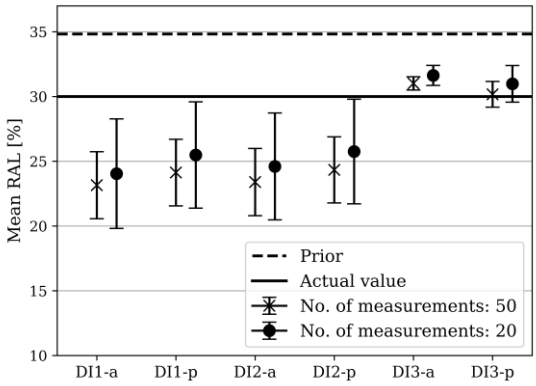

Figure 3. Mean values of the posterior distributions (mean +/– SD) for each DI, when the actual RAL= 30%.

3 BRIDGE DAMAGE INDICATOR BASED ON SENSOR DATA IN AMBIENT TRAFFIC CONDITIONS

3.1 Validation of damage indicators with temperature data

To test damage indicators and to prove that they are sensitive to stiffness change, in an alternative way, temperature measurement is used in this study. The temperature of the structural elements, and so indirectly of the air, has a small but measurable effect on Young's modulus of concrete [7-10]. Hence, when temperature changes, the stiffness of the structure changes as well. The effect of temperature change on reinforced concrete's modulus of elasticity, assuming that the temperature stays in the range of 0 to 30°C, can be expressed using a linear equation as follows [10]:

$$E_T = E_{20} \cdot (1 + \beta \cdot \Delta T) \quad (3)$$

where E_T and E_{20} are Young's modulus of concrete at temperature T and 20°C, respectively, β is the thermal hardening coefficient of concrete and ΔT is the difference between T and 20°C. For the thermal hardening coefficient, different values can be defined based on the data reported in the literature [7-10], see Table 2.

Table 2. Different β values based on the literature.

Thermal hardening coefficient: β	Reference
-0.00165	[8]
-0.00275	[10]
-0.00290	[9]
-0.00300	[7]

3.2 Data for the case study

The data available for this study is collected from a highway culvert in Slovenia, near Ljubljana (see Figure 4). It is a RC structure, carrying 2 lanes and a hard shoulder in each direction and a duct. The length of the bridge is 6.5 metres, the total width of the structure is 32.3 metres. Both the deck and the walls are made from the same grade of concrete (C25/30), the foundation is however made from C16/20 concrete.

Originally the bridge was equipped with SiWIM Weigh-in-Motion system [11] for the purpose of weighing passing trucks. This consists of strain transducers located at midspan across the width of the bridge, which are used to calculate the axle weights of the passing trucks. Additional strain sensors are placed at the quarter points in each lane to detect axles and hence to determine axle spacing and vehicle speed. Temperature sensors are also installed on the structure. Therefore, the temperature data of the deck is recorded simultaneously with the strain data.

Figure 4. View of the case study bridge.

In the case study, the two DIs defined by Equations (1) and (2), are calculated based on the strain signals recorded under the slow lane. An example of a post-processed signal can be seen in Figure 5. The sum of the signals for the four sensors in this lane can be seen in this figure too. Summing up various signals can help to reduce the influence of the truck's transverse position. The database of the signals is split into several parts depending on the temperature. Each subpart of the data then corresponds to a narrow temperature band of 2°C, from –2°C to 30°C.

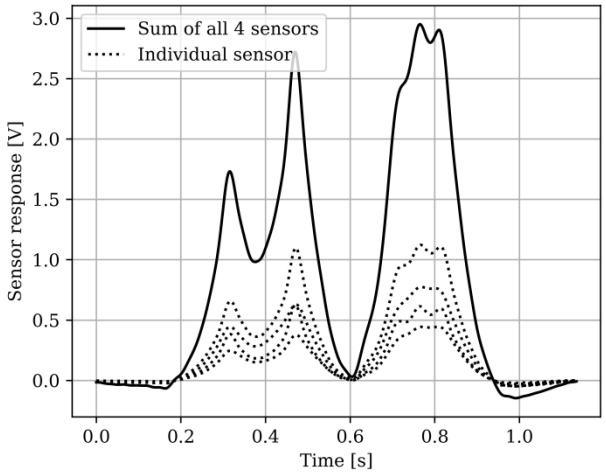

Figure 5. Measured signals during a slow lane single truck crossing event of a 5-axle truck.

3.3 Results of the case study

In Figure 6, for each temperature range, the mean +/- one standard deviation of DI_a (DI calculated with Equation (1)) are plotted. The sample size of DI is around 100, depending on the available data for each interval. Although the trend of DI with temperature is clear, the spread of the result (i.e., the standard deviation) in each interval is still significant. This is not surprising given the diversity in the truck population. The correlation between DI and temperature is positive from 0°C until about 20°C and negative beyond 20°C. A similar trend is

found by [12] in the relationship between temperature and the calculated Gross Vehicle Weights (GVW) from this bridge WIM system. The obtained correlation between temperature and DI proves that the proposed DI are indeed sensitive to stiffness change in the structure, therefore, they can potentially be used for damage detection.

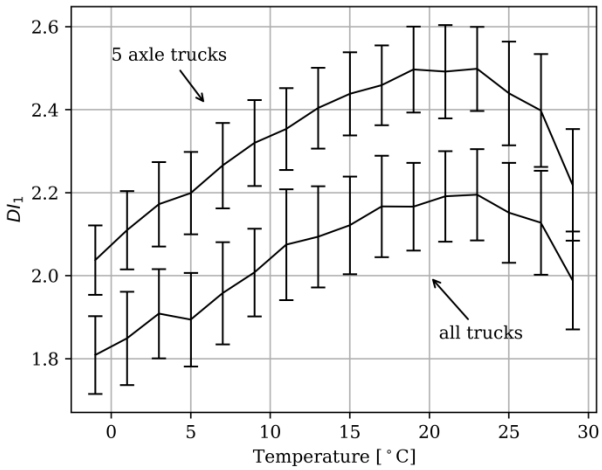

Figure 6. Mean +/– one standard deviation of DI_a versus temperature.

The simultaneously recorded temperature data can also serve for improving a damage detection tool based on the presented DIs. An alternative way for the bridge damage alerting system is proposed here, by applying a method to detect outliers of the temperature dependent DI distributions. The modified Z-score [13] can be used to identify potential outliers, based on a calculation of the median of a reference sample:

$$M_{DI} = \frac{0.6745(DI - \widetilde{DI})}{\text{median}(|DI_i - \widetilde{DI}|)} \quad (4)$$

where DI is the newly obtained damage indicator value that is investigated, $\widetilde{DI}$ is the median of the damage indicator sample and DI_i are the individual values in the damage indicator sample. This DI sample is collected during a reference period. Therefore the method's reliability would depend on the available data, i.e., the length of this reference period. The longer the reference period is, the more data can be collected and the better the reliability of the method will be. In this case study, two years of data is used.

The higher the absolute value of the modified Z score is, the more probable it is that the measured point does not belong to the original damage indicator sample, i.e., it is more probable that something other than temperature is modifying the bridge's response and so the DI. Figure 7 shows an example risk map for the case study bridge associated with the calculated modified Z-score. It can be seen how simultaneously measured temperature data can help to enhance the damage detection tool, when comparing, for example, the thresholds at 5°C and at 20°C.

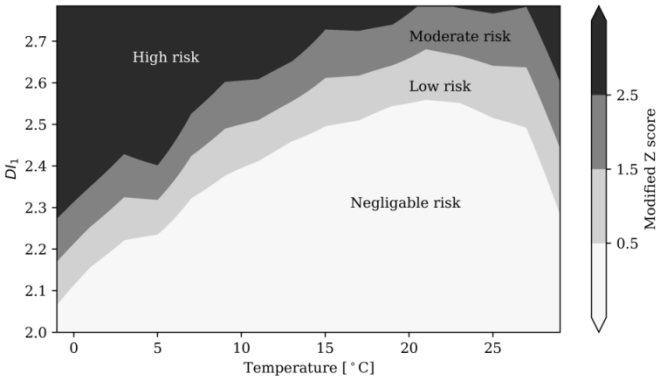

Figure 7. A proposed risk map prepared for $DI_1 = DI_a$ (5-axle trucks only) based on modified Z-scores.

4 MONITORING CHANGE IN THE SHAPE OF THE INFLUENCE LINE OF THE BRIDGE TO ESTIMATE BRIDGE SAFETY

4.1 Theory

In this contribution, an algorithm is presented that aims at finding the influence of the bridge together with the axle weights of the passing truck(s). This algorithm combines Quilligan's method [14] to calculate the influence line and Moses' method [15] to calculate the axle weights of the passing vehicles in parallel. Moses' algorithm searches for the Q vector of the axle weights that is possible to be found by solving the following equation:

$$\{Q\} = \frac{[IL]^T\{x_m(t)\}}{[IL]^T[IL]} \quad (5)$$

where (x_m) is the measured response, and [IL] is the matrix of the influence line ordinates. Equation (5) is the basis of B-WIM calculations and is the first part of the combined iterative method introduced in this contribution.

Quilligan [14] defines the matrix equation to calculate, based on the same principles as Moses' algorithm, the influence line ordinates given the measured response and the axle weights of a passing calibration vehicle. He proposes the solution in a matrix form that can be used independently from the number of axles of the vehicle. This solution of the influence line ordinates can be expressed as follows:

$$\{IL\}_{K-C_N,1} = [Q]^{-1}_{K-C_N,K-C_N}\{M\}_{K-C_N,1} \quad (6)$$

where $[Q]$ is a symmetric matrix dependent on the axle weights,$\{M\}$ is a vector dependent on the axle weights and the measured response, K is the total number of scans of the response signal and C is a vector containing the cumulative sums of the axle spacings expressed in scan numbers (starting from C_1 = 0). Hence, C_N is the total number of scans corresponding to the wheelbase of the vehicle.

The idea here is to iteratively apply the two different algorithms on the recorded signal until convergence is reached. This way, it is possible to obtain the shape of the influence line as well as the relative load distribution of the trucks based solely on measurement data. In order to verify the method and to see if the results are reliable, different tests are conducted. However, one straightforward test is to evaluate the fit between the measured and the calculated, theoretical signal by computing the coefficient of determination, i.e., the r^2 value. In

this contribution, it is also tested how temperature correlates with the calculated relative average truck weights. This is done in order to see if this value can potentially be used as damage indicator.

4.2 *Case study results*

The data used for this study is the same as described in the previous section. The iterative method is, therefore, applied to the strain measurement data of the culvert. Due to the effect of the culvert-soil interaction, it is decided to include in the influence line some metres before and after the bridge itself. The preliminary shape of the influence line (which is needed to commence the iterative method) is defined as a triangle along the bridge with two 'zero-tail' zones before and after the bridge. The total length of the influence line is set to 17 metres.

The calculated 'theoretical' signal using the obtained influence line and load distribution can be compared to the measured signal. Computing r^2 values of the two signals (the closer to 1, the better) is one way to quantify the quality of the method. Figure 8 shows the results of an example truck. The dashed line represents the measured signal while the continuous line corresponds to the calculated one. The five thin continuous lines are the individual responses of the five axles of the truck. The r^2 value, in this case, is 0.998, reflecting the very good fit.

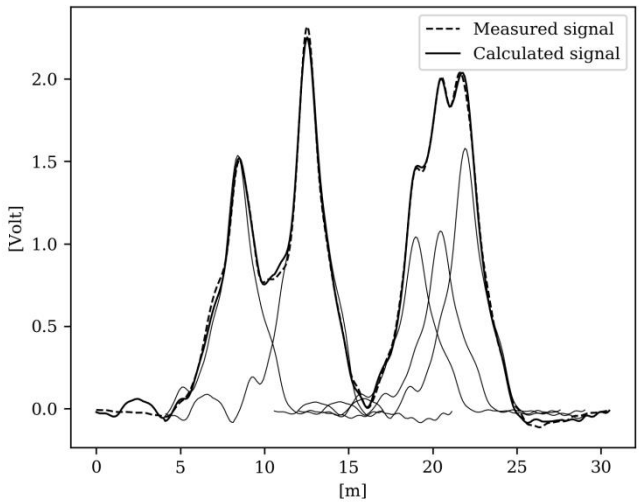

Figure 8. Comparison of the calculated truck response (the individual axle responses are marked with thin lines) with the measured response.

The iterative method is applied to the trucks' signals of each subset within a temperature range. The original sample size consists of 10000 trucks for each temperature range. However, all the cases with convergence problems are filtered out. The resulting final sample size and the average r^2 values, depending on the temperature range, can be found in Table 3. These average r^2 values suggest that the method works well and that an instantaneous IL can be found for the structure with high confidence. However, the number of cases when convergence cannot be reached (about 20%) also suggests that the method is very sensitive to the quality of the input signal.

Figure 9 presents the mean calculated relative GVW of a general population and of a population of 5-axle trucks only. As the average GVW of a population of trucks is not expected to vary with the temperature, it can be concluded that the observed variation is due to the variation of the structural behaviour that is sensitive to the temperature change. This suggests that the mean calculated relative GVW can be also used to detect stiffness change in the structure due to damage. It can be also seen that focusing on 5-axle trucks only, results in a smoother curve, i.e., a more robust relationship between calculated GVW and temperature.

Table 3. Sample size and average r^2 value for each temperature range considered.

Temperature range [°C]	Sample size	r^2 values
0-2	7945	0.9984
2-4	7937	0.9983
4-6	8131	0.9984
6-8	8057	0.9984
8-10	7904	0.9983
10-12	7891	0.9984
12-14	7902	0.9983
14-16	7843	0.9983
16-18	8060	0.9983
18-20	8072	0.9982
20-22	8050	0.9983
22-24	8097	0.9983
24-26	8034	0.9981
26-28	8138	0.9982
28-30	8165	0.9980

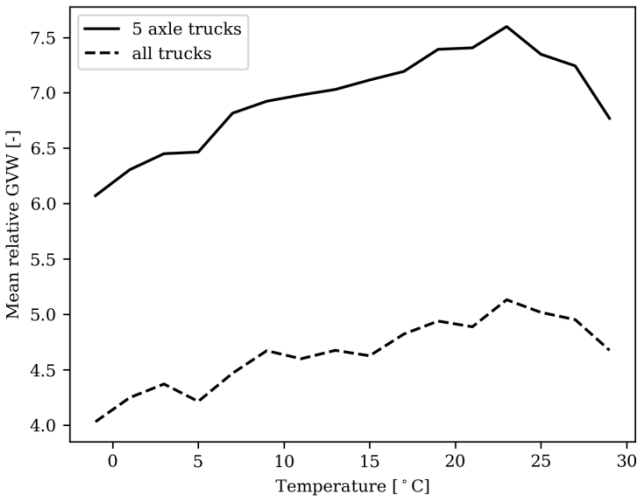

Figure 9. Mean relative GVW plotted against temperature for a population of general trucks and of 5-axle trucks.

5 CONCLUSIONS

This research project has consisted of three main contributions within the fields of bridge safety and bridge health monitoring. A Bayesian framework that can be used to better estimate bridge safety with the use of measurement data has been developed. This framework is equally appropriate to compare different SHM systems. Damage indicators have been validated based on bridge strain data and simultaneously recorded temperature data. For bridge managers, a risk map has been proposed that can incorporate the information of strain and temperature measurement and can help in decision making. The

last contribution has used an iterative approach for obtaining the instantaneous bridge influence line shape and relative axle weights of passing trucks. The mean GVW of these passing trucks has good potential for damage detection and it has been validated against temperature data.

In the on-going research, the so-called population influence lines are being studied in order to obtain, with the iterative approach, not only instantaneous but more general influence lines. A deeper investigation into the spatial variation of deterioration of bridges and how it influences damage detection is planned.

ACKNOWLEDGMENTS

This project has received funding from the European Union's Horizon 2020 research and innovation programme under the Marie Skłodowska-Curie grant agreement No. 642453.

The authors gratefully acknowledge the Federal Highway Administration's Long-Term Pavement Performance Program for access to and extensive WIM database.

Field measurement data were made available courtesy of the BridgeMon project from the Research for the Benefit of SMEs (Small and Medium-size Enterprises) scheme of the 7th Framework Programme of the European Commission.

REFERENCES

[1] Kashif Ur Rehman, S., Ibrahim, Z., Memon S. and Jameel, M. (2016), 'Nondestructive test methods for concrete bridges: A review', *Construction and building materials*, 107, 58-86.

[2] Sbartï, Z., Laurens, S., Elachachi, S. and Payan, C. (2012), 'Concrete properties evaluation by statistical fusion of NDT techniques', *Construction and building materials*, 37, 943-950.

[3] Torres-Luque, M., Bastidas-Arteaga, E., Schoefs, F., Sanchez-Silva, M. and Osma, J. (2014), 'Non-destructive methods for measuring chloride ingress into concrete: State-of-the-art and future challenges', *Construction and building materials*, 68, 68-81.

[4] Carden, E. and Fanning, P. (2004), 'Vibration based condition monitoring: A review', *Structural Health Monitoring*, 3(14), 355-377.

[5] COST Action TU1402: *Quantifying the value of Structural Health Monitoring*, accessed 2 December 2018, <http://www.cost-tu1402.eu>.

[6] Heitner, B., OBrien, E.J., Yalamas, T., Schoefs, F., Leahy, C. and Décatoire, R. (under review), 'Updating bridge reliability assessments using health monitoring data'.

[7] International Federation for Structural Concrete (fib), *Model Code 2010*, Lausanne, Switzerland, 2012.

[8] Chang, Y., Chen, Y., Sheu, M. and Yao, G. (2006), 'Residual stress-strain relationship for concrete after exposure to high temperature', *Cement and concrete research*, 36, 1999-2005.

[9] Kassir, M., Bandyopadhyay, K. and Reich, M., *Thermal degradation of concrete in the temperature range from ambient to 315°C (600°F)*, Engineering Research and Applications Division, Department of Advanced Technology, Brookhaven National Laboratory, Associated Universities, Inc., Upton, New-York, 1996.

[10] Shourky, S.N., William, G.W., Downie, B. and Riad, M.Y. (2011), 'Effect of moisture and temperature on the mechanical properties of concrete', *Construction and building materials*, 25, 688-696.

[11] Cestel d.o.o., Spruha 32, 1236 Trzin, Slovenia, accessed 2 December 2018, <http:// www.cestel.eu>.

[12] Znidaric, A. (2017), *Influence of number and quality of Weigh-in-Motion data on evaluation of load effects on bridges*, University of Ljubljana, Slovenia: Doctoral thesis.

[13] B. Iglewicz and D.C. Hoaglin, *The ASQC basic references in quality control: statistical techniques, Volume 16: How to detect and handle outliers*, Milwaukee, Wisconsin: American Society for Quality Control - Statistics Division, 1993.

[14] O'Brien, E.J., Quilligan, M. and Karoumi, R. (2006), 'Calculating an influence line from direct measurements', *Bridge Engineering* 159(1), 31-34.

[15] Moses F. (1979), 'Weigh-in-motion system using instrumented bridges', *Transportation Engineering Journal of ASCE*, 105(3), 233-249.

Chapter 3: Railway bridge condition monitoring and fault diagnostics

Matteo Vagnoli[1], Rasa Remenyte-Prescott[1], John Andrews[1]
[1]Resilience Engineering Research Group, the University of Nottingham, Science Road, University Park, NG7 2RD, Nottingham, United Kingdom
email: Matteo.vagnoli@gmail.com, R.Remenyte-Prescott@nottingham.ac.uk, John.Andrews@nottingham.ac.uk

ABSTRACT: The European transportation network is ageing continuously due to environmental threats, such as traffic, wind and temperature changes. Bridges are vital assets of the transportation network, and their safety and availability need to be guaranteed in order to provide a safe transportation network to passenger and freight traffic. At the same time, a reduction of the whole life cost of the bridge is required due to the limited amount of maintenance budget that is available to bridge owners. The aim of this project is to develop Structural Health Monitoring (SHM) strategies, in order to monitor the health state of a bridge continuously. Damage of the bridge infrastructure is required to be identified and diagnosed, by taking account of the interdependencies between different elements of the bridge. In this way, early detection of the ongoing degradation of the bridge can be achieved, and consequently, a fast and cost-effective recovery of the optimal health state of the infrastructure can be obtained. For this purpose, five condition monitoring and damage diagnostics methods are developed: *i)* a Bayesian Belief Network (BBN), which has been verified on two Finite Element Models (FEMs), by defining the Conditional Probability Tables (CPTs) using an expert knowledge elicitation process; *ii)* a data analysis methodology that relies on the definition of Health Indicators (HI) of the bridge element, which has been tested on two in-field bridges, a steel truss bridge, and a post-tensioned concrete bridge, that were subject to a progressive damage test; *iii)* a machine learning method for assessing the health state of bridges automatically, by adopting a Neuro-Fuzzy Classifier (NFC), which has been applied to a post-tensioned concrete in-field bridge; *iv)* a method to continuously update the CPTs of the BBN by considering the actual health state of the bridge elements and the knowledge of bridge engineers; the method has been verified on the post-tensioned concrete in-field bridge; *v)* an ensemble-based change-point detection method, to analyse database of past unknown infrastructure behaviour for identifying the most critical change of the health state of the infrastructure; the method has been applied to a database of tunnel behaviour, which was subject to renewal activities.

KEY WORDS: Bayesian Belief Network (BBN); Machine learning; Neuro-Fuzzy neural network; Structural Health Monitoring (SHM); Health Indicator (HI); Empirical Mode Decomposition (EMD); Genetic Algorithms (GA); Bridges.

1 INTRODUCTION

More than one million highway and railway bridges are present on the European transportation network [1]. These assets are continuously deteriorating due to aging, traffic load, and environmental effects such as strong wind and changing temperatures. Time-consuming and expensive visual inspection techniques are widely adopted to assess the health state of bridges, at fixed time intervals, ranging from one to six years. In order to overcome the limitations of visual inspections, SHM methods are used to assess the health state of bridges accurately, remotely and continuously, by relying on the analysis of static and dynamic responses of the infrastructure. Therefore, SHM methods are needed to detect ongoing degradation promptly. Such information can help in developing an optimal maintenance schedule, which can help to minimize the whole life-cycle cost of the asset [2]. At the same time, SHM methods, which are able to detect and diagnose sudden and unexpected changes of the infrastructure health state (i.e., damage of the infrastructure), are needed to guarantee the safety and reliability of the asset [3].

SHM methods rely on model-based and non-model-based strategies. The former assesses the health state of a bridge, by comparing the behaviour of the in-field bridge with the expected results provided by a FEM of the bridge; the latter assesses the health state of the bridge by analysing the measured behaviour of the in-field bridge directly. However, model-based methods, such as FEM updating methods [4], require a complex and time-consuming procedure to develop an accurate FEM. As a consequence, continuous condition monitoring might not be achieved. In contrast, non-model-based methods, such as Artificial Neural Networks (ANNs) [5], Principal Component Analysis (PCA) [6], supervised and unsupervised clustering techniques [7], show promising results for continuous condition monitoring of bridges. However, the performance of non-model-based methods strongly depends on the quality of available data. At the same time, non-model-based methods do not take into account the knowledge of structural engineers that design and maintain bridges and the influence of degradation of individual elements on the health state of the whole bridge.

Hence, bridge managers are calling for SHM methods that are able to: *i)* assess the health state of the bridge by taking account of influences between different elements; *ii)* take account of the expertise of bridge engineers without requiring time-consuming processes to develop the SHM method; *iii)* manage different sources of data, such as evidence of the bridge behaviour provided by sensors and visual inspection reports; *iv)*

update the assessment of the bridge health state every time new evidence of the behaviour becomes available; *v)* detect and diagnose slow degradation mechanisms and sudden changes in the bridge condition (damage).

This project proposes a BBN method for bridge condition monitoring and damage diagnostic. A BBN can satisfy these requirements, by providing a graphical interface to bridge managers, who can interact with the BBN model to assess the health state of the bridge and the influence between different degrading elements. The BBN method can assess the health state of a railway infrastructure, and its elements, at the same time. A pre-processing of the infrastructure behaviour is needed in order to remove the data noise, which is usually present in the measurement of the infrastructure behaviour and assess the health state of the bridge reliably.

A data analysis methodology is thus developed to analyse the vibration behaviour of the bridge and monitor the health state of bridge. The main novelty of the proposed data analysis methodology lies in the use of the Empirical Mode Decomposition (EMD), which is adopted to assess Health Indicators (HIs) of the bridge, by evaluating the trend of time and frequency-domain features of the bridge behaviour. In fact, the EMD is generally adopted in the SHM framework to identify structural changes by analysing the bridge dynamic behaviour directly, i.e., the dynamic behaviour of the bridge is used as an input to the EMD process, rather than the extracted features [8]. A machine learning method, which is based on a Neuro-Fuzzy Classifier (NFC), is also developed to automatically assess the health state of bridge elements. The HIs of the bridge are used as an input to the NFC.

A method to merge the expert judgment with the analysis of a small amount of bridge behaviour is also proposed. The method aims to define the CPTs by means of the expert knowledge elicitation process, and then to update the CPTs whenever a new measurement of the bridge behaviour is available. Indeed, an expert knowledge elicitation process is usually adopted to define the CPTs, if no data about the bridge behaviour are available [9]. However, such an approach can be subjective. On the contrary, when data of the bridge behaviour are available, the CPTs can be defined by using learning methods. This last approach requires a large amount of data usually. However, the proposed method allows defining the CPTs by merging expert judgment and bridge behaviour analysis. The updating process requires the knowledge of Cumulative Distribution Function (CDF) of an optimal HI, which is used to monitor the evolution of the bridge health state. The CDF is retrieved by analysing a database of bridge behaviour, when the bridge behaviour in different health states of the bridge is available and known in the database.

Finally, a robust data mining method for analysing database of infrastructure behaviour automatically, accurately and rapidly is developed [10]. As a result, the data of infrastructure behaviour can be transformed into valuable information for decision-makers, by pointing out past changes in the health states of the infrastructure. An ensemble-based change-point detection method is proposed in order to identify changes in the condition of railway infrastructure. This information can be used to *i)* help the construction of the quantitative part of the BBN, by providing insights about interdependencies between different elements of the asset and (or) changes of environmental condition; *ii)* identify the time when the most severe change of the asset health state occurred, and consequently diagnose the causes of such changes.

In what follows, the research aims, and objectives are discussed in Section 2, and the developed methods are presented in Section 3, followed by conclusions in Section 4.

2 OBJECTIVES

The main goal of this research project is to develop SHM methods to monitor the health state of a critical infrastructure continuously in a reliable manner. The focus is on the continuous monitoring, by taking account of the interdependencies between different elements of the infrastructure and diagnosing damage of the structure. The following objectives can be distinguished:

- Propose a method for bridge condition monitoring and damage diagnostics, to assess the health state of a bridge and its elements.
- Analyse the performance of the proposed method, by analysing both in-field bridges and FEM under different health states.
- Analyse the data of the bridge behaviour in order to remove the noise of the data and achieve a robust assessment of the bridge health state.
- Assess the health state of a bridge automatically, by taking account of the past behaviour of the bridge.
- Consider both the expertise of bridge engineer and the analysis of the bridge behaviour.
- Analyse a database of unknown infrastructure behaviour, with the aim of pointing out changes in the health state of the infrastructure.

3 CONDITION MONITORING AND DAMAGE DIAGNOSTIC

The proposed methods allow analysing the health state of the bridge throughout its life time, as shown in Figure 1: *i)* the proposed BBN allows to monitor the health state of the bridge continuously, during the life of the bridge (as depicted by the red box in Figure 1), by relying on the expertise of the bridge engineers who designed the bridge, at the early stage of the bridge life; *ii)* the proposed data analysis methodology allows to assess the health state of the bridge elements, when data of the bridge behaviour are recorded by using sensors (as depicted by the yellow box in Figure 1); *iii)* similarly, the developed machine learning method allows to automatically detect damage in the bridge elements, when a vast database of bridge behaviour is available (as shown by the orange box in Figure 1); *iv)* the novel ensemble-based change-point detection method can be adopted in order to analyse the past behaviour of the bridge, by pointing out when the health state of the bridge changed, and diagnosing the causes of such changes (as depicted by the blue box in Figure 1); *v)* the developed method to update the CPTs of the BBN allows to merge the information provided by the bridge engineers, with the analysis of the past bridge behaviour data. As a consequence, the monitoring and diagnostic performance of the BBN are significantly improved, when past data of the bridge behaviour are available to define the CPTs updating strategy (as depicted by the green box in Figure 1).

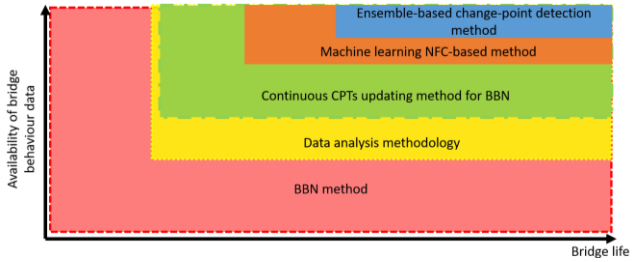

Figure 1. Novel methods developed during the research project.

It is worth noting that the procedure of merging data analysis methods with the BBN structure leads to a SHM framework that is potentially able to improve its monitoring and damage diagnostic performance over time. In fact, the higher the amount of bridge behaviour data, the more reliable the BBN-based analysis, due to the improvement of the data analysis and the CPTs update process. However, the data of the bridge behaviour need to represent different health states of the bridge and require to be validated by bridge engineers, who verify the health state of the in-field bridge. In what follows the performance of the methods proposed and verified during this research project are discussed.

3.1 The BBN method for bridge condition monitoring and damage diagnostic

The proposed BBN method offers a novel approach for a continuous SHM, by tackling the limitations of model-based and non-model-based methods. Indeed, a BBN can assess the health state of each bridge element and the whole bridge simultaneously, without requiring a complex and time-consuming process of analysis to be used. The BBN can also update the health state of the whole bridge, and its elements, whenever new evidence of the bridge behaviour becomes available. Complex information from different sources, such as data from the measurement system that is installed on the bridge, visual inspection reports, and expert judgment can be used as an input to the BBN. In this way, the knowledge of structural engineers that design and maintain bridges is merged with the evidence of the bridge behaviour. The BBN approach can also manage different sources of uncertainty, i.e. epistemic uncertainties that are caused by the incomplete knowledge of the phenomenon, and aleatory uncertainties that are caused by the randomness. Finally, the BBN offers a diagnostic property that allows diagnosing the causes of the observed health state of the bridge.

The BBN has been verified by monitoring the health state of three bridges during the project (two FEMs and one in-field bridge), by providing good damage diagnostic performance. For example, Figure 2 shows an in-field concrete post-tensioned bridge that has been damaged at the pier location, during the monitoring time. The first damage was inflicted after 19 minutes from the beginning of the monitoring time, whereas more severe damage was inflicted after 34 minutes, as depicted by dashed vertical lines in Figure 4. The bridge is monitored by the two sensors represented as circular dots in Figure 2.

The health state of the bridge is monitored by developing a BBN. The structure of the proposed BBN approach is developed by identifying major (such as the deck and spans of the bridge) and minor (such as beams and minor bridge elements) elements of the bridge. For each element of interest,

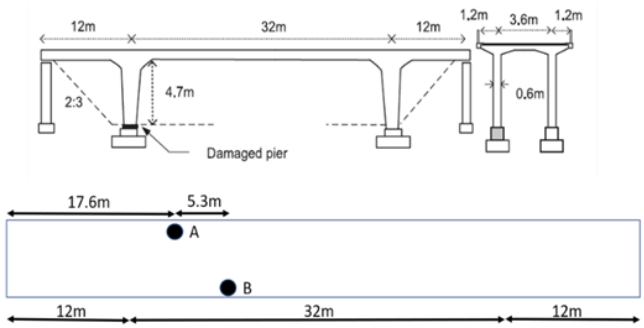

Figure 2. Post-tensioned concrete bridge.

a node is defined in the BBN framework. Different nodes are connected by considering the same order as during the construction of the real bridge, i.e., from minor to major elements, as shown in Figure 3, where the E_i nodes represent minor bridge elements. The BBN of Figure 3 allows monitoring of the health state of the bridge continuously, i.e., every time new evidence of the bridge behaviour is available, it is analysed by the proposed data analysis method, and then used as an input to the BBN. Therefore, the health state of the bridge is assessed by taking the health state of each of its elements into account.

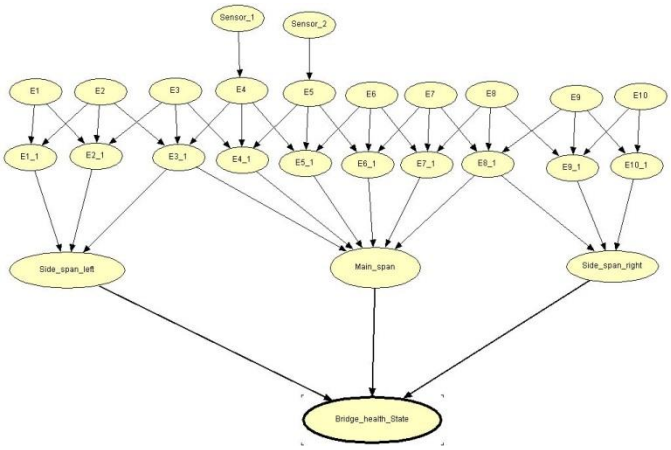

Figure 3. BBN of the post-tensioned concrete bridge.

The interdependencies between different nodes are evaluated by defining the CPTs. A Fuzzy Analytic Hierarchy Process (FAHP) of bridge expert judgements is developed in order to define the CPTs. Figure 4 shows the evolution of the health state of the whole bridge over time, which is assessed by the BBN of Figure 3. The BBN is able to point out changes of the bridge health state. At the same time, the BBN allows diagnosing the causes of such changes, by allowing an interactive visualization of the health state of the bridge and its elements to bridge managers, who can interact with the BBN structure to actively analyse the BBN results. Consequently, if the methodology was to be implemented on a touch screen system, a bridge manager can select the node of the bridge element of interest and monitor the evolution of the health state of that bridge element over time. For example, Figure 5 shows the evolution of the health state of the whole bridge, and its parent nodes, i.e., the bridge major elements that influence the health state of the whole bridge.

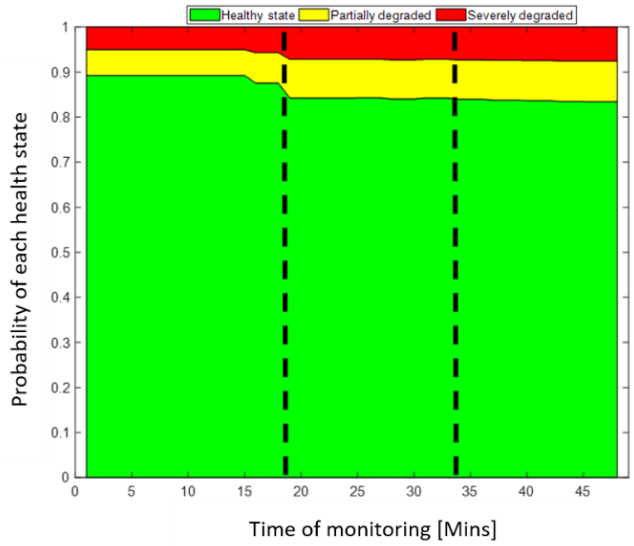

Figure 4. Evolution over time of the health state of the whole bridge.

A bridge manager can easily point out that the damaged major element of the bridge is the main span, as shown in Figure 5 by the increasing probability of the degraded health states. Similarly, the damaged elements of the bridge can be identified by the BBN.

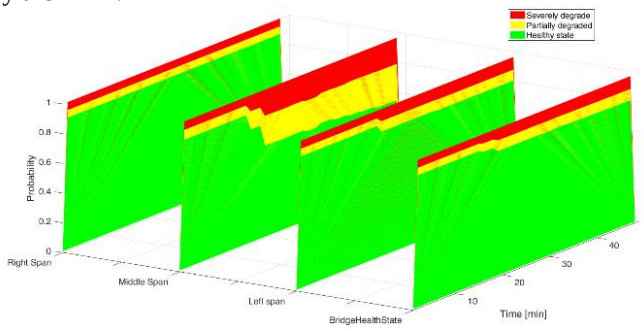

Figure 5. Evolution over time of the health state of the whole and its parent nodes, i.e., left, right and main span.

3.2 *The data methodology for bridge damage detection*

Every time when a new set of raw bridge acceleration is provided by the sensors, the proposed data analysis methodology allows to assess the bridge health state by following five steps: *1)* the raw acceleration is pre-processed with the aim of removing outliers in the data; *2)* the free vibration behaviour of the bridge is identified and *3)* a feature extraction process is developed, to reduce the dimensionality of the free-vibration bridge behaviour. Indeed, the sensors provide thousands of values of the bridge acceleration at each second in time, whereas features can extract relevant information regarding the bridge health state, by merging the thousands of sensor values into a lumped assessment. Statistical features, frequency-domain features, and vibration parameters are assessed at each τ time step in order to extract information from the free-vibration behaviour of the bridge; *4*) the feature trend over the time is computed every time interval τ^*, by assessing the residuals of the Empirical Mode Decomposition (EMD) of each extracted feature; *5)* a set of 4 bridge Health Indicators (HIs), which provides information with respect to the health state of the monitored bridge, is obtained by calculating statistical parameters (such as standard deviation and skewness) of the feature trend.

For example, the post-tensioned bridge of Figure 2 has been analysed by means of the developed data analysis method. Figure 6 shows the evolution of the optimal HIs of the bridge, which has been identified by optimizing the trend and monotonicity of the HIs. The different magnitudes of the bridge damage are represented by different classes, as shown in Figure 6. The HI-3 of both sensors allows the identification of the different health states of the bridge, i.e., the HI-3 increases when the damage magnitude increases. The proposed data analysis methodology is also verified in an in-field steel truss bridge, which was subject to a progressive damage test. The method is able to point out different health states of the bridge infrastructure in a reliable and fast manner.

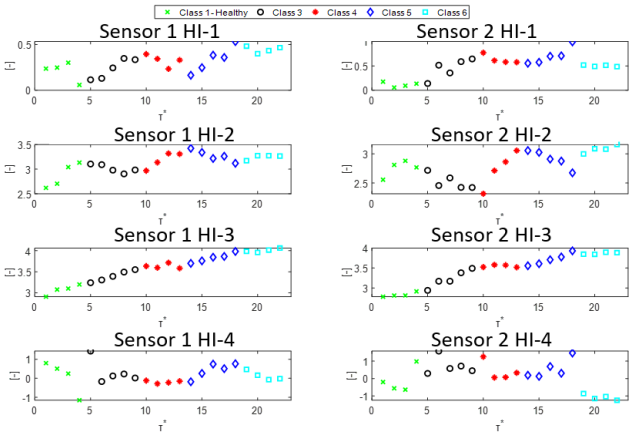

Figure 6. HIs evolution during the bridge monitoring time.

3.3 *The machine learning method for bridge damage detection and diagnostic*

An automatic assessment of bridge health state is reached by developing a machine learning method, which relies on a NFC. The NFC is trained in a supervised manner by using a dataset of bridge behaviour in different health states. The optimal subset of HIs, which has been identified by using a Modified Binary Differential Evolution (MBDE) algorithm, is used as an input to the NFC, in order to assess the health state of the bridge. The NFC is selected from amongst the machine learning classifiers because it combines fuzzy classification techniques with the learning capabilities of the Neural Networks. Therefore, the network structure is developed by means of if-then fuzzy rules, which are initially defined by using a K-means clustering algorithm. Conversely to ANNs, which require the optimization of the number of hidden layers and hidden nodes, the NFC requires only the optimization of the number of clusters of the K-means algorithm, and the performance of the NFC is slightly influenced by the number of the cluster.

The developed machine learning methods are verified by monitoring the performance of the post-tensioned concrete bridge of Figure 2. The available bridge behaviour data are divided into training, testing, and validation set. In this way, the performance of the NFC is validated by analysing a set of unknown bridge behaviour, i.e., the health state of the bridge data behaviour belonging to the validation test is not known. Therefore, the NFC is required to assess the health state of the

bridge in a reliable manner. The accuracy of the NFC, i.e., the percentage of correct classification of the bridge health state, is 79% on average. Such accuracy is a good result in monitoring the health state of an in-field bridge, due to the unknown source of uncertainty and changing environmental conditions. Indeed, similar machine learning methods, which have been previously proposed in literature by relying on ANNs and verified on FEMs by adding white Gaussian noise to the simulated bridge behaviour, have shown an average accuracy of 65% [11], whereas clustering techniques, which were verified on in-field bridges, have shown an average accuracy of 68%, with a maximum accuracy of 75% [8].

3.4 *The ensemble-based change-point detection for mining large database of infrastructure behaviour*

Usually, an SHM system generates a large quantity of data, and consequently, processing and interpreting this data can be difficult and time-consuming. Here, an ensemble-based data mining method is proposed to detect the past unexpected behaviour of civil infrastructure. An ensemble-based change-point detection analysis is developed, with the aim of identifying the time when the infrastructure behaviour starts to change rapidly and point out the duration of the health state change. The ensemble-based method is needed due to three main limitations of individual change-points detection methods: *i)* individual change-point methods, such as Cumulative Sum (CUSUM)-based or probability distribution-based [12] methods, can identify only abrupt changes in the data, without pointing out the most severe changes; *ii)* the longer the duration of the monitored behaviour of the system, the higher the number of the abrupt changes, that are identified by an individual change-point method, and thus, the most critical change of the infrastructure health state can be lost among all the change-points; and *iii)* the duration of the most critical change of the infrastructure health state is not identified by individual methods. On the other hand, the proposed ensemble-basis of change-point method allows identifying the most critical change in the data, by assessing its start and end time. As a consequence, decision-makers can initially focus only on the information regarding the most critical behaviour of the infrastructure.

The proposed method has been verified on a database of behaviour of an in-field railway tunnel, which is subject to maintenance activities. The proposed method is able to identify the critical parts of the infrastructure, and then point out the most critical change of the element behaviour. For example, Figure 7 compares the performance of the proposed ensemble-based change-point detection with the performance of four individual methods. The raw infrastructure behaviour shows a rapid change of the infrastructure health state. However, each individual method is unable to point out the start and the end of the critical infrastructure behaviour, as shown by vertical lines in Figure 7, which represent the detected change-point. Particularly, the individual methods can identify only the starting point of the change. Conversely, the proposed ensemble-based change-point method identifies a change-point interval that starts at time 50 h and ends at time 169 h. In this way, the initial point where the health state of the infrastructure starts to change, and the end point of the health state change are identified. Finally, the results of the proposed method can be used to identify the possible causes of the critical change.

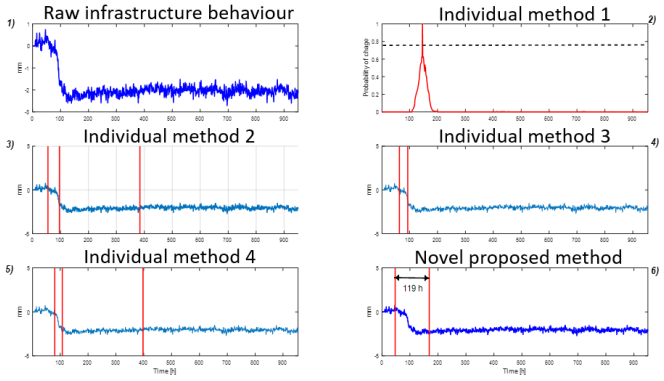

Figure 7. Change-point detection by using the proposed ensemble-based method and each individual change-point method

3.5 *The CPTs updating method for a BBN-based bridge condition monitoring and damage diagnostic approach*

A method to update the CPTs is developed by merging the expert knowledge elicitation process with the analysis of the bridge behaviour. The method requires the availability of bridge behaviour data during different known health states of the bridge elements in order to assess the dependencies between different bridge elements, by means of CDFs. The proposed method allows updating of the CPTs by taking account of the current health state of the bridge elements, whenever a new measurement of the bridge behaviour is available during the on-line monitoring of the bridge.

The diagnostic performance of the BBN is significantly improved by the CPTs updating method. For instance, Figure 8 shows the evolution of the health state of the damaged elements of the post-tensioned bridge of Figure 2, when the proposed strategy for updating the CPTs is used (Figure 8 top), and when the CPTs are defined by using the expert knowledge elicitation process (Figure 8 bottom). Both strategies allow to point out the different health states of the bridge elements, by increasing the probability of the degraded states when damages are inflicted to the bridge. However, when the CPTs are updated by adopting the proposed strategy, the probability of the degraded states increases more than the probabilities using the expert-based CPTs. Furthermore, the probability of the states of degradation increases over time in Figure 8 top, i.e., when the proposed strategy is adopted. This means that the health state of the bridge elements decreases over time. In fact, the health state of the bridge decreases over time, due to the different damages that are inflicted to the bridge pier. Therefore, the BBN that relies on the proposed strategy to update the CPTs can diagnose the damage states of the bridge more clearly.

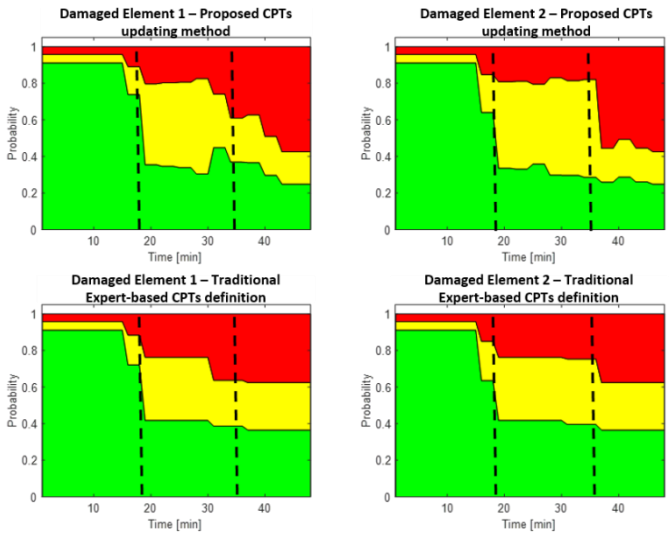

Figure 8. Comparison of the performance of the proposed updating strategy and the expert knowledge elicitation process.

4 CONCLUSIONS

The health state of bridges is usually assessed by time-consuming, expensive and subjective visual inspections at fixed time intervals, ranging from one to six years. Consequently, the degradation of the bridge health state can increase without being detected, and reduce the safety, reliability, and availability of both the bridge and the corresponding transportation network. SHM methods allow monitoring the health state of a bridge continuously, by analysing the bridge behaviour data. In this research project, the following set of methods for bridge condition monitoring and damage diagnostic has been proposed:

- A BBN method to assess the health state of a bridge by taking account of interdependencies between different elements of the bridge. The BBN method has been verified by monitoring and diagnosing the health state of two FEMs of two bridges and an in-field bridge.
- A data analysis methodology has been developed with the aim of pre-processing the data of the bridge behaviour. In this way, the noise of the data is removed, and HIs of the bridge have been provided to allow a robust assessment of the bridge health state.
- A machine learning method has been proposed by relying on an NFC. The method has been trained on past behaviour of the bridge and allowed to assess the health state of the bridge in an automatic manner.
- A method to merge expert judgment with an analysis of the bridge behaviour has been developed. Particularly, the two approaches have been merged in order to define and update the CPTs of a BBN.
- An ensemble-based change-point detection has been proposed to analyse a database of past unknown behaviour of the infrastructure. The method has allowed to point out the most critical change of the infrastructure health state.

The methods have been verified on FEMs of bridges and by assessing the health state of three in-field infrastructures, and they have demonstrated to be able to assess the health state of in-field infrastructure robustly and reliably, by taking account of interdependencies between different elements of the structure. The accuracy of SHM methods could be further improved by focusing future efforts on machine learning and data analysis methods.

ACKNOWLEDGMENTS

This project has received funding from the European Union's Horizon 2020 research and innovation programme under the Marie Skłodowska-Curie grant agreement No. 642453.

REFERENCES

[1] European Commission, *EU transport in figures, statistical pocketbook*, 2012.

[2] Vagnoli, M., Remenyte-Prescott, R. and Andrews, J., (2018) 'Railway bridge structural health monitoring and fault detection: State-of-the-art methods and future challenges ',*Structural Health Monitoring*, 17(4), 971-1007.

[3] Moughty, J.J. and Casas, J.R. (2017), 'A state of the art review of modal-based damage detection in bridges: Development, challenges, and solutions', *Applied Sciences* (Switzerland), 7(5), art. no. 510.

[4] Shabbir, F. and Omenzetter, P. (2016), 'Model updating using genetic algorithms with sequential niche technique', *Engineering Structures*, 120, 166-182.

[5] Hakim, S.J.S. and Abdul Razak, H. (2013), 'Structural damage detection of steel bridge girder using artificial neural networks and finite element models', *Steel and Composite Structures*, 14(4), 367-377.

[6] Cavadas, F., Smith, I.F.C. and Figueiras, J. (2013), 'Damage detection using data-driven methods applied to moving-load responses', *Mechanical Systems and Signal Processing*, 39(1-2), 409-425.

[7] Alves, V., Cury, A. and Cremona, C. (2017), 'On the use of symbolic vibration data for robust structural health monitoring*', Proceedings of the Institution of Civil Engineers: Structures and Buildings*, 169 (9), 715-723.

[8] Cahill, P., Hazra, B., Karoumi, R., Mathewson, A. and Pakrashi, V. (2018), 'Vibration energy harvesting based monitoring of an operational bridge undergoing forced vibration and train passage', *Mechanical Systems and Signal Processing*, 106, 265-283.

[9] Loughney, S. and Wang, J. (2017), 'Bayesian network modelling of an offshore electrical generation system for applications within an asset integrity case for normally unattended offshore installations', *Proceedings of the Institution of Mechanical Engineers, Part M: Journal of Engineering for the Maritime Environment*, p. 1475090217704787.

[10] Vagnoli, M. and Remenyte-Prescott, R. (2018), 'An ensemble-based change-point detection method for identifying unexpected behaviour of railway tunnel infrastructures', *Tunnelling and Underground Space Technology Journal*, 81, 68-82.

[11] Shu, J., Zhang, Z., Gonzalez, I. and Karoumi, R., (2013), 'The application of a damage detection method using Artificial Neural Network and train-induced vibrations on a simplified railway bridge model', *Engineering Structures*, 52, 408-421.

[12] Liu, S., Yamada, M., Collier, N. and Sugiyama, M., (2013), 'Change-point detection in time-series data by relative density-ratio estimation', *Neural Networks*, 43, 72-83.

Chapter 4: Assessment of bridge condition and safety based on measured vibration level

John J. Moughty[1], Joan R. Casas[1]
[1]Dept. of Civil and Environmental Engineering, Technical University of Catalonia, c/ Jordi Girona 1-3, 08034 Barcelona, Spain
email: john.james.moughty@upc.edu, joan.ramon.casas@upc.edu

ABSTRACT: Bridges deteriorate over time due to the influence of environmental and operational effects, and the measurement of this deterioration has been the subject of much research. Bridge damage identification methodologies have advanced considerably due to the incorporation of statistical pattern recognition and machine learning algorithms; however, the successful application of such methods has been stifled. One may argue that the continued use of model-based damage sensitive features as inputs to damage identification methodologies hindered its progression, given their sensitivity to environmental and operational effects, in addition to the difficulty of accurately determining higher, more damage sensitive, vibration modes without bridge closures and heavy loading procedures. An alternative option is to utilize vibration-based damage sensitive features which do not require external input loading or bridge closures and can be continuously recorded. The work developed in this project investigates the damage identification performance of a number of vibration-based damage sensitive features on two separate progressively damaged bridges subjected to ambient and operational loading, respectively.

KEY WORDS: Vibration; Hilbert transform; Empirical Model Decomposition (EMD); Damage.

1 INTRODUCTION

Civil engineering infrastructures are subjected to degradation due to the passage of time and as well as a great number of various external adverse actions. As of 2016, in the United States alone, 39% of the bridges in the National Bridge Inventory were built over more than 50 years ago and 9.1% of the total number of bridges were deemed structurally deficient. As a result, on average of 188 million trips were made daily across these structurally deficient bridges, and the most recent estimate projects the backlog of rehabilitation projects for these infrastructures at $123 billion [1]. Europe's highway bridge count is circa one million, and of Europe's half a million rail bridges, 35% are over 100 years old.

A review of the state-of-the-art on modal and non-modal based, output only techniques is first carried out [2,3]. The main results show that environmental and operational variations have considerable influence on a bridge's dynamic behavior, which may be mistaken for damage when using modal parameters such as natural frequencies. Data normalization techniques help determine a bridge's baseline response under a range of normal environmental and operational conditions. The process of data normalization can be challenging in itself due to the non-linear, multivariate nature of a bridge's behavior and due to the quantity of data required. On the other hand, response modeling aims at separating the variations imposed by "normal" environmental/operational actions from those caused by damage. It relies on training statistical learning algorithms so that they can accurately estimate the "normal" structural response. The most reported statistical modeling algorithms found in SHM literature consist of multilayer perceptron neural networks, support vector regressions, linear regressions, Principal Component Analysis (PCA), and cluster analysis. Non-modal-based output only techniques offer robustness in varying conditions, ease of application, and a high level of damage sensitivity. For this reason, it is considered advantageous to investigate within TRUSS new damage features and vibration-based non-modal performance indicators.

2 VIBRATION PARAMETERS

The present section introduces a number of output-only vibration parameters that can be extracted from discrete time-histories of acceleration obtained under ambient or vehicle-induced excitation conditions. For damage identification purposes, the vibration parameters must provide a measure of signal energy, vibration frequency or signal decay. Ideal vibration parameters should be representative of the discretized acceleration response from which it is obtained, sensitive to any structural changes that may occur and also being insensitive to the effects of environmental and operating conditions. The following list of vibration parameters is chosen for their ability to measure either signal energy, frequency, decay, or a combination thereof. Some parameters are novel, being first presented herein, while others are taken from other fields of engineering such as seismology and brought into a SHM context for the first time. The applicability of each vibration parameter to the specific type of vibration signal will depend on whether the parameter is suitable for extraction from short or long duration signals or from stationary or non-stationary signals. Although none of the parameters can be considered "ideal" in terms of damage identification as they do attain some degree of sensitivity to environmental and operation conditions, the addition of post-processing techniques, outlined in the following section, restrict their influence.

2.1 Cumulative absolute velocity (CAV)

CAV is an energy-based vibration parameter originally proposed by the American Electric Power Research Institute (1988) to assess the structural damage potential of earthquakes.

The concept of its original use is based on the theory that earthquakes with long duration vibration cycles result in greater structural damage. In the present study, it is used to ascertain whether or not a bridge is required to exert greater energy in resisting a repeating loading.

$$CAV = \int_0^t |\ddot{x}(t)|dt \quad (1)$$

2.2 Arias intensity (IA)

I_A, proposed by Arias [4], is another energy based vibration parameter, commonly used as an empirical indicator of an earthquake's structural damage potential and also to predict the likelihood of landslides.

$$I_A = \frac{\pi}{2g}.\int_0^{\infty} \ddot{x}(t)^2 \; dt \quad (2)$$

2.3 Destructiveness potential factor (PD)

P_D is a variation of Arias Intensity that incorporates a frequency-based denominator, as proposed by Araya and Saragoni [5]. It accounts for frequency characteristics in addition to vibration energy by including the variable ν_0, which is the number of zero crossings per unit of time.

$$P_D = \frac{\frac{\pi}{2g}.\int_0^{\infty} \ddot{x}(t)^2 \; dt}{{\nu_0}^2} \quad (3)$$

2.4 Mean frequency (FM)

F_M is an adaptation of a parameter originally developed by Rathje et al [6] called Mean Period (TM), which was developed to assess Earthquake ground motions. It uses Fourier amplitude values {FA_i} within an associated frequency range to yield a weighted average period between 0.25 Hz and 20 Hz. As this parameter requires accurate Fourier amplitude values of each frequency, it is not suitable for use on non-stationary signals where the frequency content changes with time; therefore it is only applied herein to the data obtained from the ambient induced excitation case study data.

$$FM = \frac{\sum_{i=m}^{n} {FA_i}^2.(f_i)}{\sum_{i=m}^{n} {FA_i}^2} \quad \text{for } m \le f_i \le n \text{ (in Hz)} \quad (4)$$

2.5 Cumulative absolute displacement (CAD)

This parameter is used to assess the variation in displacement at each sensor over time for a repeated loading, i.e., a repeated vehicle crossing. As a vehicle crossing results in a short duration vibration signal, an accurate approximation of transient displacement can be obtained from the acceleration signal using integration and band-pass filtering to avoid drift. It is, however, necessary to ensure that the bridge is close to static behavior at t = 0 s in the neutral axis position to avoid ambient environment induced variations.

$$CAD = \int_0^t |x(t)|dt \quad (5)$$

2.6 Distributed vibration intensity (DVI)

DVI, first detailed herein, utilizes vibration intensity, which in simple harmonic motion context can be defined as ($I = a^2/f$), where a is acceleration amplitude and f is frequency. The SI units of vibration intensity are mm^2/s^3, but its logarithmic power form of decibels (*dB*) is more commonly used. For the distributed variant employed in the present study, a Fourier transformation is applied to the acceleration response and the summation of the vibration intensity values is taken within a frequency range, denoted by (f_i) within the limits *m*-*n* in Equation (6). The frequency range should encompass the first few modes of vibration of the structure in question. In this way, *DVI* may capture the damage sensitivity associated with energy and modal changes, while unwanted variation due to adjusting ambient conditions and frequency domain noise can be diminished over sufficient duration length, in addition to the application of Mahalanobis Squared Distance (MSD), as those variations are assumed to be Gaussian in nature.

$$DVI = \sum_{i=m}^{n} 10log_{10}\left(\frac{\ddot{x}_i^2.(f_i)}{f_i}/I_S\right) \quad (6)$$

$$\text{for } m \le f_i \le n \text{ (in Hz)}, I_S = 10\ mm^2/s^3$$

2.7 Mean cumulative vibration Intensity (MCVI)

MCVI, first presented herein, is the second of three parameters based on the concept of vibration intensity (energy /frequency). In *MCVI*, the energy portion, i.e., the numerator, is the square of the aforementioned vibration parameter *CAV*, while the denominator is a weighted mean value of Fourier frequency within a specified frequency range. As per Equation (7), the weighting is applied to the discrete frequencies (f_i) via their corresponding Fourier Amplitude values (FA). As highlighted for *DVI*, it is important that the frequency range selected encompasses the first few modes of vibration of the structure; in the present study, the frequency range is taken as (*m* - *n* = 1 Hz - 20 Hz).

$$MCVI = \frac{\int_0^t \ddot{x}\,(t)^2 \; dt}{\left(\sum_{i=m}^{n} {FA_i}^2.(f_i) \;/\; \sum_{i=m}^{n} {FA_i}^2\right)} \quad (7)$$

$$for\ m \le f_i \le n \text{ (in Hz)}$$

2.8 Vibration envelope area (VEA)

VEA is another novel vibration parameter proposed that can be considered as a pseudo energy-based parameter. It is obtained by calculating the area enclosed by two spline interpolated lines that link the positive and negative peaks, respectively. *VEA* is best used after a low-pass has been applied to the vibration signal to remove potential high-frequency peaks that may obscure the resulting area calculation. Figure 1 presents an example of how *VEA* is obtained, with the vibration envelope shaded.

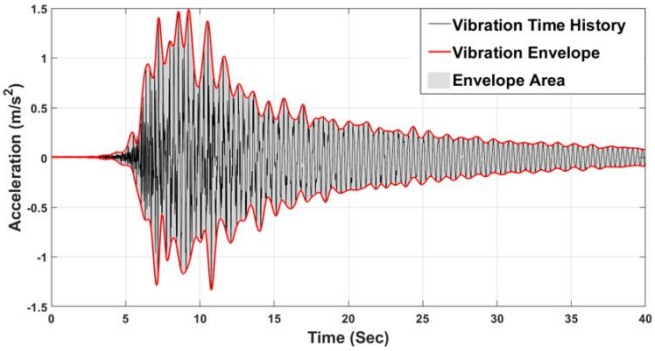

Figure 1. Example of vibration envelope area obtained from a vehicle induced vibration response.

2.9 Vibration energy decay parameters

Equation (8) provides the exponential decay function, where its components y_0 and a represent the Exponential Decay Intercept (ED_I) and Exponential Decay Constant (ED_C), respectively. These two parameters (ED_I and ED_C) can be utilized for the purposes of damage identification.

$$y(t) = y_0 e^{at} \tag{8}$$

However, applying this function to the raw signal will not result in the required decay profile as negative values will hinder its application. Firstly, the vibration signal must be transformed into a suitable form for the exponential decay function. This is completed in two ways in the present study. The first method aims to find the exponential decay of vibration energy. This is achieved by squaring the acceleration response before applying the exponential decay function to obtain the parameters ED_I and ED_C. Note that the exponential decay is only taken from the point at which the vehicle has exited the bridge. The second method that incorporates the exponential decay function is explained in the following section.

2.10 Hilbert envelope decay parameters

Equation (9) depicts the Hilbert Transform of the original vibration signal $x(t)$ where the integral is evaluated as a Cauchy principal value. Combining $x(t)$ and $j.H\{x(t)\}$, produces the analytical signal $z(t)$, where j indicates the complex form of the Hilbert Transform. The Hilbert envelope $e(t)$ is obtained from the absolute analytical signal using spline interpolation (Equation (11)). Finally, the exponential decay function (Equation (8)) is fitted to the Hilbert envelope to provide the required vibration parameters ED_I and ED_C.

$$H\{x(t)\} = \frac{1}{\pi}\int_{-\infty}^{\infty}\frac{\mathrm{x}(\tau)}{\mathrm{t}-\tau}\mathrm{d}\tau \tag{9}$$

$$z(t) = x(t) + j.H\{x(t)\} \tag{10}$$

$$e(t) = |z(t)| \tag{11}$$

The Hilbert Transform can identify the additional frequency bursts as it acts as a filter. This is advantageous in the case of structural vibration responses, as modes of vibration can be emphasized by using a Hilbert filter. Leaving only the sinusoidal frequency content, and as the Hilbert envelope is applied only to the part of the vibration response that occurs after the vehicle has exited the bridge, the sinusoidal frequencies present in the signal should be the structural modes of vibration. It is also recommended to apply band-pass filtering to the vibration signal prior to applying the Hilbert Transform to remove high-frequency noise and low-frequency drift. Figure 2 provides a graphical example of the exponential decay function plotted over the Hilbert envelope. Note that the Hilbert Transform envelope begins spikey, then gradually settles to flow smoothly along the free vibration peaks. This is indicative of the presence of multiple frequencies (modes of vibration) at the start of the signal, which decay quickly, leaving only the first mode of vibration, whose peaks decay identically in both the real and complex parts of the analytical signal. The Hilbert envelope, depicted in Figure 2 contains the peaks of the individual structural modes of vibration. As they decay through time, the resulting exponential decay constant (ED_C) is representative of modal damping across all excited modes simultaneously.

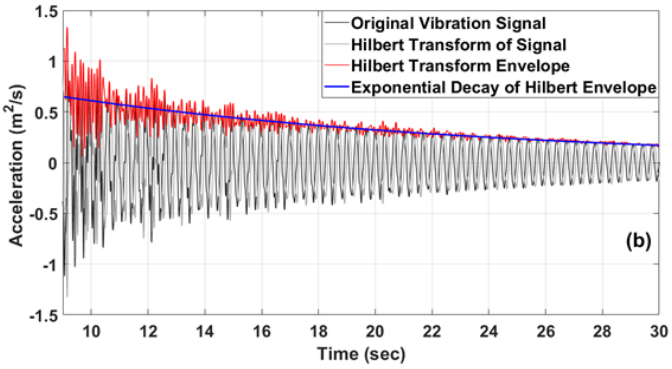

Figure 2. Hilbert Transform envelope of the original signal and its analytical form.

2.11 Application suitability of vibration parameters

The variables of each bridge monitoring campaign, such as monitoring duration, excitation method, number and type of sensors can differ widely from project to project. This may be due to the influence of external conditions associated with each bridge, such as the traffic volume and type, socioeconomic factors and the financial budget available. The result is that the vibration data obtained may attain different properties that may render some damage sensitive features, such as those presented here, unsuitable for the application. Furthermore, Fourier-based damage sensitive features, such as modal parameters, are unsuitable for application to short duration non-stationary vibration responses that would be typical of vehicle induced excitation bridge testing. For this reason, Table 1 is provided to give a breakdown of the applicability of each of the selected vibration parameters to specific vibration properties that may influence their damage identification performance.

3 METHODOLOGY

The present section provides a theoretical overview of the algorithms utilized within the present study.

3.1 Outlier detection for ambient excitation condition

For the ambient condition test, the vibration parameters are assessed using Mahalanobis Squared-Distance (MSD), which is a common multivariate outlier detection algorithm that uses mean and covariance data to train and assess dataset continuity. MSD is determined as shown in Equation (12), where $\{X\}_\zeta$ is the potential outlier, $\{\bar{X}\}$ is the mean of the training data and $[\Sigma]$ is the covariance matrix of the training data.

$$D_\zeta = \left(\{\bar{X}\}_\zeta - \{X\}\right)^T [\Sigma]^{-1}\left(\{X\}_\zeta - \{\bar{X}\}\right) \tag{12}$$

In addition to the MSD, the Minimum Covariance Determinate (MCD) estimator is also employed to enhance robustness and reduce uncertainty regarding sources of ambient excitation by identifying and removing outliers from the training data prior to MSD. Although environmental conditions may remain relatively constant throughout the bridge test, the assumption of Gaussian distributed sources of ambient loading cannot be applied in some cases (one traffic lane under the bridge in operation throughout the test or feasible construction

work nearby). This leaves a case where the undamaged vibration data used to train the MSD may contain outliers itself due to passing traffic or construction vehicle activity, which if left included in the training data may negatively impact the subsequent test/damaged data results, particularly if the training data outliers are significantly dissimilar to the remaining data set. The MCD employed in the present study is the FAST MCD algorithm [7].

Table 1. Vibration parameter application classification.

Property \ Vib. Para.	*CAV*	I_A	P_D	F_M	*DVI*	*MCVI*	*CAD*	*VEA*	ED_I	ED_C
Fourier-Based Parameter	×	×	×	✓	✓	✓	×	×	×	×
Non-Stationary Signal Applicability	✓	✓	✓	×	×	×	✓	✓	✓	✓
Long Duration Signal Applicability	✓	✓	✓	✓	✓	✓	×	×	×	×
Suitability to Ambient Induced Excitation	✓	✓	✓	✓	✓	✓	×	×	×	×
Suitability to Vehicle Induced Excitation	✓	✓	✓	×	×	×	✓	✓	✓	✓

3.2 Damage localization methodology

In addition to the use of MSD for damage detection purposes under ambient excitation conditions, the present study also assesses the change in vibration parameters in a spatial context. This is achieved by assessing changes in the distribution of the vibration parameters from each sensor location through time. Vibration parameters are obtained in discretized windowed datasets of 30 min duration with 10 min overlap, to which a suitable distribution is fitted. For energy-based parameters, such as *CAV*, their value can never be less than zero and have no theoretical maximum, as such, their distribution fit can be taken as Log-Normal. For parameters that include a frequency-based component, their values can be considered to be centered about a specific mean value, as such, their distribution fit can be taken as Gaussian/Normal.

To measure the degree of variation through time of the windowed distributions, symbolic data objects are used. Symbolic data objects are representative values of a larger data set that can be used in an SHM context, as demonstrated in [8]. In the present study, the overlapping Normal and Log-Normal distributions of the vibration parameters are reduced to their symbolic data objects of Median and Interquartile Range for Normal distributions and Interquartile Values (0.25 and 0.75) for Log-Normal distributions. Using these symbolic objects as a two-dimensional damage feature vector, changes to the overlapping windowed distributions through time can be calculated using pairwise Euclidean distance.

4 TEST DATA

The present section gives explicate information regarding the data collection methodology, structural testing regimes, and collected output data.

4.1 S101 bridge – ambient excitation

The S101 Bridge was a pre-stressed 3-span flyover near Vienna, Austria that had a main span of 32 m and two 12 m side spans. The deck cross-section was 7.2 m wide double-webbed t-beam, whose webs had a width of 0.6 m. The height of the beam varied from 0.9 m in the mid-span to 1.7 m over the piers. In 2008, it was decided to replace the S101 Bridge due to insufficient carrying capacity and deteriorating structural condition being identified from visual inspection data. A progressive damage test was conducted on the S101 bridge across 3 days in 2008 through the completion of a number of sequential damage actions, which are presented in Table 2. During the test the bridge was closed to traffic, meaning that excitation was mainly ambient, although one traffic lane beneath the bridge was kept in use throughout the test which resulted in vibrations being transmitted through the foundations. Additionally, construction work was also in progress nearby that used heavy machinery and affected the vibratory response of the bridge at times, particularly during the cutting of the first pre-stressed tendon when it was noted that a vibrating impact roller was in operation close by. These additional sources of excitation add a level of uncertainty to the vibration data as no specific information on traffic volume was recorded. As for environment sources of excitation, very little temperature variation was observed throughout the test duration as sub-zero temperatures were kept within a 3 to 4-degree range due to persistent heavy cloud cover [9]. After the pier settlement phase was halted, the pier was hydraulically lifted back to its original position and compensation plates were inserted. Vibration data were recorded by 13 tri-axial accelerometers, with a sample rate of 500 Hz, spaced out along on the West side of the bridge deck. Vibration recordings from the sensors did not cease throughout the progressive damage test.

4.2 Steel truss bridge - vehicle-induced excitation

The second set of test data utilized within the present study is obtained from a progressive damage test conducted on a Japanese bridge that was subjected to a moving vehicle excitation [10]. The bridge in question was a simply-supported steel truss bridge that spanned 59.2 m with a width of 3.6 m and a max height of 8 m. It was scheduled to be replaced in 2012, before which a progressive damage test was carried out while the bridge was closed to the public. Damage induced to the bridge structure consisted of the severing and partial severing of vertical members of the main truss structure. In all, three damage scenarios were competed with a recovery action also carried out in between. The progression of the damage states is detailed in Table 3. The dynamic behavioral response was recorded from 8 uniaxial accelerometers with sample rates of 200 Hz. For each damage scenario, a 21 kN double-axle vehicle was driven across the bridge three times at approximately 40 km/h to induce excitation. Note that no vehicle dynamics were obtained; however, the dynamic response of the bridge has been assessed in detail by Kim et al [10], who identified the first five modes of vibration for each damage scenario, which are utilized at the end of the present study as a comparison of damage identification performance for the vibration parameters assessed herein.

Table 2. Damage actions conducted on the S101 bridge.

State	Start Time	End Time	Description of Damage Actions
1	10.12.2008 05:16 pm	11.12.2008 07:13 am	Undamaged
2	11.12.2008 07:13 am	11.12.2008 10:21 am	North-Western (NW) column cut through
3	11.12.2008 10:21 am	11.12.2008 11:49 am	First pier lowering step of 1 cm (1 cm total)
4	11.12.2008 11:49 am	11.12.2008 01:39 pm	Second pier lowering step of 1 cm (2 cm total)
5	11.12.2008 01:39 pm	11.12.2008 02:45 pm	Third pier lowering step of 0.7 cm (2.7 cm)
6	11.12.2008 02:45 pm	12.12.2008 01:12 pm	Compensating plates inserted and pier returned to original position
7	12.12.2008 01:12 pm	12.12.2008 03:03 pm	First pre-stressed tendon cut over NW pier
8	12.12.2008 03:03 pm	13.12.2008 05:44 am	Second pre-stressed tendon cut over NW pier
9	13.12.2008 05:44 am	13.12.2008 10:08 am	Third pre-stressed tendon cut over NW pier
10	13.12.2008 10:08 am	13.12.2008 11:14 am	Forth pre-stressed tendon cut over NW pier

Table 3. Damage actions conducted on the steel bridge.

Damage State	Description of Damage Actions
INT	Undamaged
DMG1	Half cut in vertical member at mid-span
DMG2	Full cut in vertical member at mid-span
RCV	Mid-span member reconnected
DMG3	Full cut in vertical member at 5/8th span

5 RESULTS AND CONCLUSIONS

5.1 Detection of S101 bridge under ambient excitation

CAV and *IA* have detected the cutting of the pier with ease and showed signs of step changes at each pier lowering stage, however as the pier is repositioned, only *IA* seems to mirror that behavior by veering back towards and below the damage threshold line, whereas *CAV* stays entirely above the damage threshold. Both parameters have depicted a slight upturn as the third pre-stressed tendon is severed, however, the change in trend is slight, save for a few data points that briefly shot over the threshold. The latter appears to be an anomaly caused by external sources of vibration, rather than a sudden and temporary change in structural behavior. As *PD* is calculated using *IA* as a numerator before dividing it by the number of zero crossing per unit of time, it is to be expected that they should share a similar pattern. However, it seems that *PD* provides greater detail of each stage of the damage test. The trend of *PD* during the pier settlement stages has been upward, save for the second lowing step which is depicted by a steep step change downwards. As the pier is repositioned to its original position, *PD* has failed to signify an improvement in structural condition, however, after the second pre-stressed tendon is cut there has been a trend downwards below the damage threshold line. Overall, *MCVI* has produced similar results to *PD* but in a more compact manner, which is positive as it indicates a low standard deviation. Figure 3 depicts the damage detection results of *DVI*, which provides a compact scatter of data points through time. Not much variation is seen between each pier lowing stage, however, the moment at which the pier is returned to its original position has been clearly captured, although the data points do not fully return under the threshold line, as expected. Thereafter, the *DVI* values remain quite stationary, even throughout the night, until soon after the third tendon is severed, at which point an increase in damage is exhibited.

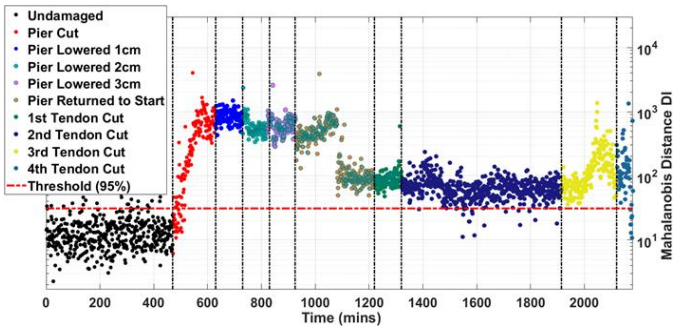

Figure 3. Mahalanobis squared-distance using *DVI*.

To advance the assessment with the parameters *DVI* and *MCVI* further, cross power spectral densities have been employed. As both *DVI* and *MCVI* utilize Fourier based parameters in their derivation, this can be replaced by a cross power spectrum instead. The rationale to this is that the cross power spectrum provides a Fourier Transform of the cross-correlation function of the power shared at each frequency between two signals. Therefore, with the use of a reference sensor, a more comparative representation of change can be obtained. When damage is introduced at a specific location, then the cross-correlation of frequency power will change for that location compared to the reference sensor and should be detectable with Mahalanobis Squared-Distance. In the case of *DVI* obtained from cross power spectral densities (Figure 4), a significant improvement has been achieved, whereby after the pier is repositioned the data points return below the damage threshold entirely, which is what is expected given that the bridge is pre-stressed.

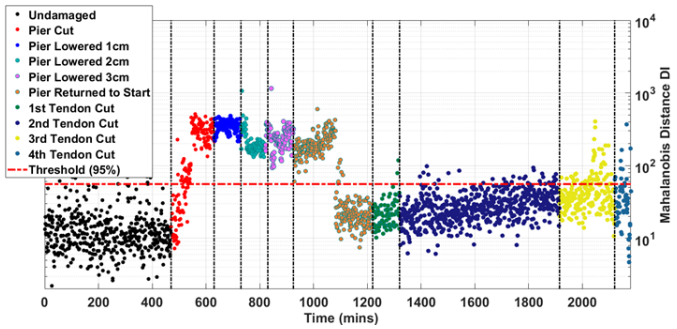

Figure 4. Mahalanobis Squared-Distance damage detection using *DVI* obtained from the cross-power spectrum.

Thereafter there is a slight upward trend, but not substantial enough to cross the threshold to a large extent until after the

third pre-stressed tendon is severed, although this occurs in a gentler manner than its original form in Figure 3. In summary, the parameter *DVI* obtained from the power-spectrum from the cross-correlation using an accelerometer as reference sensor has been the one performing better using ambient induced vibration.

5.2 *Localization of S101 bridge under ambient excitation*

The method described in Section 3.2 is applied for damage localization. From all vibration parameters examined, the best results correspond again to the *DVI*. In fact, Figure 5 presents the damage localization results of *DVI*, which provides a very clear location of damage at the North pier. The damage hotspot begins, like all others, at the moment of pier cutting, after which it increases in intensity after the third pier lowering step, before returning to an undamaged stage after pier repositioning. Significantly, the second damage hotspot occurs before the third pre-stressed tendon is cut and increases in intensity as the third and fourth tendon are severed, indicating that it is most likely caused as a result of damage.

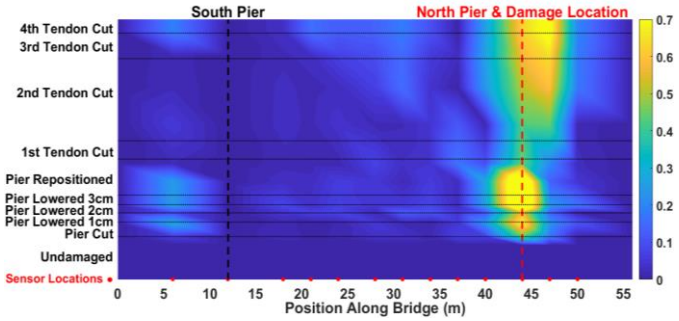

Figure 5. Evolution of *DVI* through time at each sensor.

5.3 *Damage identification methodology for steel truss bridge vehicle - induced excitation*

In this case, empirical vibration parameters labelled *CAV*, *CAD*, ED_I, ED_C and Instantaneous Vibration Intensity (*IVI*) have been assessed [11], and successfully identified the required damage events, with *CAD* providing the greatest resolution [12]. To evaluate the damage identification capability, the percentage variation observed at the damage location for condition states DMG2, RCV and DMG3 are given in Table 3 and can be compared against modal frequency changes in Table 4, as obtained by Kim et al [10]. From the comparison, all of the vibration parameters assessed appear to have outperformed the modal frequency changes, with *IVI*'s percentage differences producing the best overall. The study has demonstrated that *IVI* is suitable for quantifying the instantaneous outputs of the HHT and that it is an effective damage parameter for short non-stationary signals, provided that an appropriate method such as EMD (Empirical Model Decomposition) is used to decompose the signals initially and that only physically meaningful Intrinsic Mode Functions (IMFs) are chosen. Overall, the research has demonstrated that many of the novel empirical vibration parameters assessed are suitable for damage identification (detection, localization and quantification), provided that they are applied to a suitably applicable vibration signal type, as per the criteria set out in Table 1, and provided that a suitable outlier detection method is chosen based on the distribution type of the extracted vibration parameter. Further investigation is required in the case of vehicle induced excitation case to adjust for the variability of induced loads of each vehicle passage.

Table 3. Vibration parameter variation at damage locations.

Parameter	DMG2	RCV	DMG3
CAV	+9.1%	+0.1%	+19.8%
CAD	+10.2%	-0.1%	+22.2%
ED_I	+8.9%	+0.1%	+36.1%
ED_C	-0.4%	0.0%	+13.8%
IVI	+10.31%	-25.56%	+36.40%

Table 4. Modal frequency variation.

Mode	DMG2	RCV	DMG3
1st B. Mode	-2.67%	-0.13%	+0.31%
2nd B. Mode	+0.20%	-0.25%	-5.67%
3rd B. Mode	-0.21%	-0.87%	-9.05%
4th B. Mode	+0.22%	-0.72%	-6.87%
5th B. Mode	+0.58%	+0.19%	-0.16%

ACKNOWLEDGMENTS

This project has received funding from the European Union's Horizon 2020 research and innovation programme under the Marie Skłodowska-Curie grant agreement No. 642453.

REFERENCES

[1] American Society of Civil Engineers, ASCE, *2017 Infrastructure Report Card ASCE*, 2017.

[2] Casas, J.R. and Moughty, J.J. (2017), 'Bridge damage detection based on vibration data: past and new developments', *Frontiers in Built Environment*, https://doi.org/10.3389/fbuil.2017.00004.

[3] Moughty, J.J. and Casas, J.R. (2017),'A state of the art review of modal-based damage detection in bridges: Development, challenges, and solutions', *Applied Sciences*, 7, 510.

[4] A. Arias, *A measure of earthquake intensity*, R.J. Hansen, ed. Seismic Design for Nuclear Power Plants, MIT Press, Cambridge, Massachusetts, 438-483, 1970.

[5] Araya, R. and Saragoni, R. (1984), 'Earthquake accelerogram destructiveness potential factor', *Proceedings of the 8th World Conference of Earthquake Engineering*, San Francisco, US, 2, 835-841.

[6] Rathje, E.M., Faraj, F.S. and Russell, J.D. (2004), 'Empirical relationships for frequency content parameters of earthquake ground motions,' *Earthquake Spectral*, 20(1), 119-144.

[7] Rousseeuw, P.J. and Van Driessen, K. (1999), 'A fast algorithm for the minimum covariance determinant estimator', *Technometrics* 41(3), 212-223.

[8] Santos, J.P., Orcesi, A.D., Cremona, C. and Silverira, P. (2013), 'Baseline-free real-time assessment of structural changes', *Structure and Infrastructure Engineering*, 11(2), 145-161.

[9] Vienna Consulting Engineers (VCE), *Progressive Damage Test S101 Flyover Reibersdorf*, Report No. 08/2308. Vienna, Austria, 2009.

[10] Kim, C.W., Kitauchi, S. and Sugiura, K. (2013), 'Damage detection of a steel bridge through on-site moving vehicle experiments', *Proceedings of 2nd International Conference on Smart Monitoring, Assessment and Rehabilitation of Civil Structures (SMAR2013)*, Istanbul, Turkey.

[11] Moughty, J.J., and Casas, J.R. (2018), 'Damage identification of bridge structures using the Hilbert-Huang transform', *Proceedings of the 6th International Symposium on Life-Cycle Civil Engineering (IALCCE 2018)*, Ghent, Belgium.

[12] Moughty, J.J. and Casas, J.R. (2018), 'Noninvasive empirical methods of damage identification of bridge structures using vibration data', *Proceedings of the 6th International Symposium on Life-Cycle Civil Engineering (IALCCE 2018)*, Ghent, Belgium.

Chapter 5: Development of optical fibre distributed sensing for SHM of Bridges and large-scale structures

António Barrias[1], Joan R. Casas[1], Sergi Villalba[2]
[1]Department of Civil and Environmental Engineering, Technical University of Catalonia, c/ Jordi Girona 1-3, 08034 Barcelona, Spain
[2]COTCA SL, Barcelona, Spain
email: antonio.jose.de.sousa@upc.edu, joan.ramon.casas@upc.edu, sergi.villalba@cotca.com

ABSTRACT: This project investigates the performance of Distributed Optical Fibre Sensors (DOFS), more specifically the case of the Optical Backscattered Reflectometry (OBR) based system for the Structural Health Monitoring (SHM) of bridges and large-scale structures. This technology has demonstrated promising results for monitoring applications in a wide range of fields but due to its novelty, still presents several uncertainties which prevent its use more systematically and efficiently in civil engineering infrastructures. This is particularly true for the application of this sensing technique to concrete structures due to their long-term deployment and exposure to extreme weather. Therefore, different laboratory experiments are devised where multiple aspects of the instrumentation of DOFS technology in civil engineering applications are assessed and scrutinized. This includes new implementation methods, and comparison and performance analysis of different bonding adhesives and their spatial resolution. The long-term performance of this sensing technology is also evaluated. Furthermore, the OBR system technology is applied to two real-world structures in Barcelona, Spain, where new imperative conditions, such as the long-term effect of temperature variation and its compensation, are addressed. Differing conclusions are drawn related to the capabilities and limitations of this optical sensing system in concrete structures.

KEY WORDS: Distributed Optical Fibre Sensors (DOFS); Structural Health Monitoring (SHM); Concrete; Bridges; Monitoring.

1 INTRODUCTION

Civil engineering infrastructures are subjected to degradation due to the passage of time in addition to a significant number of various external adverse actions, which compromise their structural integrity, and consequently the safety of its users. As of 2016, in the United States alone, 39% of the bridges in that National Bridge Inventory were built over more than 50 years ago, and 9.1% of the total number of bridges were deemed structurally deficient despite 188 million daily trips across these bridges. The most recent estimate of the backlog of rehabilitation for these infrastructures is at $123 billion [1]. Consequently, the development of measures that extend the lifetime period of civil engineering infrastructures is of great importance. In this way, assessment and maintenance strategies that can target and identify those structures in most needs of attention are highly in demand. In this context, the field of SHM has been widely studied and advanced for the past few decades. Nonetheless, SHM has not yet been implemented on a large scale and in a regular manner on civil engineering structures. One of the reasons being that there is still a deficit of reliable and affordable generic monitoring solutions [2].

The most common SHM systems have been based until now on traditional electric based strain sensors, accelerometers, and inclinometers among others, which present different challenges when applied in real-world conditions [3]. On the other hand, Optical Fibre Sensors (OFS), when compared with the conventionally used electrical sensors, provide the enhanced advantages of being immune to electromagnetic interference, withstanding a wide range of temperature variations, chemically inert and also being small and lightweight which facilitates its handling and transport [4]. It is in this way that these types of sensors have become one of the most popular research topics looking at its use in SHM practices. Furthermore, this technology has been mostly applied through the use of Fibre Bragg Gratting (FBG) sensors [5], which are point sensors.

However, in the case of large-scale infrastructures, the number of point sensors necessary to obtain a complete and global strain monitoring, becomes impractically high. Additionally, for the specific case of concrete structures, where beforehand, it is practically impossible to know with certainty the exact location of possible crack formations, these point sensors present severe limitations. Also, in practical terms, a large number of sensors present the difficulty of requiring an associated large number of connecting cables making all the monitoring system more complex. In this regard, DOFS provide unique advantages allowing the strain and temperature monitoring of virtually every cross-section of the element where it is attached to, while requiring the use of just one single sensor and with it one connecting cable.

2 DISTRIBUTED OPTICAL FIBRE SENSORS

Due to the novelty of this technology, the use of DOFS in SHM of civil engineering infrastructures is still a relatively recent practice. These sensors share the same advantages of the other OFS, but as mentioned before, present the unique privilege of enabling the monitoring over greater length extents of the infrastructure and with a very short distance between each measuring point, in the order of millimetres.

These sensors can be bonded or embedded to the structure to be monitored, and when temperature or strain variations occur, these changes are going to be transmitted from the material to the sensor, which then generates a deviation of the scattered

signal, which is being reflected within the fibre cable core. This is the phenomenon behind the distributed optical fibre sensing as defined by the interaction between the emitted light and the physical optical medium. Three different scattering processes occur, which are the Raman, Brillouin and Rayleigh scattering [6]. The research conducted within this project is focused on the capabilities and potential of this last scattering technique, more specifically in the form of the Optical Backscatter Reflectometry (OBR) since it provides an unprecedented spatial resolution (up to 1 mm) which makes it suitable for crack detection and localization in concrete structures.

3 LABORATORY EXPERIMENTS

After performing an initial literature review on the use of this technology in civil engineering infrastructures [6], an experimental design is undertaken. Currently, one of the major concerns related to the use of this technology is the strain transfer effectiveness between sensor and substrate material. Moreover, when the sensors are bonded on the surface, the challenge presented by the case of concrete structures due to the roughness and heterogeneity of its surface needs to be considered. Hence, the study and identification of the optimal bonding adhesive and alternative installation methods for these applications become essential for more widespread use of this technology in current and future concrete structures. Additionally, there is insufficient information regarding the long-term performance of these types of sensors in fatigue loading scenarios. For this reason, a set of laboratory experiments is devised to investigate these topics.

3.1 Performance assessment of embedded DOFS

As mentioned before, one of the key challenges on the use of DOFS in reinforced concrete structures is related to the compromise between the required accuracy and mechanical protection of the sensor [7]. Therefore, it is decided to perform an experimental test with the main goal of assessing the performance and feasibility of deploying a thin polyimide coated low bend loss fibre in the rebar of RC members without previous mechanization. This setup is meant to provide better protection from the external environmental conditions to the fibre sensor without the need of a special thick coating, while assuring an enhanced stress-transfer between the monitored material and the sensor.

As a result, after assessing the feasibility of the direct deployment of the DOFS sensor without previous mechanization of the rebar, through a tensile test, two single reinforced concrete beam specimens [100x180x800 mm] are instrumented with a 5.2 m length DOFS and then tested. The DOFS are bonded in each sample, initially to the rebar and, after hardening of the concrete, to the external surface,). The bonded segments are positioned in such a manner that strains are measured at the rebar and at multiple locations of the concrete surface (both in compression and tension) simultaneously. A single fibre is used. The main difference between the two RC beams is the bonding adhesive used for the instrumentation of the DOFS to the rebar, being cyanoacrylate in Beam 1 and a two-component epoxy in Beam 2. Figure 1 shows that the DOFS perform very satisfactorily in all segments until the occurrence of cracking.

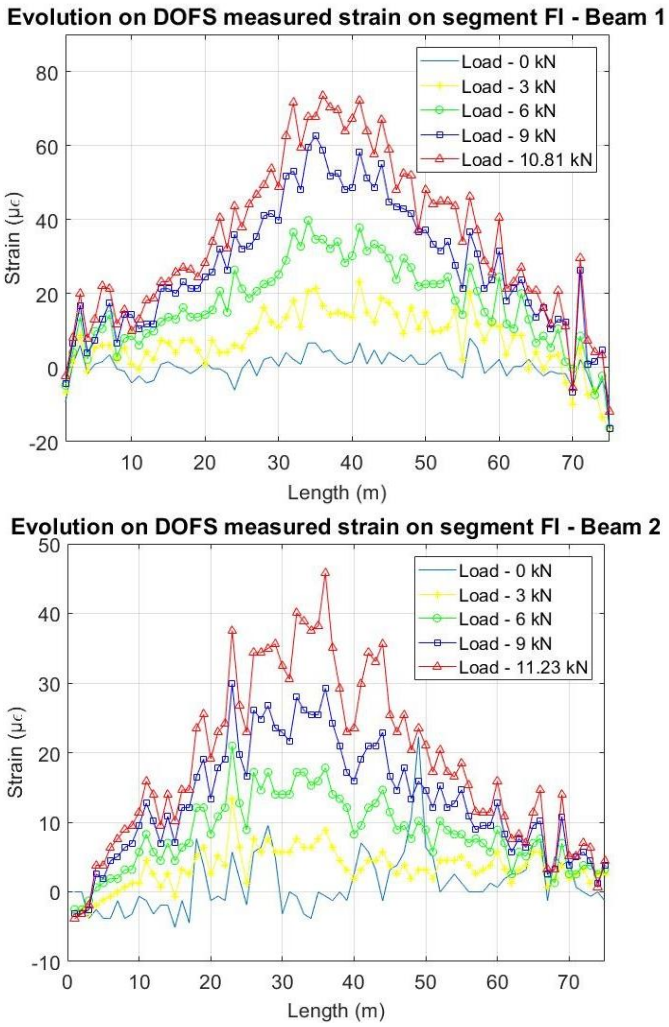

Figure 1. Strains measured by DOFS on the embedded segment (FI) of each instrumented beam.

In both beams, sometime after the occurrence of damage, the DOFS measurements start alternating huge positive and negative peaks at the crack location. In order to deal with the latter, it is proposed to perform a post-processing routine, where the inaccurate measurements are removed being identified by their inherent Spectral Shift Quality (SSQ), followed by a surface interpolation of the remaining accurate values. After completing this process, a good agreement is observed for both beams when comparing the strain values after cracking with what was measured by the strain gauges and with what was visually observed directly on the beam specimens for the corresponding load level. Additionally, the superior performance of the cyanoacrylate adhesive bonded segment in the rebar of Beam 1 p compared with the epoxy bonded one in Beam 2 is demonstrated. It is concluded that good results can be obtained within the undamaged stage of the specimen and that the proposed installation method can effectively detect and locate the damage formation once it is produced. For the following stage, a post-processing technique is proposed to eliminate the identified inaccurate peak values, which are originated after crack formation. This experimental campaign shows the feasibility of deploying a single polyimide coated Rayleigh OFDR based DOFS, simultaneously to the rebar and

external surface of a reinforced concrete element, as fully explained in [8].

3.2 *DOFS spatial resolution and adhesives comparison analysis*

As mentioned before, in order to obtain the optimal strain transfer between the sensor and the monitored material, the topic of its deployment is of considerable importance. In addition to the removal of any grease or dust present in the surface of the host material and the smoothening of the surface, the decision on the adhesive to bond the optical fibre sensor to the surface must be assessed. To this end, a laboratory experiment is devised where a single 5.2 m polyimide DOFS is attached to the surface of a reinforced concrete beam using four different adhesives: epoxy, cyanoacrylate, polyester, and neutral cure silicone and tested under a three-point load test. These adhesives are chosen based on previous experience of the research group and the available literature on the topic. The DOFS are bonded to the concrete performing a pattern with four equal segments (each one bonded with aforementioned selected adhesives) on the bottom surface of the beam as per Figure 2, with the objective of inducing the same strain levels, allowing a direct comparison between them. Additionally, the influence of different spatial resolution inputs on the used DOFS system is assessed, given that an increased detail provided by an enhanced spatial resolution would be of interest, mainly for the case of sub-mm crack detection.

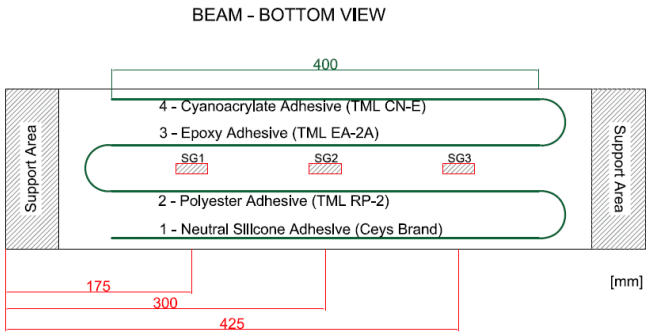

Figure 2. Instrumented sensors at the tested concrete beam.

3.2.1 *Spatial resolution comparison*

To perform the analysis of the influence of different spatial resolutions, three separate, but identical, load cycles are conducted with different spatial resolution under a maximum applied a load of 11 kN and therefore, without inducing cracking. Three spatial resolutions are tested: 1 cm, 3 cm and 1 mm, thus representing 520, 174 and 5191 measuring points respectively. The obtained results are depicted in Figure 3. It is observed how the data collected with a 1 mm spatial resolution present a significantly higher spatial variability when compared with the other two. Table 4 gives the nominal difference between these sets the values.

Although the differences in mean value (μ) are very close to zero, the calculated standard deviations (σ) are very different between the analyzed sets. Moreover, even after applying a moving average filter to the initially measured data collected with the 1 mm, relatively erratic measurements remain when compared with the other data sets. Therefore, the researchers conclude that no real advantages are accomplished by using a sub-cm spatial resolution, being the use of 1 cm spatial resolution preferred when using this type of experimental setup.

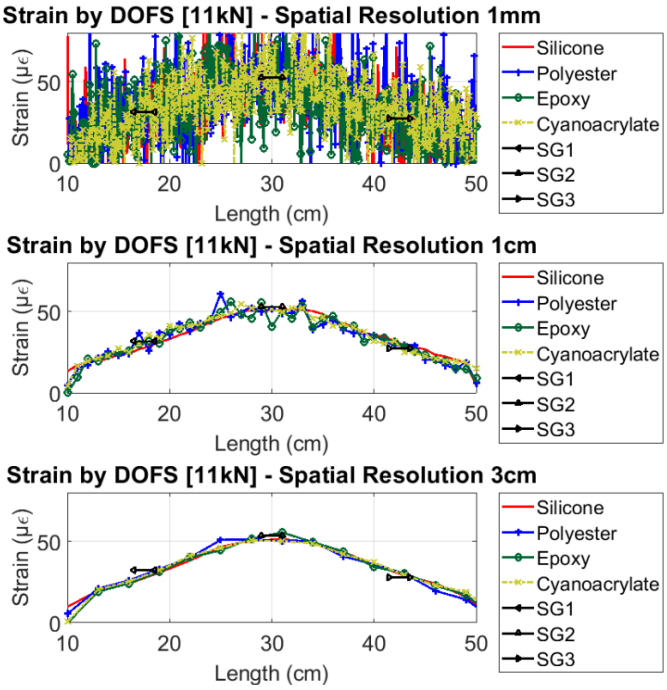

Figure 3. Strain measured for a load of 11 kN using different spatial resolutions.

Table 4. Comparison of spatial resolution sets difference [All units represent microstrain (με)].

Spatial Resolution	Δ(1mm-3cm)		Δ(1mm-1cm)		Δ(1cm-3cm)	
Statistical Property	Mean (μ)	std (σ)	Mean (μ)	std (σ)	Mean (μ)	std (σ)
Average DOFS segments	-1.07	19.19	-1.23	19.34	0.29	3.38

3.2.2 *Different bonding adhesives comparison*

The performance of the different used bonding adhesives is assessed using the same load cycles as in the previous study of the spatial resolution influence (i.e., without inducing cracking). Figure 4 confirms that all bonded segments are able to follow the applied load correctly and present a good agreement with the data from the strain gauges. In fact, at the beam mid-span, where higher strain levels are produced, the higher difference between DOFS bonded segments and the strain gauge at that location is of 5.54 με, while all others are close or below 2 με, which corresponds to the strain resolution provided by the used DOFS interrogator system. Additionally, when assessing the measured strain spatial variability achieved by each bonded segment throughout the applied load sequence, it is observed how the silicone bonded segment presents smoother and more homogenous readings. This is related to its inherently lower elasticity modulus, which allows for a fibre adjustment movement within the adhesive.

When analysing these adhesives for a load cycle where cracking was induced in the specimen and further loaded until rupture, it is verified that all four different bonded segments are able to effectively detect and locate the crack formation although with different performances. Whereas the polyester,

epoxy, and cyanoacrylate bonded segments present strain peaks with narrow bases at the location of the crack (around 2 cm), the silicone bonded segment, while also displaying a strain peak at the crack location, it has a broader base (about 20 cm). This issue turns the detection of further cracks formations within this area (20 cm) impractical when using this particular bonding adhesive.

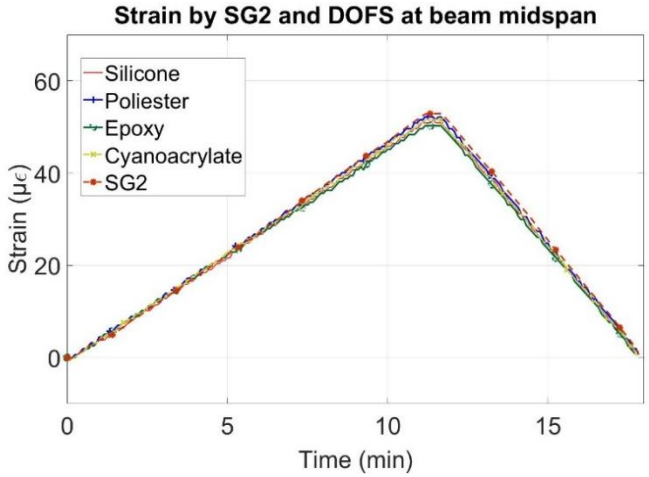

Figure 4. Measured strain at beam mid-span by different bonding adhesives DOFS segments and Strain Gauge 2 (SG2).

When continuing the assessment of how each segment performs after crack initiation, apart from the silicone bonded segment, all other adhesives present alternating positive and negative strain peaks at the crack locations, where only positive increasing strains corresponding to applied tension should be observed given that stresses in the bottom surface will be always tensile stresses. As in the previous experimental campaign, a post-processing routine is applied to remove unreliable values (i.e., the points where SSQ values are below the acceptable threshold of 0.15). Since negative values, which are not consistent with the expected tension being developed in the bottom surface of the concrete beam, still remain after this action, these values are also removed. In the end, a surface interpolation is performed replacing removed and inaccurate data points. With this operation, the silicone bonded segment presents the fewer identified inaccurate data points, leading therefore to fewer removed data from the original measurements. Nevertheless, the latter still presents a significantly wide area of influence for the developed crack, corresponding to almost 2/3 of the total length of the bonded segment. For the other segments, relatively more data were replaced, especially involving the removal of negative strain measurements. In conclusion, the neutral cure silicone can be a good option as a bonding adhesive for situations where the quantification of crack damage is not relevant or even where cracking is not foreseen as in prestressed concrete elements. Regarding the other adhesives, they can also be considered for the same situations as suggested for the silicone adhesive, although with a higher spatial variability and more susceptible to the differently sized aggregates in the concrete material.

3.3 Long-term performance of DOFS

The experiment described here is not a completely independent campaign from the one detailed in the previous section, as it is conducted in the same period and using a very similar setup. The primary objective is to assess the accuracy and reliability of DOFS measurements over time when monitoring structures over a long-term period when several load cycles are applied. This contribution will add to the literature on the performance of Rayleigh based OFDR DOFS under fatigue loading, which is currently reduced to a few publications. A laboratory experiment consisting of 2 million load cycles induced on two reinforced concrete beams (FA1 and FA2), instrumented with Rayleigh based DOFS as in Figure 2, is devised. The applied load cycles replicate expected real-world conditions for the case of a standard highway bridge. No other work is found on the application to concrete structures under fatigue testing with this type of DOFS setup. Two different load stages are considered for the stress range of the load cycles. The lower value of the stress range correspond to the actuation of the structures' self-weight and permanent loads, whereas the upper one correspond to the addition of the traffic load. The traffic load is represented by a 4-axle truck with a load of 120 kN by axle and multiplied by a dynamic factor of 1.3 as described in Fatigue Load Model 3 of EN 1991-2 [9].

The main difference between the test in each beam is that for beam FA1 the load is applied directly to the beam in an un-cracked condition, whereas for beam FA2, the beam is initially loaded statically until a 28 kN load (inducing in this way cracking), unloaded and then finally loaded with the same 2 million cycles as beam FA1. The goal is to assess the fatigue performance in both un-cracked and cracked concrete, simulating the cases where the DOFS will be bonded to prestressed (no cracking) or reinforced (cracking) concrete bridges. The measured strain by the different segments of the DOFS at the beam midspan over the applied number of load cycles for beam FA1 is depicted in Figure 5. The DOFS measurements follow the strain gauge with a good agreement along the number of cycles. In addition, it is important to point out that the applied load frequency was of 4 Hz, the sampling acquisition of the DOFS was of one measurement every five seconds (i.e., 0.2 Hz), and the readings from the strain gauges were collected at 1 Hz. This partly explains the difference between both sets of sensors, for a magnitude of the applied strain range of around 12 με.

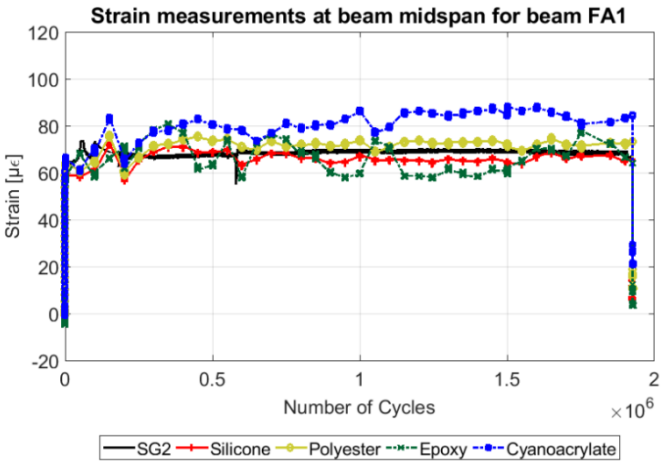

Figure 5. Strain measured at beam midspan for test in beam FA1.

In the case of beam FA2, the DOFS measurements present a good agreement with the strain gauge at the same location

(SG2) until cracking was initiated. After the cracking detection, all DOFS segments and strain gauges measurements follow with more or less agreement the applied load until the beginning of the 2 million load cycles application. Nonetheless, it is observed how after the post-cracking stage and unloading stage, the strain measurements slightly diverge between the different DOFS segments and the strain gauges, especially in the case of the silicone bonded segment. When assessing the measured strain during the 2 million load cycles, a reasonable agreement is again found with the data measured by the strain gauges. Summarizing, encouraging results on the use of this novel technology are obtained for long-term monitoring periods with fatigue-induced behaviour. The distributed optical fibre technology displays a good performance under fatigue loading for both the un-cracked and cracked scenarios by comparison to strain gauges' measurements.

4 REAL WORLD APPLICATIONS

As a result of the internship at COTCA during the TRUSS training period, it becomes possible to assess and interpret the results of the application of this novel technology to two real-world existing structures located in Barcelona, Spain. This is an excellent opportunity to evaluate the feasibility of implementing these sensors in real scenarios, which present different challenges in comparison to the case of laboratory experiments in controlled environments, as fully documented in [7].

4.1 Sant Pau hospital

The first application of DOFS is conducted at the historical and UNESCO world heritage site Sant Pau Hospital, one of the most superb examples of the Catalan architectural modernism movement. In one of the buildings, some dangerous cracks appeared in brick masonry columns on one of its floors. Therefore, after a structural assessment, it was decided to replace two of those columns by new structural elements made of steel. This procedure implied the installation of a temporary bearing steel structure around the columns to support the load while the masonry element was cut, removed and substituted by the new steel profile columns. Afterwards, the load was transferred from the temporary bearing structure to the new columns. Moreover, the floor above these elements was being used to treat and accommodate recovery drug patients and their relocation was not possible. As a consequence, it was necessary to perform the replacement of the fault columns while the building was in regular functioning service. For this reason, a structural monitoring scheme was necessary in order to ensure that no harm was being inflicted in the building occupants due to the conducted restoration works.

Consequently, a 50 m long DOFS is deployed in the upper masonry vaults ceiling, which using a spatial resolution of 1 cm, allowed for the monitoring of 5000 different points. The use of DOFS here, being able to monitor such a large area using just one sensor, clearly constitutes a more cost-effective solution than a traditional set-up based on a large number of point sensors. The monitoring procedure is conducted over 18 days. Hence, it is possible to conclude that the replacing operation caused an increment (in compression) of the strain in the vault in the order of 80 με, which was almost uniform along the whole roof. During the entire duration of the rehabilitation works, the structural response is under the serviceability and ultimate limit states, given that the strain increment generated minimal stresses of 0.14 MPa compared to the characteristic compressive strength of 3 MPa of the material. Moreover, there are not new formation of cracks detected. The implementation of DOFS technology in this historic structure shows that it is possible to monitor the strains developed as a result of rehabilitation works and the structural safety while maintaining the building in operation as required by the owner.

4.2 Sarajevo bridge

The second application of DOFS takes place at the Sarajevo Bridge, shown in Figure 6. This is a structure located over one of the main roadway entrances of the city of Barcelona, Spain with high traffic flow during peak hours. It is a two-span bridge with span lengths of 36 and 50 m and where each span is built up by three box-girder prestressed concrete beams connected by an upper reinforced concrete slab.

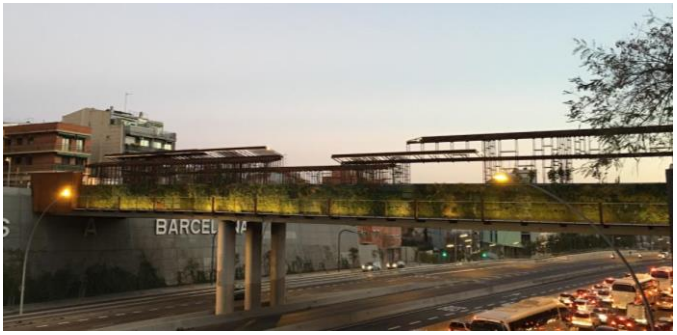

Figure 6. Sarajevo bridge after the rehabilitation works.

This structure was subjected to rehabilitation works to enlarge the existing deck while introducing new steel elements to increase pedestrian traffic and improve its aesthetics. Due to the high traffic volume in the bridge and the underneath lanes, it was not possible to close the bridge to traffic or place temporary support beneath the rehabilitated structure. As in the previous real-world case, it was compulsory to perform the required rehabilitation works while maintaining the structure in its normal service operation without the possibility of adding temporary support. Given the strategic importance of this structure to the city's road network, it was paramount to perform close monitoring follow up of the induced stresses during and after the execution of the works.

The adopted solution consists of a pair of 50 m length DOFS (DOFS 1 and DOFS 2) placed in the internal bottom surface of the box-girder beam, that is most susceptible to a significant load increment in the 36 m length span. The monitoring period in this application was between June of 2015 and February of 2016 (8 months). The DOFS measurements are conducted in chosen days throughout this period, being the maximum and minimum measured values in each of those dates used to generate envelope response graphs. One important aspect of this application is that, due to the vast duration of the monitoring period, the influence of temperature on the readings needs to be considered. Both the refractive index of the backscattered light and the materials which compose the DOFS are dependent on these temperature changes, so a correction of this thermal-induced error on the monitoring output is required. Using the data from 14 m of the DOFS, which are not bonded to the structure, it is possible to perform the thermal

compensation. It is noticed that the main responsible for the strain variation measured in the structure is the decrease of temperature between summer and winter, which is translated into an uniform shortage of the box-girder. Moreover, these stress variations do not induce changes in the bridge behaviour, given that they are acceptable for these types of structures and increase the compression state of the concrete in a limited and permissible amount.

5 CONCLUSIONS

This research has investigated the use of the promising novel technology of DOFS in SHM applications of bridges and large-scale structures. Different experiments and analysis have been conducted within the TRUSS project in order to provide more relevant results and conclusions as guidelines for its future use in SHM of concrete structures. In summary, the following contributions have been achieved:

- A novel implementation technique of the fibre to a reinforced concrete member has been proposed and positively tested.
- Different bonding adhesives for deployment in concrete members have been performed and assessed.
- A study of the influence of the spatial resolution in DOFS measurements have been conducted, being 1 cm spatial resolution the most convenient one.
- The performance of DOFS when applied to RC members under a high number of load cycles has been evaluated in order to replicate the long-term reliability of this technology when applied to a standard bridge structure.
- The deployment of this technology in two real-world structures in Barcelona where new imperative conditions, such as the long-term effect of temperature variation and its compensation, have been addressed.

ACKNOWLEDGMENTS

This project has received funding from the European Union's Horizon 2020 research and innovation programme under the Marie Skłodowska-Curie grant agreement No. 642453.

REFERENCES

[1] American Society of Civil Engineers (ASCE), *2017 Infrastructure Report Card ASCE*, 2017.
[2] Glisic, B., Hubbell, D., Sigurdardottir, D.H. and Yao, Y. (2013), 'Damage detection and characterization using long-gauge and distributed fiber optic sensors', *Optical Engineering*, 52, p. 87101.
[3] Kudva, J.N., Marantidis, C., Gentry, J.D. and Blazic, E. (1993), 'Smart structures concepts for aircraft structural health monitoring', P*roceedings of the 1993 North American Conference on Smart Structures and Materials*, 964–971.
[4] Casas, J.R. and Cruz, P.J.S. (2003), 'Fiber Optic Sensors for Bridge Monitoring', *Journal of Bridge Engineering*, 8(6), 362-373.
[5] Ferdinand, P. (2014), 'The evolution of optical fiber sensors technologies during the 35 last years and their applications in structure health monitoring', *Proceedings of the 7th European Workshop on Structural Health Monitoring (EWSHM)*, Nantes, France.
[6] Barrias, A., Casas, J.R. and Villalba S. (2016), 'A review of distributed optical fiber sensors for civil engineering applications', *Sensors*, 16(5), p. 748, May.
[7] Barrias, A., Rodriguez, G., Casas, J.R. and Villalba, S. (2018), 'Application of distributed optical fiber sensors for the health monitoring of two real structures in Barcelona', *Structure and Infrastructure Engineering*, 14(7), 967-985.
[8] Barrias, A., Casas, J.R. and Villalba, S. (2018), 'Embedded distributed optical fiber sensors in reinforced concrete structures - A case study', *Sensors*, 18(4), 980.
[9] European Committee For Standardization (CEN), *EN 1991-2: Eurocode 1: Actions on structures - Part 2: Traffic loads on bridges*, 2002.

Chapter 6: Bridge damage localisation using displacement and velocity measurements

Daniel Martinez[1], Eugene OBrien[1]
[1]School of Civil Engineering, University College Dublin, Dublin 4, Ireland
email: daniel.martinez-otero@ucdconnect.ie, eugene.obrien@ucd.ie

ABSTRACT: This project considers two different strategies for bridge damage detection and localization using indirect deflection and velocity measurements by an instrumented vehicle, and direct deflection measurements on the bridge. First, curvature - the second spatial derivative of deflection - is proposed as an indicator of damage. The rate of the curvature is also considered as this can be measured using Laser Doppler Vibrometers (LDVs). Curvature is proportional to the reciprocal of the flexural stiffness of the bridge cross-section. Consequently, a sharp increase in bridge curvature results from a local loss of stiffness and indicates damage of the type associated with a bridge strike. The second strategy employs bridge deflection for the direct calculation of the bridge stiffness profile using the theorem of virtual work. As deflection can be calculated for a bridge with a known stiffness profile, back-calculation of the stiffness can be formulated as an inverse problem.

As part of the first strategy, it is proposed here to measure curvature using sensors in a passing vehicle over a bridge (drive-by bridge monitoring). Instantaneous Curvature (*IC*) is investigated as a means of finding a local loss of stiffness in a bridge using drive-by measurements. Absolute displacements of the bridge cannot be directly measured from the vehicle. However, it is assumed that relative displacements between vehicle and bridge can be measured. It is shown that a sharp increase occurs at the damage locations. Vehicle-bridge interaction is modelled using the Finite Element (FE) method. Road profile and white noise are considered as the main sources of inaccuracy. The use of LDV measurements taken from a specialist vehicle is proposed as an alternative for the first strategy. The use of LDVs is inspired by the Traffic Speed Deflectometer (TSD), a truck instrumented with several LDVs which is used for road pavement monitoring. In this project, the concept of using a TSD is explored for bridge damage detection. It is assumed that relative velocities between bridge and vehicle can be directly obtained from the LDVs. The Rate of Instantaneous Curvature (*RIC*), which is the first derivative of *IC* respect to time, is introduced as a bridge damage indicator. RIC could be obtained using simulated relative velocity measurements. A TSD is modelled as a half-car using the FE method. Provided measurements are sufficiently accurate, bridge damage is detectable by comparing the RIC measurements from healthy and damaged bridges. Moving Average Difference (*MAD*) is introduced based on *RIC* to make the method robust when noise is included in the measurements. It is shown that, in simulations, the damage location can be detected using the *MAD* in the presence of noise.

A novel method is proposed for the direct calculation of bridge stiffness from deflection measurements as part of the second strategy. The relation between bridge deflection and stiffness is well known from the theorem of virtual work. Hence the bridge stiffness profile, represented as a vector of point stiffnesses, can be theoretically obtained by solving an inverse problem using drive-by measurements of deflection. However, the inverse problem is ill-conditioned which means that the final solution is profoundly affected by noise. Therefore, a filtering method based on the Blackman window is employed to solve the ill-conditioning. A numerical case study is employed to evaluate the effectiveness of the approach using bridge deflections and measurements collected from simulated displacement transducers. It is also assumed that axle spacings of vehicles are provided. The approach provides an opportunity to use measurements from random traffic passing over a bridge. This has the considerable advantage that measurements can be repeated every time a vehicle crosses the bridge. Absolute deflection measurements at a fixed location (e.g., mid-span) are simulated, and the influence lines found from every (simulated) passing truck are converted into a stiffness profile. This technique provides constant monitoring of the bridge and cracks can be detected after the passage of a few vehicles.

KEY WORDS: Bridge damage detection; Structural Health Monitoring (SHM); Curvature; Instantaneous curvature; Rate of instantaneous curvature; Damage localisation; Traffic Speed Deflectometer (TSD); Stiffness; Drive-by monitoring.

1 INTRODUCTION

There is an increasing concern about bridge structural health monitoring methods to identify whether a bridge is in good condition. Highway bridges are particularly vulnerable due to the rising trend of heavy loads and traffic flow on the road networks [1-4]. In addition, aging and overloaded heavy trucks crossing bridges are a prevalent issue [5-9]. Solutions to these problems have been proposed, but the most popular involves visual inspection [10]. Among the inconveniences of this method, it can be identified the lack of accurate damage quantification and the infrequent surveys due to the high costs [11]. In consequence, different possibilities to sensor the bridge have been studied. The most popular alternative involves using direct instrumentation installing the sensors on the bridge [12]. Wu et al [13] install a long-gauge FBG (Fiber Bragg Grating)

sensor in Xinyi River Bridge in China to measure strain. Area values of strain histories are used to obtain damage location and extent. Whelan et al [14] measure strain and acceleration from accelerometers and strain transducers. Embedded software allows a wireless solution that facilitating large-scale structural monitoring.

Recently, indirect monitoring (or drive-by) is used as an alternative strategy in which the evaluation of bridge condition is performed from a moving vehicle [12,15]. Elhattab et al [16] conduct a numerical analysis using accelerations from an instrumented vehicle to calculate the bridge displacement profile. Damage location can be extracted from the apparent profile. Tan et al [17] adopt drive-by accelerations to implement a wavelet analysis. Drops in bridge frequency are obtained as damage increases.

One of the major objectives in bridge engineering is damage detection and location, commonly referred to as level 2 damage identification [18]. Much research has been done on this topic [11,18-22]. To obtain damage location, the curvature is a common parameter [23]. OBrien et al [24] perform a simulation of a passing vehicle measuring deflections. Curvature calculated from these deflections is used to locate damage. The TSD has been proposed as a suitable vehicle for bridge damage detection [11,25,26]. A TSD [27] is a specialized vehicle design for road pavement assessment. High axle weights are used to create a deflection basin. LDVs installed in the vehicle are used to measure relative velocities between the road pavement and the vehicle [28].

Bridge damage assessment by calculating the stiffness profile provides level 3 damage identification, focusing on damage extension and location [29]. One of the most popular methods is the use of Cross entropy (CE). An iterative procedure is involved in the use of CE in which random data are generated with the aim of improving the result at every iteration step [30]. Dowling et al [31] use CE to calibrate the stiffness and to reduce the error in the Moving Force Identification (MFI) problem. Gonzalez et al [32] estimate the stiffness profile of an experimental beam using CE. Unfortunately, the algorithm is susceptible to noise. An alternative to Cross-Entropy can be obtained in the Genetic Algorithm (GA). GA starts by usually assuming a random population and improved reproductive solutions from this initial population are obtained [33]. Chou and Ghaboussi [34] use the GA and the Implicit Redundant Representation (IRR) to detect damage extension and location.

This chapter covers two methods for bridge damage localisation based on curvature and a method for damage location and quantification. The first method proposes Instantaneous Curvature (*IC*) to locate damage assuming that relative deflections between road pavement and vehicle can be measured. The second method is based on the *IC*, but it is adapted to the TSD. Considering that relative velocities can be obtained from the TSD, Rate of Instantaneous Curvature (*RIC*) is proposed. *RIC* is the first derivative respect to time of *IC*. The simulations consider measurements obtained from LDVs as a real TSD would do.

The third method performs damage location and quantification by stiffness calculation. Stiffness profile is calculated by inverting the relationship between stiffness and deflection in the theorem of virtual work. The method uses a random population of trucks traversing the bridge. The analytical model considers three sensors that measure deflection at different locations on the bridge. The novelty of this work is that no Bridge Weigh-in-Motion system is used to measure the axle weights of the random population of trucks.

2 INSTANTANEOUS CURVATURE (IC) FOR BRIDGE DAMAGE DETECTION

2.1 Method explanation

Three measurements at different locations are needed for the calculation. A distance between sensors of $\Delta x = 1$ is considered to be a realistic approach. This distance is assumed to be constant for all the sensors. The curvature of a function is commonly defined as its second derivative. Consequently, curvature can calculated based on the central difference method given by Equation (1).

$$IC(x,t) = \frac{u(x-\Delta x,t)-u(x,t)+u(x+\Delta x,t)}{\Delta x^2} \quad (1)$$

where t is the time.

As *IC* is measured from a passing vehicle, time is related to the position by the speed $c = \frac{\Delta x}{\Delta t}$. However, normal curvature calculation is performed only at a particular time and *IC* is considering this with the use of the three sensors. Random noise is added to the model based on the maximum deflection of the bridge. Equation (2) defines the simulated noisy signal.

$$u_{noise}(x,t) = u(x,t) + E_P \times N_{noise} \times u_{max} \quad (2)$$

where u_{noise} represents the noisy signal, u_{max} is the maximum deflection of the bridge, $E_P$is the noise level (0 for 0% noise and 1 for 100% noise) and N_{noise} is a random vector with zero mean value and unit standard deviation. The noise of each of each sensor is considered to be independent, affecting the accuracy severely.

2.2 Results

As the vehicle travels, the deflection responses are measured by a sensor. Before and after the second axle, two sensors are used at distance x and 1 m (Δx). Figure 1 shows the results of *IC* obtained for a defined damage situation. Loss of stiffness at specific locations is the approach adopted to model damage here. It can be seen in Figure 1(a) that 20% loss of stiffness is difficult to be detected if the damage is close to the support and 1% noise is considered. At other damage locations and greater damage extents, *IC* is able to locate the damage. Figure 1(b) considers a 50% stiffness reduction for the same damage locations as in Figure 1(a). The results are improved by assuming that the specialised vehicle is going to cross the bridge ten times and calculating the average.

3 THE FEASIBILITY OF USING A TSD FOR BRIDGE DAMAGE DETECTION USING RIC

3.1 Method explanation

Although *IC* can locate damage, deflection is difficult to be measured from a vehicle. However, LDVs installed in the TSD are able to measure relative velocity between vehicle and bridge at different points. Relative velocity contains information of both vehicle and bridge components. Based on

IC, *RIC* is obtained using relative velocities instead of deflections.

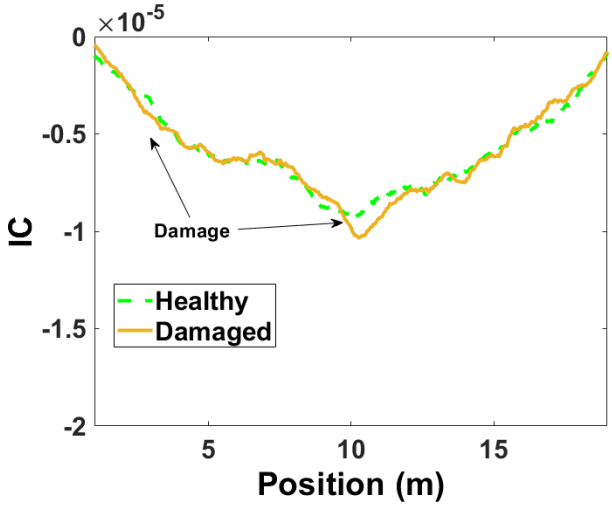

(a)

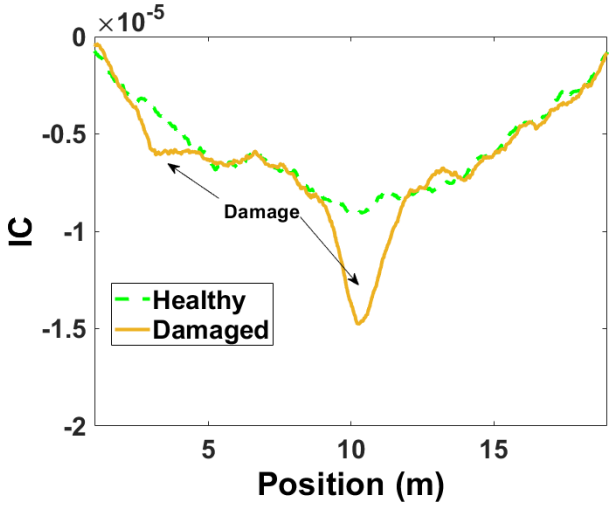

(b)

Figure 1. Damage localisation using *IC* for 1% noise and: (a) 20% loss of stiffness, (b) 50% loss of stiffness.

A crack model to simulate bridge damage is used based on the assumptions described by Sinha [35]. As for the *IC*, three LDVs are needed to calculate one *RIC*:

$$RIC(x,t) = \frac{\dot{q}(x-\Delta x,t)-2\dot{q}(x,t)+\dot{q}(x+\Delta x,t)}{\Delta x^2} \quad (3)$$

where $\dot{q}(x,t)$ is the relative velocity when the central laser vibrometer is located at a distance of x from the left end of the bridge. Six sensors are used, totalising four *RIC* calculations. These four *RIC*s are used to improve the accuracy of the measurements by calculating the mean RIC_{av}. A moving average filter is proposed as a damage indicator based on RIC_{av}. Measurements at healthy (RIC_{av}^{hea}) and damaged (RIC_{av}^{dam}) states are used to remove high-frequency effects to calculate Moving Average Difference (*MAD*):

$$MAD(x) = \frac{\frac{1}{z}\sum_{i=-\frac{z-1}{2}}^{i=\frac{z-1}{2}} RIC_{av}^{dam}(x+idx) - \frac{1}{Z}\sum_{i=-\frac{z-1}{2}}^{i=\frac{z-1}{2}} RIC_{av}^{hea}(x+idx)}{min(RIC_{av}^{hea})} \times 100\ (\%) \quad (4)$$

where z is the number of points used for the moving average, and dx is the sampling interval in space. $z = 51$ is considered to filter the RIC_{av}^{dam} and RIC_{av}^{hea}. This is equivalent to filtering over 1 m length of the bridge.

3.2 Results

In Figure 2, the *MAD* attenuates the fluctuations due to the phase shift. Noise is added to the model based on the ideal noise of the LDVs. 20% of the bridge depth crack (50% loss of stiffness) is used at every damage location. Figure 2 shows MAD calculated from noisy relative velocities. Damage locations are obtained for single and multiple damage situations. The crest of the function indicates the damage locations. Figure 2(b) shows that multiple damages are also located, but the second peak is lower compared to the first one.

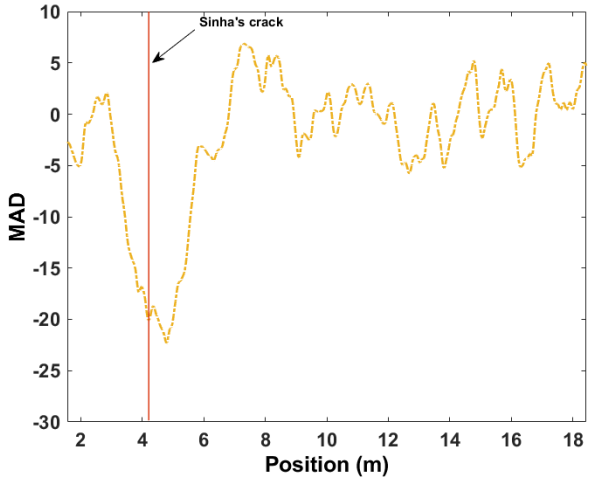

(a)

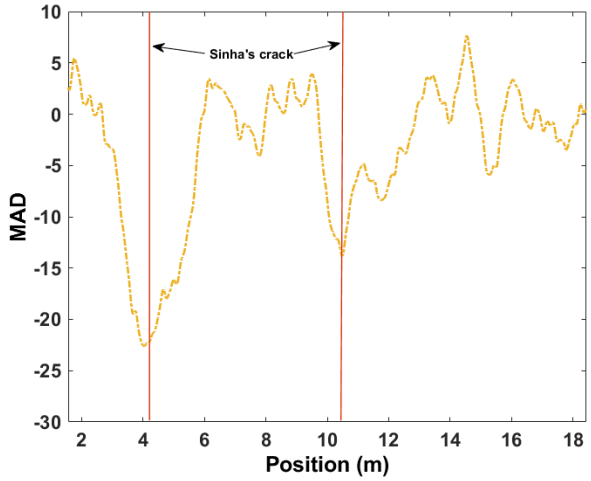

(b)

Figure 2. *MAD* for damage detection in the case of: (a) a single damage location, (b) two damage locations.

4 BRIDGE DAMAGE DETECTION USING RANDOM TRAFFIC

4.1 Method explanation

Deflection measurements are simulated at three different locations to calculate the stiffness (*EI*) profile of the bridge. A 3% noise normal distribution respect to the maximum deflection of the bridge is used. The relation between deflection and stiffness is set in the well-known theorem of virtual work.

In this theorem, a virtual unitary force is applied at the point in which the deflection is calculated. The theorem of virtual work can be expressed as a matrix product as shown by Equation (5):

$$\{\delta\}_{T\times 1} = [P]_{T\times N} \times \{J\}_{N\times 1} \quad (5)$$

where $\{\delta\}$ is a column vector representing the histogram of deflections measured by a sensor at every time step. $[P]$ is a matrix that contains the product of bending moments (real and virtual) in every element and at every time step. $\{J\}$ is a column vector equating the reciprocals of the stiffness at every analysed location. T and N represent the total number of time steps and the total number of analysed locations respectively. In pursuance of stiffness profile calculation, Equation (5) has to be inverted. As $[P]$ is not a squared matrix, a direct inversion cannot be done. For this reason, Moses algorithm [36] is adapted to this equation. Moses algorithm is used to minimise the objective function of the square of the differences between measured and theoretical deflections as per Equation (6).

$$E = min[(\{\delta\} - [P]\{J\})^2] \quad (6)$$

where E in the error that has to be minimised.

The minimum is calculated by deriving the squared of the differences. As a result, a squared matrix is obtained and Equation (5) is transformed into Equation (7):

$$\{\delta_M\}_{N\times 1} = [P_M]_{N\times N} \times \{J\}_{N\times 1} \quad (7)$$

where $\{\delta_M\}$ and $[P_M]$ represent the equivalent vector and matrix obtained using Moses algorithm.

Stiffness profile can be calculated by $[P_M]$ matrix inversion. However, this system of equations is ill-conditioned. It is well-known that adding a value to the main diagonal improves the condition of a matrix at the cost of obtaining a solution further from true solution [37]. In this project, a matrix based on the Blackman window is added to the original matrix instead of a simple diagonal matrix. The main advantage of using the Blackman window matrix is its ability to maintain the maximums and the minimums of the true solution. The algorithm can be split into two blocks, as shown in Figure 3.

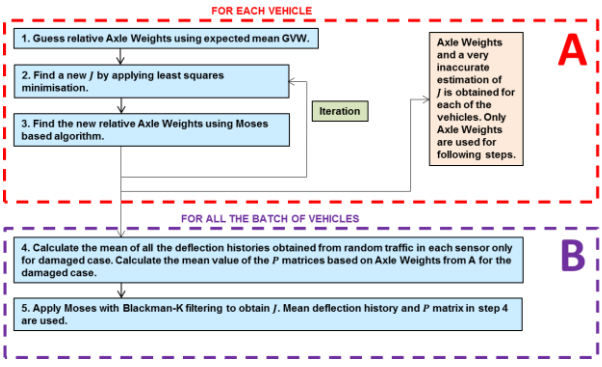

Figure 3. Flow chart of the algorithm for static deflections.

In Block A, an iteration-optimisation process is applied to obtain an estimation of the axle weights for each vehicle. The iteration-optimisation starts with a guess of the Gross Vehicle Weight (GVW) based on the average of the expected population of vehicles. The mean GVW used is 160 kN as a first guess. Two optimisation steps are used in the iteration process. The first step calculates the stiffness reciprocal values based on the axle weights prediction. These axle weights are used to calculate the bending moments created by the vehicle in the $[P]$ matrix of Equation (7). Conjugate gradients optimisation is used to obtain the solution from the least squares minimisation. Axle weights are calculated in the following step applying Moses algorithm. The optimised reciprocals of the stiffness of the previous step are used. The iteration-optimisation process is applied regardless of the deflections being dynamic or static.

The second part of the algorithm (Block B) uses the information of all the vehicles to calculate the stiffness profile. Ideally, when static deflections are measured, only one batch of vehicles is needed to assess the bridge (Figure 3). The histograms of deflections of all vehicles in each of the sensors are averaged. Consequently, the mean of all the $[P]$ matrices is calculated using the axle weights in Block A. This $[P]$ matrix is adapted to the mean deflection, and the $\{J\}$ vector in Equation (7) can be obtained by adding the Blackman matrix to improve the $[P]$ matrix condition.

Obtaining the stiffness profile from dynamic deflection also requires the use of a different batch of vehicles for a previous health state of the bridge (Figure 4). The use of the extra batch of vehicles allows the calculation of a deflection based on a prismatic vector. This assumption considers that, for the previous condition analysis of the bridge, the stiffness profile is constant at every analysed location. A deflection with no dynamic influence is obtained, allowing more accurate estimation of the mean deflection history. To calculate the deflection caused by the damage, the difference between the two first mean deflections is calculated. The subtraction removes most of the dynamics caused by the velocity of the random traffic population.

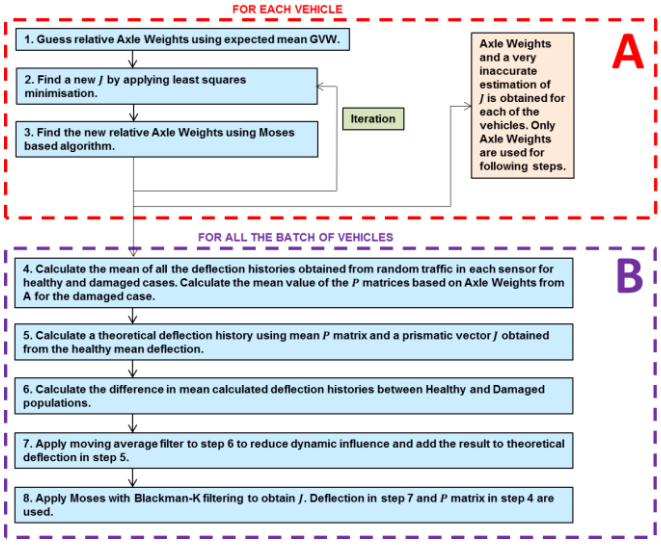

Figure 4. Flow chart of the algorithm for dynamic deflections. Steps 5-7 are different from Figure 3.

This deflection contains information about the damage location and extent, but it is noisy, and dynamics still influence it. A moving average is applied to the deflection difference, filtering the noise and the dynamics. This deflection difference is added to the deflection with no dynamic influence. The total

deflection is used as in the static case and the stiffness profile can be calculated from this deflection and the [*P*] matrix of the damaged batch.

4.2 Results

Repeatability and consistency of the stiffness profile have to be checked as random traffic is used. To analyse if the calculated stiffness profile is acceptable, 10 batches of 1000 trucks are used. In Figure 5, the batches are analysed for three scenarios. Figure 5(a) shows that all the calculated stiffness profiles are always close to the real values. The mean of all the histograms of stiffness is significantly closer to the actual damage scenario than individual batches. It is shown that in spite of the effect of dynamics and noise, no false positives are obtained in any of the runs. Similar conclusions can be extracted from the damage scenarios in Figures 5(b) and 5(c). The damage location is detected in both cases, and damage extent can be obtained.

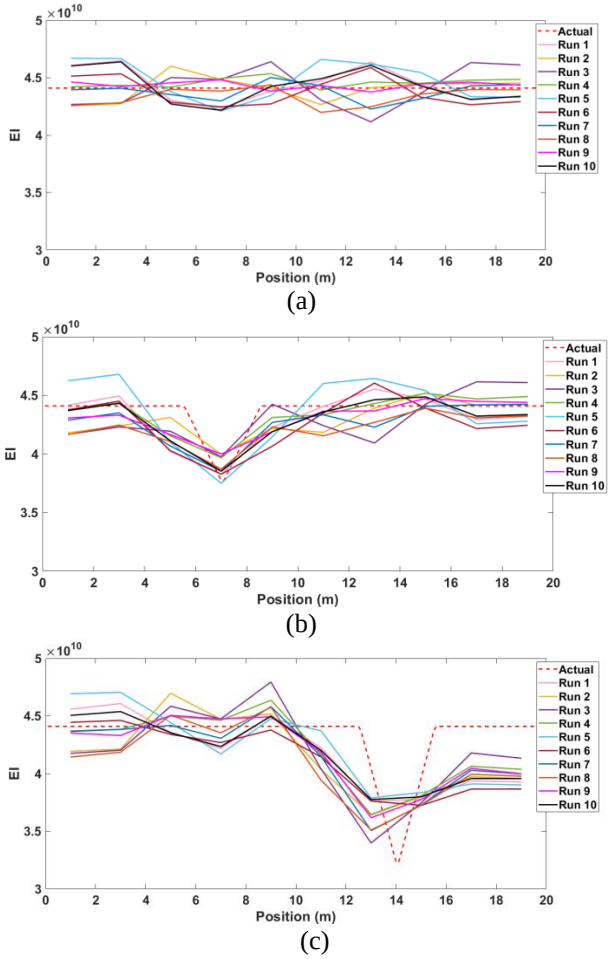

(a)

(b)

(c)

Figure 5. Ten different runs using the stiffness calculation for: (a) non-damaged bridge, (b) a 5% depth crack at 7 m, (c) a 10% depth crack at 14 m.

5 CONCLUSIONS

An instantaneous curvature denoted by *IC* has been used for drive-by bridge damage location. It has been shown that *IC* can detect the damage and localise it in a noisy environment. To adapt it to a specialised vehicle, the curvature has been calculated based on relative velocities. Therefore, the rate of *IC* or *RIC* has been used to locate damage with a similar effect to the *IC*. A moving average difference, abbreviated as *MAD*, has been proposed to filter the difference in phase out. *MAD* provides the damage location taking the noise from the LDVs into account.

A novel method that calculates the stiffness profile using bridge deflections due to random traffic has been explained using a numerical model. The key novelty here is that there is no need to measure random traffic axle weights to detect damage. This method has allowed for level 3 damage detection, i.e., estimation of location and extent of the damage. Further research is needed to test these concepts in real highway bridges.

ACKNOWLEDGMENTS

This project has received funding from the European Union's Horizon 2020 research and innovation programme under the Marie Skłodowska-Curie grant agreement No. 642453. Greenwood Engineering, designers of the TSD, are also acknowledged for their cooperation and support.

REFERENCES

[1] Green, M. and Cebon, D. (1994), 'Dynamic response of highway bridges to heavy vehicle loads: theory and experimental validation', *Journal of Sound and Vibration*, 170, 51-78.

[2] Hwang, E.-S. and Nowak, A. S. (1991), 'Simulation of dynamic load for bridges', *Journal of Structural Engineering*, 117, 1413-1434.

[3] Cai, C.S. and Shahawy, M. (2004), 'Predicted and measured performance of prestressed concrete bridges', *Journal of Bridge Engineering*, 9, 4-13.

[4] Garlock, M., Paya-Zaforteza, I., Kodur, V. and Gu, L. (2012), 'Fire hazard in bridges: Review, assessment and repair strategies', *Engineering Structures*, 35, 89-98.

[5] Sumitro, S. and Wang, M. (2005), 'Sustainable structural health monitoring system', *Structural Control and Health Monitoring*, 12, 445-467.

[6] Patjawit, A. and Kanok-Nukulchai, W. (2005), 'Health monitoring of highway bridges based on a global flexibility index', *Engineering Structures*, 27, 1385-1391.

[7] Feng, M. Q., Chen, Y. and Tan, C.-A. (2005), 'Global structural condition assessment of highway bridges by ambient vibration monitoring', *Nondestructive Detection and Measurement for Homeland Security III*, San Diego, California, US.

[8] Han, W., Wu, J., Cai, C. and Chen, S. (2014), 'Characteristics and dynamic impact of overloaded extra heavy trucks on typical highway bridges', *Journal of Bridge Engineering*, 20, 1-11.

[9] Guo, T., Frangopol, D.M. and Chen, Y. (2012), 'Fatigue reliability assessment of steel bridge details integrating weigh-in-motion data and probabilistic finite element analysis', *Computers & Structures*, 112, 245-257.

[10] Moughty, J.J. and Casas, J.R. (2017), 'A state of the art review of modal-based damage detection in bridges: Development, challenges, and solutions', *Applied Sciences*, 7(5), 510.

[11] Malekjafarian, A., Martinez, D. and O'Brien, E. J. (2018), 'The feasibility of using laser doppler vibrometer measurements from a passing vehicle for bridge damage detection', *Shock and Vibration*, 9385171, p. 10.

[12] Malekjafarian, A., McGetrick, P. J. and O'Brien, E.J. (2015), 'A review of indirect bridge monitoring using passing vehicles', *Shock and Vibration*, 2015, id 286139, p. 16.

[13] Wu, B., Wu, G., Yang, C. and He, Y. (2018), 'Damage identification method for continuous girder bridges based on spatially-distributed long-gauge strain sensing under moving loads' *Mechanical Systems and Signal Processing*, 104, 415-435.

[14] Whelan, M.J., Gangone, M.V. and Janoyan, K.D. (2009), 'Highway bridge assessment using an adaptive real-time wireless sensor network', *IEEE Sensors Journal*, 9, 1405-1413.

[15] Yang, Y. and Yang, J. P. (2018), 'State-of-the-art review on modal identification and damage detection of bridges by moving test vehicles', *International Journal of Structural Stability and Dynamics*, 18(2), id 1850025.
[16] Elhattab, A., Uddin, N. and O'Brien, E. (2016), 'Drive-by bridge damage monitoring using bridge displacement profile difference', *Journal of Civil Structural Health Monitoring*, 6, 839-850.
[17] Tan, C., Elhattab, A. and Uddin, N. (2017), '"Drive-by''bridge frequency-based monitoring utilizing wavelet transform', *Journal of Civil Structural Health Monitoring*, 7, 615-625.
[18] Limongelli, M. (2019), 'The surface interpolation method for damage localization in plates', *Mechanical Systems and Signal Processing*, 118, 171-194.
[19] Yan, A. and Golinval, J.-C. (2005), 'Structural damage localization by combining flexibility and stiffness methods', *Engineering Structures*, 27, 1752-1761.
[20] Sun, Z, Nagayama, T., Nishio, M. and Fujino, Y. (2018), 'Investigation on a curvature-based damage detection method using displacement under moving vehicle', *Structural Control and Health Monitoring*, 25(1), p. 18.
[21] Zhu, X., Law, S., Huang, L. and Zhu, S. (2018), 'Damage identification of supporting structures with a moving sensory system', *Journal of Sound and Vibration*, 415, 111-127.
[22] Hong, W., Zhang, X., Lv, K., Jiang, Y., Fang, X. and Hu, X. (2017), 'A novel method for structural diagnosis based on passing vehicle response', *Advances in Mechanical Engineering*, 9, 1-11.
[23] Catbas, F.N., Gul, M. and Burkett, J.L. (2008), 'Conceptual damage-sensitive features for structural health monitoring: laboratory and field demonstrations', *Mechanical Systems and Signal Processing*, 22, 1650-1669.
[24] O'Brien, E., Martinez, D., Malekjafarian, A. and Sevillano, E. (2017), 'Damage detection using curvatures obtained from vehicle measurements', *Journal of Civil Structural Health Monitoring*, 7, 333-341.
[25] Keenahan, J.C. and O'Brien, E.J. (2018), 'Drive-by damage detection with a TSD and time-shifted curvature', *Journal of Civil Structural Health Monitoring*, 8, 383-394.
[26] OBrien, E.J., Sevillano, E. and Martinez, D. (2016),'Monitoring the condition of a bridge using a traffic speed deflectometer vehicle travelling at highway speed', *Proceedings of the 3rd International Balkans Conference on Challenges of Civil Engineering*, Tirana, Albania.
[27] Flintsch, G.W., Ferne, B., Diefenderfer, B., Katicha, S., Bryce, J. and Nell, S. (2012), 'Evaluation of traffic speed continuous deflection devices', *Proceedings of the 91st Annual Transport Research Board Meeting*, Washington, US.
[28] Rasmussen, S., Krarup, J. A. and Hildebrand, G. (2002), 'Non-contact deflection measurement at high speed', *Proceedings of the 6th International Conference on the Bearing Capacity of Roads, Railways and Airfields*, Lisbon, Portugal.
[29] Rytter, A. (1993), *Vibration Based Inspection of Civil Engineering Structures*, Dept. of Building Technology and Structural Engineering, Aalborg University, Aalborg, Denmark: Doctoral thesis.
[30] De Boer, P.-T., Kroese, D.P., Mannor, S. and Rubinstein, R.Y. (2005), 'A tutorial on the cross-entropy method', *Annals of operations research*, 134, 19-67.
[31] Dowling, J., OBrien, E.J. and González, A. (2012), 'Adaptation of Cross Entropy optimisation to a dynamic Bridge WIM calibration problem', *Engineering Structures*, 44, 13-22.
[32] González, A., Covián, E., Casero, M. and Cooper, J. (2013), 'Experimental testing of a cross-entropy algorithm to detect damage', *Key Engineering Materials*, 569, 1170-1177,
[33] Whitley, D. (1994), 'A genetic algorithm tutorial', *Statistics and Computing*, 4, 65-85.
[34] Chou, J.-H. and Ghaboussi, J. (2001), 'Genetic algorithm in structural damage detection', *Computers and Structures*, 79, 1335-1353.
[35] Sinha, J., Friswell, M. and Edwards, S. (2002), 'Simplified models for the location of cracks in beam structures using measured vibration data', *Journal of Sound and vibration*, 251, 13-38.
[36] Moses, F. (1979), 'Weigh-in-motion system using instrumented bridges', *Journal of Transportation Engineering*, 105, 233-249.
[37] Neumaier, A. (1998), 'Solving ill-conditioned and singular linear systems: A tutorial on regularization', *SIAM review*, 40, 636-666.

Chapter 7: On the secondary use of truck sensors and asset management data to monitor the performance of road infrastructures

Federico Perrotta[1], Tony Parry[1], Luis C. Neves[1], Mohammad Mesgarpour[2], Emma Benbow[3], Helen Viner[3]
[1]Faculty of Engineering, University of Nottingham, University Park, Nottingham, NG7 2RD, England
[2]Microlise Ltd, Farrington Way, Eastwood, Nottingham, NG16 3AG, England
[3]TRL Ltd, Crowthorne House, Nine Mile Ride, Wokingham, RG40 3GA, England
email: perrottafederico2@gmail.com, tony.parry@nottingham.ac.uk, luis.neves@nottingham.ac.uk

ABSTRACT: This project aims to assess the impact of road surface characteristics, such as unevenness and macrotexture, on the fuel consumption of heavy-duty vehicles, such as trucks, using a 'Big Data' approach. In the past, several studies claimed that road pavement in poor condition could increase road vehicle's fuel consumption. However, in these studies, only a few vehicles were tested on selected road segments and under specific drive-cycle conditions, which may not produce results fully representative of real driving and network level conditions. For this reason, there is still a high level of uncertainty in the topic, which does not allow road managers to account for the extra costs and environmental impact that this can produce. Here, the potential for secondary use of the large quantities of data from standard sensors installed on modern trucks and information from the database of road agencies is investigated to assess the impact of road surface characteristics on vehicle fuel economy in the United Kingdom. Advanced statistics, data mining, and regression techniques have been combined to develop a new methodology based on 'Big Data' to provide pavement engineers and road asset managers with robust model prototypes capable of giving more reliable estimates about the impact of roughness and macrotexture on truck fleet fuel consumption. This chapter summarises findings over the last three years, points out possible implications of the results at the strategic and managerial level, and discusses future developments of the project.

KEY WORDS: Fuel consumption; Big data analysis; Road asset management; Machine learning.

1 INTRODUCTION

Road transport is one of the critical contributors to the economic growth of countries. However, since road vehicles rely on fossil fuels, the sector also represents one of the highest contributors to the emissions of pollutants [1]. Recent statistics show that road transport contributes about a quarter of the total emissions of Greenhouse Gases (GHGs) in Europe and worldwide [1].

In the past, several studies claimed that due to their effect on rolling resistance [2-4], road surface characteristics such as roughness and macrotexture can impact fuel consumption by up to 5% [2,5-11]. This could be of particular interest for governmental authorities and road managers since, if poor conditions of the road surface affect vehicle fuel consumption, maintenance will represent an opportunity to reduce costs and emissions of GHGs from the road transport industry significantly [5,11-13]. This, at a global level, implies significant reductions of costs and emissions of pollutants from the road transport industry, with possible significant direct and indirect benefits for society, and therefore, represents an opportunity which cannot be neglected [13-17]. However, in the past, researchers tested only a few vehicles driven at a relatively constant speed [8,9,18], or performed coast-down measurements [7,19-21] on selected and short road segments and, for this reason, their conclusions cannot be considered fully representative of real driving and network level conditions. Because of this, there is still a high level of uncertainty in the topic, and road managers cannot justify a re-evaluation of the current road maintenance strategies.

In this project, the impact of road surface characteristics on truck fleet fuel consumption is assessed. A 'Big Data' approach is undertaken combining advanced statistics, neural networks and other machine learning techniques to point out the complex correlations existing between road surface characteristics and fuel consumption [22-27]. In particular, secondary use of data from standard sensors [28] installed on modern trucks is made, and analysed in combination with data from the databases of road asset managers and meteorological agencies to model how fuel consumption is affected by roughness, macrotexture of road surfaces and other factors. This represents a more holistic approach, which allows investigation of the variation of fuel consumption under conditions representative of real driving. In particular, new models capable of estimating the effect of road surface characteristics on truck fleet fuel consumption are developed, and their performance improved throughout the project in conditions representative of typical motorways and primary roads in the United Kingdom. Additionally, thanks to the standard nature of the data used in the study and availability of these (or similar) at international level, the developed methodology promises to be able to provide answers in regards to the impact of road surface characteristics on vehicle fuel economy globally. That offers an opportunity to investigate the performance of the road infrastructure regarding vehicle fuel economy; it will support engineers' decisions towards the review of the current road maintenance policies, and, in the future, it may help drivers in selecting the most eco-friendly route between two locations. Although in its current state the developed method might be applicable only to trucks and heavy-duty vehicles, future standardization of sensors for cars and other vehicle types may extend its applicability.

The present chapter summarizes results of the research work carried out within this project, highlighting implications of its results at a strategic and managerial level, and discussing possible future developments.

2 BIG DATA

When data are collected in a large volume, from a variety of sources of unknown quality or veracity, streamed at high velocity, it is common to refer to them as 'Big Data' [29]. Today, companies in any sector collect vast quantities of information from disparate sources. For example, truck fleet managers and manufacturers do that to monitor the performance of their vehicles, plan maintenance and optimize operational costs. That is done thanks to SAE J1939 sensors [28], which are installed as standard on modern trucks and that measure geographical position, vehicle weight, the performance of the engine and fuel consumption, among other parameters.

Similarly, road agencies periodically collect data about the condition of the road infrastructure by means of monitoring vehicles [30]. This includes measurements of road geometry (e.g., gradient, crossfall, radius of curvature, etc.) and road conditions, which in England are measured as Longitudinal Profile Variance (LPV) at 3, 10 and 30 meters wavelengths for roughness and as Sensor Measured Texture Depth (SMTD) for macrotexture [30]. This is different from international standards which use International Roughness Index (IRI) for roughness and Mean Depth Profile (MPD) for the macrotexture, but other studies showed good correlation between these measurements [31,32]. Collection of this information allows Highways England and road agencies in general to plan future road works and maintenance of the infrastructure [30]. In order to assign road conditions from road agencies to truck performance data from truck fleet managers, geographical filters are applied. For instance, given a certain journey of a truck along a particular road segment between points A and B, the average of LPV and SMTD for that specific road segment are assigned to that journey of that truck. That allows comparison of fuel consumption with road condition measurements and inclusion of that information in the developed fuel consumption models.

Meteorological agencies collect real-time data about the weather to provide the public and industry with information about the current and future meteorological conditions. This data is attached to a truck performance by assigning information from the nearest weather station to each journey. These data can then be considered in the development of fuel consumption models, including investigating the variation of fuel consumption in different weather conditions such as in summer and winter, rain and/or wind, etc.

The idea behind this project is that using a large amount of information from these various sources, might offer the opportunity to model truck fleet fuel consumption and understand how this varies with changes in road surface characteristics and other factors such as meteorological conditions. The data are provided by Microlise Ltd and TRL, two privately owned companies involved in the project, which allowed the use of these data for research purposes only. Additionally, in a final stage of the project, meteorological data are collected from the Met Office, the weather forecast agency in the UK. This is used to investigate the effect of air temperature, atmospheric pressure, humidity, rainfall and wind speed on truck fleet fuel consumption.

3 METHOD

In the past, fuel consumption models have been developed [9,11,33-35] with the aim of estimating the impact of road surface conditions on vehicle fuel economy, based on physical-mechanistic principles to be used in road asset management applications. However, due to improvements in vehicle technology and continuous deterioration or changes in road pavement conditions, these models generally require constant re-calibration. In the past, that has been done by testing a few vehicles under selected pre-defined conditions, along with selected, short road sections. This facilitates accurate and interpretable models but may not allow the model to give reliable estimates in regards to situations different from those tested. This may represent a limitation for the traditional approach, which may not produce models representative of real driving and network level conditions. For example, recent studies showed that existing models recently developed or calibrated in Europe [11,36,37] are already obsolete and require re-calibration for them to be used to make decisions at managerial level [38-40]. For this reason, currently available tools are considered unreliable and rarely used for maintenance planning in practice.

This is why within this project a different approach is adopted. A large quantity of the data available in the databases of truck fleet managers, truck manufacturers, road agencies and weather forecast institutions are collected to derive models capable of taking into consideration the effects of various factors including road surface conditions. In an initial phase of the study, linear regression models are developed [12,23,24]. These models are built to produce a baseline for performance, which allow interpretation and comparison with results from previous studies adopting similar techniques to model road vehicles' fuel consumption [8,9,41-43]. In a second phase, advanced analytics are used to boost the performance of the developed models and take advantage of the large quantity of information available to point out complex correlations, achieve better accuracy and improve the reliability of the obtained estimates [22,25]. Finally, results are validated with conditions representative of motorways and primary roads in the UK.

3.1 Linear regression

Initially, linear regression is used to model the fuel consumption of trucks based on the available data from Microlise and TRL. This technique was used in the past to model road vehicle fuel consumption [41,44,45], which provides a way to have a baseline for comparison of performance between previous studies and the machine learning techniques applied later in the project.

3.2 Machine learning

Machine learning techniques are, at the current state of knowledge, the best techniques to deal with 'Big Data' [46]. These techniques apply advanced statistics to detect patterns and recognize trends through the data. However, there are a number of machine learning techniques available and knowing

which one performs best for a specific problem is not possible a-priori [46]. For this reason, three different techniques are applied [22,25,26]: artificial neural networks [46-48], support vector regression [46,49] and random forests [50]. These techniques are tested in various case studies throughout the project, and compared in terms of R^2, root-mean-squared error (RMSE), mean absolute error (MAE), and required training time. Machine learning algorithms (such as those used in regression analysis) require 'training' before being able to make an estimate. Working on an initial dataset representative of the phenomenon of interest, the algorithms automatically identify trends and patterns across the data [51]. This approach may require lots of data and some time, but it is necessary to ensure that the model is robust enough to deal with new information [46,51]. Based on that, the algorithms are then able to make accurate estimates about new conditions in almost real-time [46,51].

The main advantage of these techniques is that they automatically apply probabilistic methods to detect trends and, for this reason, they are robust to outliers [46]. Additionally, equations which characterize patterns and trends across the data are directly generated by the algorithm so that users do not need to specify them. However, this might also be seen as a disadvantage of machine learning algorithms as it is generally said that they work like 'black-boxes'; That is because the algorithms operate complex transformations of the input variables to higher dimensional spaces which makes the process difficult to replicate [46]. However, in order to reduce doubts about the reliability of the techniques applied and models developed in the study, interpretability is investigated, and performance also evaluated in these terms. For example, various variable selection algorithms are used to include in the developed models only variables which show some correlation with the fuel consumption of the considered fleet of trucks, and the results compared to those of past studies. In particular, p-values, the adjusted-R^2, the Akaike Information Criterion (AIC) [52], the Lasso [53] and random forests [50] have been analyzed and their results compared. Only variables identified by both the used algorithms and studies conducted in the past are used for modelling fuel consumption. Additionally, the architecture of the developed machine learning models is kept as simple as possible while achieving low error (RMSE and MAE) and reasonable training time. This improved the accuracy of the linear regression significantly.

Finally, a parametric analysis of all input variables is performed. The models developed in the project are used to make estimates for 50 values evenly distributed between the 5^{th} and 95^{th} percentiles of the considered input variable, while other variables are set to their mean value. This procedure tests consistency of the developed machine learning models and assists interpretation.

4 RESULTS

In the first phase of the project, some multiple linear regression models are developed to understand the type of data available and explore opportunities within the available information. For example, in one of these initial studies some 1,420 records from 260 trucks, driving at constant speed on the M18 motorway in the UK, are analysed [23]. Based on these data, the resulting linear regression model is derived:

$$FC = 62.42 + 0.00024GVW + 14.84g\% + \\ - 0.57s + 0.26LPV10 + 0.87SMTD \quad (1)$$

where *FC* is Fuel Consumption (in l/100 km), *GVW* the Gross Vehicle Weight (in kg), *g%* the road gradient (in %), *s* the vehicle speed (in km/h), *LPV10* unevenness as Longitudinal Profile Variance at 10 m wavelength (in mm^2), and *SMTD* macrotexture as sensor measured texture depth (in mm).

The model above is followed by other attempts using different datasets from trucks driving along the same road, which show the possibility of using high-resolution fuel consumption data to model truck fleet fuel consumption and the available information to make estimates about the impact of road roughness and macrotexture on the fuel consumption of the considered vehicle fleets. Perrotta et al [23] show that for trucks driving on motorways in the UK fuel consumption can be affected by road roughness (LPV10) by up to 3% and by the macrotexture of the road surface by up to 5%. That, together with other attempts performed on smaller [12,24] and larger [22,27] datasets, confirm the finding of studies conducted in the past and increase confidence that the 'Big Data' approach could work.

In the second phase of the project, improving the accuracy of the developed models is the primary goal. A larger quantity of information is made available by Microlise and TRL, to test the usability of machine learning techniques and produce results representative of conditions typical of the whole strategic road network of England, which includes motorways and strategic primary roads. In a case study, 14,281 records from 1,110 trucks are used and performance of a linear regression of the inputs is compared to results from machine learning techniques [22,27]. This analysis includes data from heavy trucks [54] driving at relatively constant speed along the motorways M1 and M18 in England, representative of the condition of motorways in the UK. Figure 1 shows two of the developed models and compares linear regression with Artificial Neural Network (ANN) for the same data. For brevity, only results of the ANN are reported, but similar trends are found by support vector regression and random forests, demonstrating their ability to outperform linear regression models [26]. A parametric analysis of the input variables is performed to investigate how each relates to the variation of fuel consumption for the considered truck fleets. Figure 2 reports trends identified by parametric analysis of the developed linear model and ANNs [22,27]. Again, results of support vector regression and random forests are not reported for brevity, however, they show trends similar to those identified by the ANN and, for this reason, their interpretation can be considered robust and reliable. In particular, from Figure 2 it is possible to see that, in regards to road conditions and their impact on vehicle fuel consumption, the ANN identifies higher fuel consumption in road segments characterized by higher LPV at 30 meters wavelength. That represents an interesting result which partially confirms results of studies conducted in the past [2,8,9,11], but it also opens discussion towards the impact of road surface conditions on vehicle fuel economy at motorway speed.

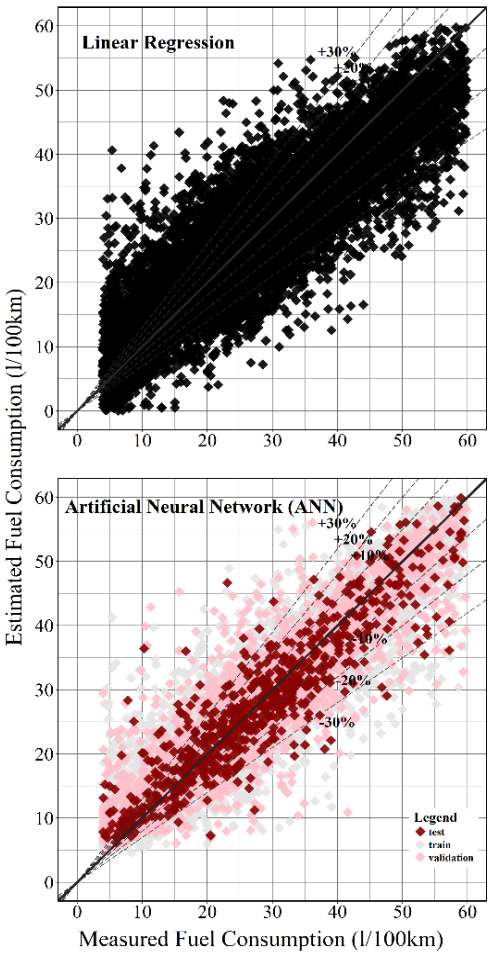

Figure 1. The fit of the ANN model developed by Perrotta et al [22,27] and comparison with a linear regression model developed using the same data.

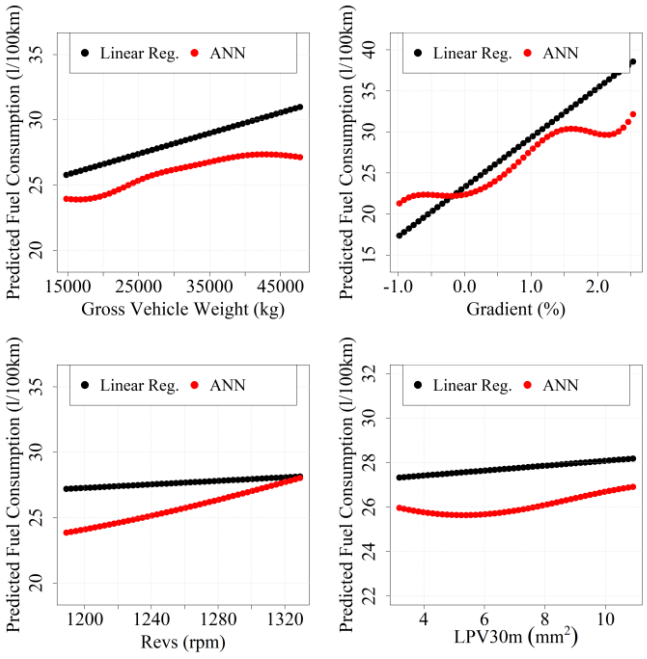

Figure 2. Examples of parametric analysis and comparison of estimates between the linear regression and the artificial neural network model developed in [22,27].

5 VALIDATION

In the final phase of the project, the main goal is to test the developed methodology and models for conditions representative of the whole UK strategic road network, i.e., to validate the obtained results and extend their applicability to the national level. Therefore, data from a mix of truck types driving along different road types, such as motorways and primary roads in England, are considered. In particular, roads are selected to be representative of conditions of the entire strategic road network and included the whole M18, part of the M1, the whole A21 and part of the A47, A49, and A259. The sample ended up considering 29,536 records from light trucks, 197,572 records for medium trucks and 256,678 records from heavy trucks (classified as specified by EPA [54]). Again, all considered records are from journeys of trucks performed at relatively constant speed along the considered road segments. Additionally, in this case, weather conditions are considered in the investigation. Figure 3 reports trends identified by parametric analysis of the developed linear model and artificial neural network.

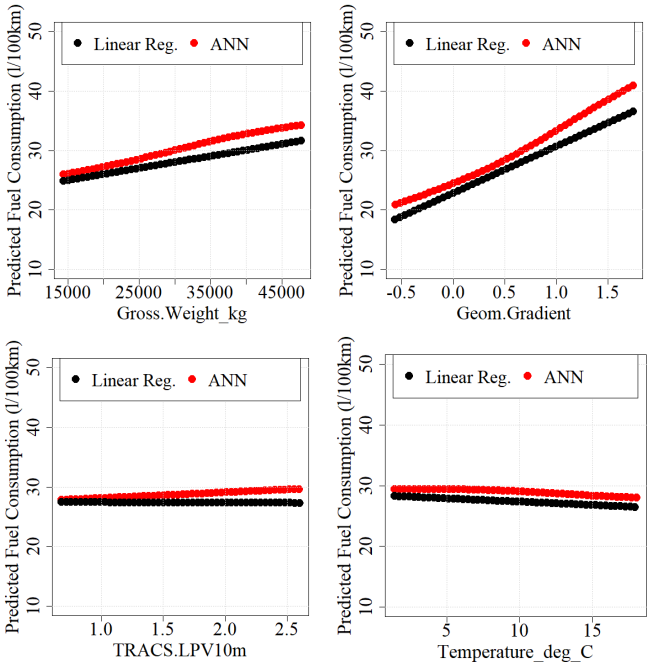

Figure 3. Examples of parametric analysis and comparison of estimates between the linear regression and ANN developed in the validation phase.

Once again, trends identified by support vector regression and random forest are very similar to those identified by the ANN which makes conclusions based on machine learning models robust. In particular, it is possible to notice that the ANN shows that fuel consumption is higher for roads characterized by higher LPV at 10 meters wavelength and lower for higher temperature, which seems reasonable and in line with results of studies based on physical/mechanical approaches.

6 CONCLUSIONS AND FUTURE DEVELOPMENTS

This project has shown the great potential of the 'Big Data' approach and secondary use of truck sensors and road asset management data to model the variation of fuel consumption due to the impact of road surface condition. The results have

demonstrated that machine learning algorithms are able to outperform linear regression, in terms of RMSE, MAE, and R^2. They have also showed that inclusion of more data and types of measurements could allow the models developed using machine learning to further improve in precision, accuracy, and reliability.

Performing a parametric analysis has proven to be a good way to partially interpret results of machine learning algorithms as its output graphs are easily readable and allow identification of how fuel consumption varies in different situations. Further work should test and explore the impact of road surface conditions on truck fleet fuel consumption in urban environments using the developed method. The latter would provide an insight into how road roughness and macrotexture affect fuel consumption when low speed, and different traffic and road geometry from motorways and primary roads intervene in the process. This will improve the applicability of the approach and may help engineers in justifying a review of current road design and maintenance strategies helping highway authorities in saving costs and reducing the emissions of pollutants from the road transport industry.

In the future, when data for different vehicle types, such as cars or motorbikes, became available, this approach could be extended to support engineers in estimating the excess costs and environmental impact that the conditions of the road surface produce. This work can also be relevant for electric vehicles since batteries could last longer on smoother road pavements and possibly increase the distance that a vehicle can travel with a single charge.

ACKNOWLEDGMENTS

This project has received funding from the European Union's Horizon 2020 research and innovation programme under the Marie Skłodowska-Curie grant agreement No. 642453.

The authors would like to thank Microlise Ltd, for allowing analysis of anonymized sets of telematic data, and TRL together with Highways England, for enabling analysis of the asset management data in the HAPMS, for their collaboration and assistance provided during the whole project.

REFERENCES

[1] A. Hoen, A. van Grinsven, B. Kampman, J. Faber, H. van Essen and I. Skinner, *Research for TRAN Committee - Decarbonisation of EU transport*, Policy Department B: Structural and Cohesion Policies, Transport and Tourism, Directorate General for Internal Policies, European Parliament, 2017.

[2] Sandberg, U., Bergiers, A., Ejsmont, J.A., Goubert, L. and Karlsson, R., *MIRIAM SP1 D.4: Road surface influence on tyre/road rolling resistance*, Report from Project: Models for Rolling Resistance in Road Infrastructure Asset Management Systems (MIRIAM), 2011.

[3] P.D. Cenek, *Rolling resistance characteristics of New Zealand road surfaces* in *Vehicle-Road Interaction*, ASTM STP 1, B.T. Kulakowski, Ed. Philadelphia: American Society for Testing and Materials, 248-262, 1994.

[4] G. Descornet, *Road-surface influence on tire rolling resistance* in *Surface characteristics of roadways: International research and technologies*, vol. ASTM STP 1, W. E. Meyer and J. Reichert, Eds. Philadelphia: American Society for Testing and Materials, 401-415, 1990.

[5] E. Beuving, T. De Jonghe, D. Goos, T. Lindahl and A. Stawiarski, *Environmental impacts and fuel efficiency of road pavements*, European Asphalt Pavement Association (EAPA), Fuel efficiency report March, 2004.

[6] R. Laganier, R. and J. Lucas, *Influence of pavement evenness and macrotexture on fuel consumption*, in *Surface characteristics of roadways: International research and technologies*, ASTM STP 1, W.E. Meyer and J. Reichert, Eds. Philadelphia: American Society for Testing and Materials, 454-459, 1990.

[7] H.W. du Plessis, A.T. Visser and P.C. Curtayne, *Fuel consumption of vehicles as affected by road-surface characteristics*, in *Surface characteristics of roadways: International research and technologies*, ASTM STP 1, W.E. Meyer and J. Reichert, Eds. Philadelphia: American Society for Testing and Materials, 480-496, 1990.

[8] U. Sandberg, *Road macro-and megatexture influence on fuel consumption*, in *Surface characteristics of roadways: International research and technologies*, ASTM STP 1, W.E. Meyer and J. Reichert, Eds. Philadelphia: American Society for Testing and Materials, 460-479, 1990.

[9] K. Chatti and I. Zaabar, *Estimating the effects of pavement condition on vehicle operating costs*, NCHRP report 720, Transportation Research Board, 2012.

[10] Zaabar, I. and Chatti, K. (2014), 'Estimating vehicle operating costs due to pavement surface conditions',*Proceedings of Transportation Research Board 93rd Annual Meeting*, Washingto n, US.

[11] E. Benbow, S. Brittain and H. Viner, *MIRAVEC D3.1: Potential for NRAs to provide energy reducing road infrastructure*, Report from project 832615: Modeling Infrastructure Influence on Road Vehicle Energy Consumption (MIRAVEC). Deliverable D3.1, 2013.

[12] Perrotta, F., Trupia, L., Parry, T. and Neves, L.C. (2017), 'Route level analysis of road pavement surface condition and truck fleet fuel consumption', *Proceedings of Pavement Life-Cycle Assessment Symposium*, Illinois, US, 51-57.

[13] D. Gleave, R. Frisoni, F. Dionori, L. Casullo, C. Vollath, L. Devenish, F. Spano, T. Sawicki, S. Carl, R. Lidia, J. Neri, R. Silaghi and A. Stanghellini, *EU road surfaces: Economic and safety impact of the lack of regular road maintenance*, Policy Department B: Structural and Cohesion Policies, Transport and Tourism, Directorate General for Internal Policies, European Parliament, 2014.

[14] Wang, T., Lee, I.S., Kendall, A., Harvey, J., Lee, E.B. and Kim, C. (2012), 'Life cycle energy consumption and GHG emission from pavement rehabilitation with different rolling resistance', *Journal of Cleaner Production*, 33, 86-96.

[15] Wang, T., Harvey, J. and Kendall, A. (2014), 'Reducing greenhouse gas emissions through strategic management of highway pavement roughness', *Environmental Research Letters*, 9(3).

[16] Santero, N.J. and Horvath, A. (2009), 'Global warming potential of pavements', *Environmental Research Letters*, 4(3), p. 034011.

[17] Trupia, L., Parry, T., Neves, L.C. and Lo Presti, D. (2016), 'Rolling resistance contribution to a road pavement life cycle carbon footprint analysis', *International Journal of Life Cycle Assessment*, 22(6), 972-985.

[18] Zaabar, I. and Chatti, K. (2010), 'Calibration of HDM-4 models for estimating the effect of pavement roughness on fuel consumption for U. S. conditions', *Transportation Research Record: Journal of the Transportation Research Board*, 2155, 105-116.

[19] U. Hammarström, R. Karlsson and H. Sörensen (2008), *Road surface effects on rolling resistance - coastdown measurements with uncertainty analysis in focus*, Report from Project: Energy Conservation in Road Pavement Design, Maintenance and Utilisation (ECRPD), Deliverable D5(a), 2008.

[20] R. Karlsson, U. Hammarström, H. Sörensen and O. Eriksson, *Road surface influence on rolling resistance coastdown measurements for a car and an HGV*, VTI notat 24A-2011, Swedish Road and Transport Institute, Linköping, Sweden, 2011.

[21] U. Hammarström, J. Eriksson and R. Karlsson, *Rolling resistance model, fuel consumption model and the traffic energy saving potential from changed road surface conditions*, Report VTI-code 748A, Swedish Road and Transport Institute, Linköping, Sweden, 2012.

[22] Perrotta, F., Parry, T. and Neves, L.C. (2017), 'Application of machine learning for fuel consumption modelling of trucks', *Proceedings of the 2017 IEEE International Conference on Big Data*, Boston, US.

[23] Perrotta, F., Parry, T. and Neves, L.C. (2017), 'Using truck sensors for road pavement performance investigation', *Safety and Reliability - Theory and Applications, Proceedings of 27th annual European Safety and Reliability Conference (ESREL 2017)*, Portoroz, Slovenia, 392-396.

[24] Perrotta, F., Parry, T. and Neves, L.C. (2017), 'A big data approach to assess the influence of road pavement condition on truck fleet fuel

consumption', *Transport, Infrastructure and Systems: Proceedings of the AIIT International Congress on Transport, Infrastructure and Systems*, G. Dell'Acqua and F. Wegman, Eds. Rome, Italy, CRC Press, 33-38.

[25] Perrotta, F., Parry, T., Neves, L.C. and Mesgarpour, M. (2018), 'A machine learning approach for the estimation of fuel consumption related to road pavement rolling resistance for large fleets of trucks', *Proceedings of the 6th International Symposium on Life-Cycle Civil Engineering (IALCCE 2018)*, Ghent, Belgium.

[26] Perrotta, F., Parry, T., Neves, L.C., Mesgarpour, M. Benbow, E. and Viner, H. (2018), 'A big data approach for investigating the performance of road infrastructure', *Proceedings of Civil Engineering Research in Ireland (CERI 2018)*, Dublin, Ireland.

[27] Perrotta, F., Parry, T. and Neves, L.C. (2018), 'Evaluation of road pavements fuel efficiency using truck sensors data', *TRAVISIONS Young Researchers Competition 2018, Transportation Research Arena (TRA)*.

[28] SAE International, *SAE J1939-71, Vehicle Application Layer - Surface Vehicle Recommended Practice*, SAE International Standard, 2016.

[29] IBM, *The four V's of Big Data,* IBM Big Data & Analytics Hub, 2018, accessed 21 August 2018, <http://www.ibmbigdatahub.com/info-graphic/four-vs-big-data>.

[30] The Highways Agency, *HD 29/08 Data for pavement assessment,* in *Design manual for roads and bridges*, 7(3), Part 2, Standard, 2008.

[31] E. Benbow, D. Wright, K. Nesnas and A. Wright, *Measures for assessing ride quality on trunk roads,* Report CPR1553, Crowthorne, UK, 2011.

[32] H. Viner, P. Abbott, A. Dunford, N. Dhillon, L. Parsley and C. Read, *Surface Texture Measurement on Local Roads*, TRL report PPR148, Crowthorne, UK, 2006.

[33] G. Carlsson, *VEjstandard og Transport-Omkostninger (VETO)*, Report VTI 307, Swedish Road and Transport Institute, Linköping, Sweden, 1986.

[34] U. Hammarström and B. Karlsson, *VETO - A computer program for calculation of transport costs as a function of road standard*, Report VTI/MEDDELANDE 501, Swedish Road and Transport Institute, Linköping, Sweden, 1987.

[35] H.R. Kerali, J.B. Odoki and E.E. Stannard, *Overview of HDM-4, Volume 1*, Paris: World Roads Association (PIARC), 2006.

[36] Odoki, J. B., Anyala, M. and Bunting, E. (2013), 'HDM-4 adaptation for strategic analysis of UK local roads', *Proceedings of the Institution of Civil Engineers - Transport*, 166, 65–78.

[37] University of Birmingham, *Development of socio-economic models for highway maintenance, Analysis of DfT Road Network Using HDM-4*, Final report for WSP 4/068/005, March, 2011.

[38] Perrotta, F., Parry, T., Neves, L.C., Buckland T., and Mesgarpour, M. (2018), 'Comparison of HDM-4 fuel consumption estimates with real measurements from trucks on motorways: a UK case study', *Proceedings of the Transportation Research Board 97th Annual Meeting*, Washington, D.C., US.

[39] Perrotta, F., Parry, T., Neves, L.C., Buckland, T., Benbow, E. and Mesgarpour, M. (2019), 'Verification of the HDM-4 fuel consumption model using a Big Data approach: a UK case study', *Transportation Research Part D: Transport and Environment*, 67, 109-118.

[40] Perrotta, F., Parry, T., Neves, L.C., Buckland, T., Benbow, E. and Viner, H. (2018), 'Comparison of truck fuel consumption measurements with results of existing models and implications for road pavement LCA', *Proceedings of the 6th International Symposium on Life-Cycle Civil Engineering (IALCCE 2018)*, Ghent, Belgium.

[41] Bifulco, G., Galante, F., Pariota, L. and Spena, M. (2015), 'A linear model for the estimation of fuel consumption and the impact evaluation of advanced driving assistance systems', *Sustainability*, 7(10), 14326-14343.

[42] Rakha, H. A., Ahn, K., Moran, K., Saerens, B. and Van den Bulck, E. (2011), 'Virginia Tech comprehensive power-based fuel consumption model: Model development and testing', *Transportation Research Part D Transport and Environment*, 16(7), 492-503.

[43] Wang J. and Rakha, H.A. (2016), 'Fuel consumption model for conventional diesel buses', *Applied Energy*, 170, 394-402.

[44] N. Clark, G. Thompson and O. Delgado, *Modeling heavy-duty vehicle fuel economy based on cycle properties*, WVU Final report ICCT, West Virginia University Center for Alternative Fuels, Engines, and Emissions, 2009.

[45] Delgado, O.F., Clark, N.N. and Thompson, G.J. (2011), 'Modeling Transit Bus Fuel Consumption on the Basis of Cycle Properties', *Journal of the Air & Waste Management Association*, 61(4), 443-452.

[46] I. Goodfellow, Y. Bengio and A. Courville, *Deep Learning*, Cambridge, MA: The MIT Press, Massachussets Institute of Technology, 2016.

[47] Riedmiller, M. and Braun, H. (1993), 'A direct adaptive method for faster backpropagation learning: The RPROP algorithm', *Proceedings of IEEE International Conference on Neural Networks (ICNN)*, 1(7), 586-591.

[48] McCulloch, W. S. and Pitts, W. (1943), 'A logical calculus of the ideas immanent in nervous activity', *The Bulleting of Mathematical Biophysics*, 5(4), 115-133.

[49] S.R. Gunn, *Support vector machines for classification and regression*, Technical Report, School of Electronics and Computer Science, University of Southampton, UK, 1998.

[50] Breiman, L. (2001), 'Random forests', *Machine Learn*ing, 45(1), 5-32.

[51] G. James, D. Witten, T. Hastie and R. Tibshirani, *An Introduction to Statistical Learning*. New York, NY: Springer Science+Business Media New York, 2013.

[52] Akaike, H. (1974), 'A new look at the statistical model identification', *IEEE Transactions on Automatic Control*, 19(6), 716-723.

[53] Tibshirani, R. (1996), 'Regression shrinkage and selection via the Lasso', *Journal of the Royal Statistical Society B*, 58(1), 267-288.

[54] EPA, *Vehicle Weight Classifications for the Emission Standards Reference Guide*, U.S. Environmental Protection Agency, 2017, accessed 13 December 2017, <https://www.epa.gov/emission-standards-reference-guide/vehicle-weight-classifications-emission-standards-reference-guide>.

Chapter 8: Reduction of uncertainty through regularized, automated road inspection

Siyuan Chen[1], Debra F. Laefer[1,2], Eleni Mangina[3]
[1]School of Civil Engineering, University College Dublin, Ireland
[2]Center for Urban Science and Progress and Department of Civil and Urban, New York University, US
[3]Department of Computer Science, University College Dublin, Ireland
email: siyuan.chen.1@ucdconnect.ie, debra.laefer@nyu.edu, eleni.mangina@ucd.ie

ABSTRACT: This chapter reports on the research contributions of the project 'Reduction of uncertainty through regularized, automated road inspection'. This research applies Unmanned Aerial Vehicles (UAVs) and the photogrammetry method to road and bridge inspections. Associated data processing, quality evaluation, and damage extraction solutions are also created. The results show that low cost commercial UAVs have the capabilities to acquire high-quality images and to be used for 3D documentation and surface damage detection. In this project, the Structure From Motion (SFM) method is employed for images based 3D point cloud generation. Subsequently, automatic noise reduction and damage segmentation method are developed for the point cloud post-processing. Following a lab test, the entire pipeline is applied in several field surveys, such as the Wicklow road, Wicklow Bridge, and Boyne viaduct in Ireland, thus establishing that the proposed UAV inspection method can reduce surveying costs significantly and provide a competitive result in terms of quality.

KEY WORDS: Unmanned Aerial Vehicle (UAV); Photogrammetry; Structure From Motion (SFM); Inspection; Infrastructure.

1 INTRODUCTION

The safety of a community's road network is fundamental to an efficient public transportation system and highly related to its economic prosperity. Therefore, such networks must be inspected and maintained on a regular basis. The primary approach has been in-person inspection, which has considerable limitations such as the generation of traffic interruptions, reliance on expensive and/or heavy equipment, and creation of safety risks for inspectors.

As a possible alternative, the use of UAVs with remote sensing capabilities has received significant interest in baseline documentation and surface evaluation for roads [1] and bridges [2]. The viability of using UAVs for infrastructure inspection relies upon a pipeline of four components: (1) high quality and comprehensive data acquisition, (2) 3D data reconstruction and evaluation, (3) quality optimization, and (4) damage extraction. These four areas are the focus of this TRUSS project. This chapter summarizes the background to the work and the contributions made as part of the research program.

2 BACKGROUND

2.1 UAV-based data acquisition

The UAV-based data acquisition for infrastructure inspection can be achieved from a multitude of sensors. For visual inspection, the most common approaches involve Light Detection and Ranging (LiDAR) or imagery data (photographs or video) from a camera. LiDAR is a line of sight technology that sends out a laser beam and back calculates the position of the beam intersection with an object in the real world. The resulting set of points with its co-registered intensity and x,y,z positional data are used to generate a three-dimensional (3D) point cloud directly. However, full capability LiDAR equipment is comparatively expensive and heavy for UAV usage. As such, cameras are more commonly deployed, especially for smaller and less costly UAVs. However, imagery natively only provides 2D information. To extract 3D information, a reconstruction process is required, as will be introduced in the next section.

For road inspection, selecting an appropriate UAV platform for sensor mounting and data collection involves: (1) having enough payload to carry the sensors, (2) having adequate battery life for sufficient flight time for data collection, (3) having adequate flexibility to avoid obstacles, and (4) providing enough stability to ensure high data quality. This last factor is crucial, as UAV vibration can significantly compromise data quality [3]. Image blurring and the 'Jello' effect on videos may both generate heavy noise in a 3D point cloud. Mitigating this problem requires both hardware design and/or algorithm development, such as better stabilizing the UAV frame, redesigning the camera mounting, improving the flight control program, and post-processing of the datasets.

Furthermore, Caroti et al [4] demonstrate that, in addition to instrument and processing methodologies, the data capturing strategies also affect the output. This issue relates to the flight path planning, such as flight height, incidence angle, and offset distance, as well as the data density control. However, the impact of the image capturing strategies on the final dataset has yet to be systematically evaluated concerning both flight path coverage and data acquisition density.

2.2 3D reconstruction and evaluation

As the acquired images or videos cannot directly provide 3D scene information, a further step is required in the form of 3D scene reconstruction. To achieve this, a common strategy is the SFM method [5]. This method relies on images taken from multiple viewpoints. By detecting key points in each image, the geometric relationship between images can be calculated and used for triangulation. Thus, the depth information of key points is derived and placed into a unique coordinate system.

Using this approach Hallermann et al conducted a series of experiments [6-8] in which they used an AscTec platform with a Sony NEX camera for image acquisition. The SFM enabled generation of 3D point clouds. The 3D data were then used to detect locations of surface damage and inclination of a historic German tower, the Bad Frankenhausen. Wu [9] noted that the direct application of SFM is problematic for long strip structures, such as a road, because of radial distortion. To overcome this, Wu's research presented a self-calibration method to fix the curvature problem in a few critical configurations, but failed to study the underlying phenomenon of radial distortion comprehensively. Therefore, a reliable method for UAV-derived point cloud quality evaluation is necessary.

Compared to the point cloud generated by the traditional laser scanner, the UAV imagery reconstructed point clouds include data from more viewpoints and are less restricted by the view angle, therefore providing better coverage. However, point cloud-based images are often much noisier than those obtained from active sensors (e.g., laser scanners). Possible reasons can be mismatching of feature points, low-quality images, distortions of a camera lens or environmental effects like light reflection and shadows. Those noise points can impair surface reconstruction, point classification, and damage detection. To minimize the effect, an optimization processing should be included to remove noise within the point cloud.

2.3 Quality optimization

To date, quality optimization research has mainly focused on noise reduction. Generally, noise can be classified as small-amplitude noise or distant outliers [10]. The small-amplitude noise has points randomly distributed around the surface. To reduce such noise points, the main idea is to move the points to an estimated surface. I.e., a Moving Least Squares (MLS) algorithm can be used to generate a smoothed surface [11]. Shen et al [12] defined the implicit moving least-squares (IMLS) approach for building interpolating or approximating implicit surfaces from polygonal data, while Yingjie and Liling [13] included the weighting least squares method and hierarchical clustering algorithm to optimize the speed of the MLS method. However, these methods are usually sensitive against a large number of outliers and over smooth the data points.

Distant outliers are points clustered together far from the actual surface. This commonly occurs due to structural artefacts in the acquisition process or caused by mismatching features in image based-reconstruction process [14]. Outliers must be removed from the dataset before any surface fitting. Two typical methods to remove outliers are statistical and geometric. Statistical methods assume noise to have different performance characteristics than regular points in a k-dimensional space when fitting the data to a standard probability distribution [15]. Geometric methods use distance to a neighbour point or a local density to set a threshold for noise removal [16].

As mentioned above, several methods are available for point cloud noise removal. However, the performance of each technique on a high noisy SFM dataset is unclear [17]. Therefore, it is necessary to find an efficient method for removing noise from UAV image derived point clouds.

2.4 Damage identification and extraction

In an inspection context, damage identification activities typically aim to find cracks, discolourations, spalling, and other forms of damage (Figure 1), as well as the underlying baseline geometry of the scanned structure. Initially, such feature extraction was done manually by trained operators, as in the mentioned work by Hallermann [6-8]. Subsequent efforts have attempted to automate the process, such as the semi-automatic approach developed by Sui [18] for post-disaster, building damage detection. In that work, building heights, textures, and shapes were compared between pre-disaster and post-disaster models, and changes became the basis for damage determination. Similarly, by comparing multiple scans over time, Lucieer [19] used SFM to map landslide displacements. At a flight elevation of 40 m with 39 ground control points, they achieved a 7.4 cm horizontal accuracy and a 6.2 cm vertical accuracy for land movement tracking. Notably, in both of these examples, there was an assumption of the existence of and reliance upon historical data. However, more often than not, such information is not available.

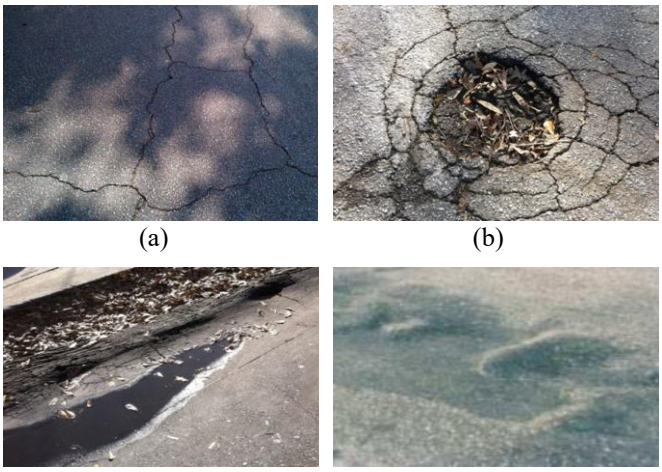

(a) (b) (c) (d)

Figure 1. Typical road damages [20]: (a) Cracks, (b) pot holes, (c) rut, (d) shoving.

Thus, the question arises as to how to extract features based exclusively on current data. With LiDAR data, the lines of research are both extensive and fairly well-established such as the artificial neural network-based approach for damage extraction [20], the topology graphing for building extraction [21], and the supervised machine learning approach for road extraction [22]. An equivalent set of efforts have yet to be developed for SFM point clouds. A possible reason is that SFM-generated point clouds are generally less homogeneous and have more noise than those produced directly from LiDAR, as the UAV flight paths are less consistent than data acquired from the greater heights of the more controlled helicopters and plane flightpaths. Thus, identification and extraction of relatively small features (as would be representative of damage on the surface of infrastructure) become especially challenging with UAV-based images. For this reason, developing a feature extraction algorithm applicable to SFM outputs of imagery-based point clouds that is robust against low-quality and inconsistently dense point clouds would be a significant advancement in UAV usage.

3 METHODOLOGY AND RESULT

Thus, for UAVs to be viable for automatic road network inspection, problems related to the input data quality and coverage and its post-processing must be solved. These problems are addressed through the following four objectives:

- Design a reliable UAV platform and proper strategies for data acquisition.
- Find a robust solution for images-based 3D reconstruction.
- Data quality evaluation and optimization.
- Algorithm development for automatic damage extraction and its evaluation.

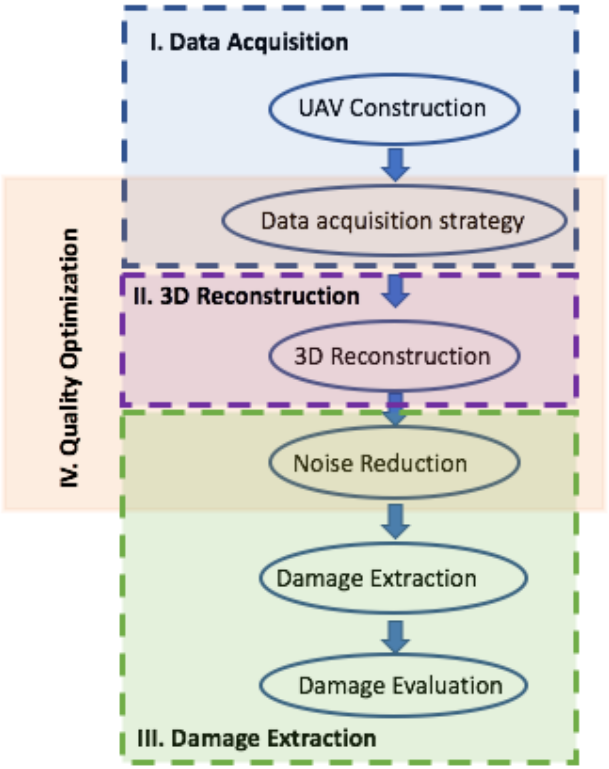

Figure 2. Research structure of the three areas of data acquisition, 3D reconstruction, and damage extraction.

3.1 UAV-based data acquisition

To achieve high-quality data, a reliable and extendable UAV platform must be employed. A 2015 review of the state of the technology [23], identifies that low-cost UAVs (those under 4000 euros) could not simultaneously satisfy all requirements of flight times, payload, hovering capabilities, and flight speed needed for road network inspection. Additionally, at that time, a further disadvantage of commercial UAVs laid in that they were closed source. This means that fight path control data (such as the cruising speed, turning radius and camera angle) were not easily accessible or alterable.

In response, a multi-rotor UAV with a real-time video system for road and bridge inspection is designed and built as part of this project (Figure 3). This involves the design and 3D printing of the frame, the assembly of various commercially available components, and the programming of the flight controller.

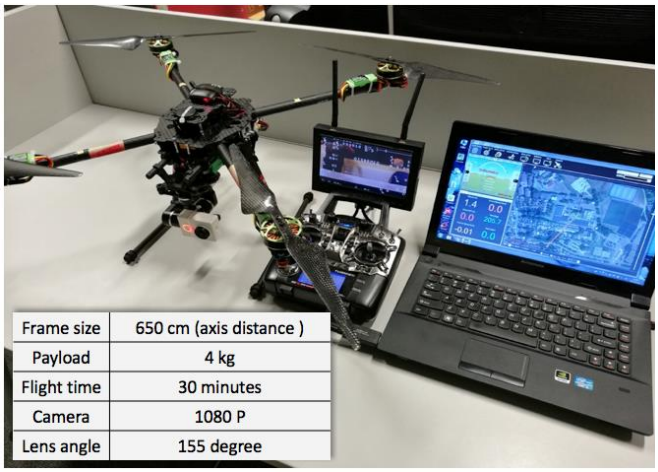

Figure 3. Customized multi-rotor UAV system.

The system is tested during 10 aerial surveys through which more than 2,000 still images and 100 minutes of video are collected (examples shown in Figure 4). Additionally, the UAV design is based on open source projects and can be updated to meet future requirements (e.g., adding additional sensors, enhancing on-board computing power, and customising the data capturing strategies).

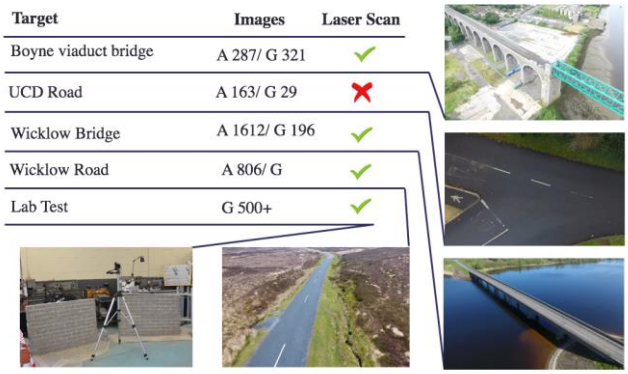

Figure 4. UAV-based surveys.

To ensure the stabilization and increasing the image quality by avoiding blurring, the flight control system needs to be adjusted. The main goal of tuning the control system is to minimise the difference between the real location and the intended location, as shown by Equation (1), where $e(t)$ is the error between the desired and measured locations.

$$e(t) = x^{des}(t) - x^{real}(t) \quad (1)$$

To make the adjustments more rapid and smoother, dynamic control mechanisms are required [24]. Proportional Integral Derivative (PID) control methods are applied as per Equation (2), in an attempt to minimize errors over time by adjusting the control variable $u(t)$, which is the thrust..

$$u(t) = K_p e(t) + K_i \int_0^t e(\tau)d\tau + K_d \frac{de(t)}{dt} \quad (2)$$

$$\begin{cases} K_p = 0.6K_u \\ K_i = \dfrac{2K_p}{T_u} \\ K_d = \dfrac{K_p T_u}{8} \end{cases} \quad (3)$$

where the terms K_p, K_i, and K_d denote the coefficients for the proportional, integral, and derivative terms respectively. The $K_p e(t)$ term accounts for present values of the error, while the term $K_i \int_0^t e(\tau)d\tau$ accounts for errors accumulated in the past, and the term $K_d \frac{de(t)}{dt}$ accounts for trends of error changing rate in the future.

By tuning the three model parameters (K_p, K_i, and K_d), the controller can have a rapid and accurate reaction to pose adjusting. To identify the best parameters, the UAV is set to be rotatable in only one degree of freedom (shown in Figure 5) to measure the tuning feedbacks.

Figure 5. PID tuning test.

3.2 3D reconstruction and quality evaluation

Creating a robust 3D reconstruction approach for imagery/video based data streams requires the creation of a pipeline for point cloud generation, as well as for the collection of significant data to test the approach. The SFM method is chosen as it can be applied to a single camera. By detecting common features from a group of images taken from different angles, this method can calculate the geometric relationship between each frame. After the relative location of each frame is calculated, more common feature points can be projected to the 3D coordinate system. To increase the accuracy, image selection, camera calibration, and control image orientation are useful [26].

However, before this method can be used in real inspection scenarios, possible quality issues must be identified and addressed systematically. These relate to the collection angles, the offset distances, the light conditions, and the camera model. Among those factors, the angles and distances are most intrinsic to the survey process. To date, however, their impact on the results and means to optimize their accuracy have yet to be addressed systematically. The investigation into this topic starts by conducting a laboratory experiment [27]. The experiment involves the construction of the masonry wall (130 x 90 cm) in Figure 6. To replicate field conditions, a lightweight digital camera or action camera commonly used in UAVs is selected for image capture, more specifically, the Cannon IXUS 175 camera. The camera is tripod mounted to control the shooting angles. Image capturing occurs at offsets from 1, 2, and 3 meters from the wall's front surface. Angles are set as 30, 45, and 60 degrees to the wall's normal direction. SFM is used to generate a point cloud from these images (Figure 7).

Figure 6. Camera set up.

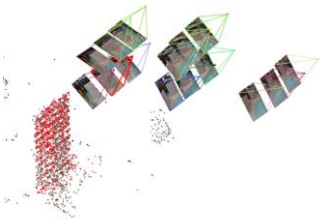

Figure 7. SFM-based point cloud.

As a reference dataset, laser scanning is carried out with the Leica ScanStation P20 shown in Figure 8. Figure 9 illustrates the resulting point cloud directly taken from the data.

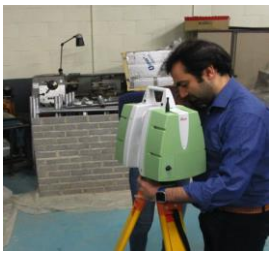

Figure 8. Laser scanner set up.

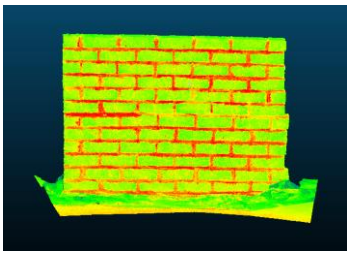

Figure 9. Laser scanning-based point cloud.

By aligning the image-based data and laser scanning-based data in the same coordinate system, the absolute distance between the two datasets can be calculated leading to the results in Figure 10. The distance distribution shown on the right side indicates that the error is from 0.02 mm to 2 mm. The average error is about 1 mm demonstrating that in this type of situation, with a relatively short distance and multiple shooting angles, an image-based point cloud is considered quite reliable.

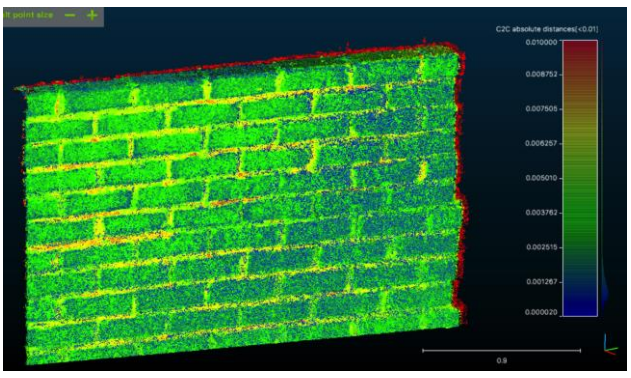

Figure 10. Image-based point cloud compared to a laser-scanning-based point cloud.

In real inspection scenarios, access may be restricted, and the cost-effectiveness of multiple scan stations may not be feasible. To understand the effect of shooting angles, and distances with respect to the quality of the result, the datasets are processed first individually and then in groups (Figure 11).

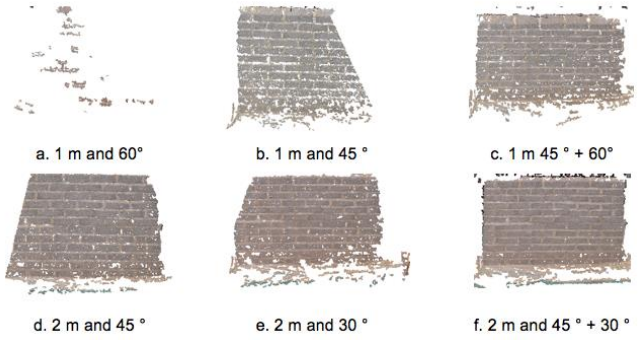

Figure 11. Point clouds from the various camera positions.

Figures 11(a), 11(b), 11(d) and 11(e) demonstrate that images obtained from closer locations and with larger shooting angles are less reliable. This defies common perceptions that closer data capture would be superior. For example, Figure 11(f) taken from 2 m away is clearly superior to an image taken from only 1 m (Figure 11(c)). A possible reason is that the longer shooting distance increases the field of view of the images, allowing the overlapping and matching between images to increase, which is significant for the SFM process. Furthermore, by processing two sets of images together (Figures 11(c) and 11(f)), the deformation problem can be overcome. The results provide meaningful insight into real inspection strategies. With a fixed lens, compared to a close but big shooting angles flight trajectory, a relatively longer distance but small shooting angle flight path is more appropriate for image-based 3D reconstruction.

3.3 Noise reduction

During a field test conducted on a concrete bridge in county Wicklow of Ireland, the point clouds reconstructed from bundle images from UAV contain a large amount of noise in the data. The majority are outlier noise clusters around the bridge, especially under the bridge, which are caused by the waves, water reflection, and self-shadows. As previously mentioned, denoising is important as noise can negatively impact further production-oriented processing for documentation and damage detection. Statistical and geometric-based filters are used in this investigation for denoising, and implemented in Cloud compare [28] and the Point Cloud Library (PCL) [29].

The Statistical Outlier Removal (SOR) filter firstly computes the average distance of each point to its neighbours through *k*-nearest neighbours searching function [30,31]. The point is considered an outlier if this distance is larger than the average distance derived from all points in the dataset plus *t* times of the standard deviation (σ) of the average distance. Thus, the outlier removal is controlled by two thresholds: *k* and *t*.

The geometric-based filter considers the distance from a given point to the object's surface [32]. The algorithm locally fits a plane through each point in the dataset, which is based on neighbour points of the given point extracted by either kNN search or a range search method. Next, if the distance of a point to the fitting plane is larger than the threshold known as the max error rate (*r*), the point will be labelled as a noise point.

The test result shows that the SOR filter can efficiently remove most of the outlier noise in this situation. By searching 400 neighbors at each point, the False Positive Rate (FPR) achieves 2.54%, which means that 97.46% of the noise is detected and removed, as shown in Figure 13, when compared to the laser scanned ground truth.

Figure 13. The classified noise pints (red points are outlier).

3.4 Automated damage detection

Identifying damage using a 3D model is the final goal. To this end, quite a few methods are tested in different scenarios. For cracks in the concrete surface, a simple plane fitting method is applied to analyse the surface changes and locate cracks. In the case study, through the SFM point cloud, the crack is measured as 1.4 cm, which is close to the 1.2 cm obtained from the in-situ measurement. In addition, the 3D model shows that the right-side wall is about 1 cm in front of the left side, which cannot be observed from the 2D images and may provide insight as to the likely failure mechanism (Figure 14).

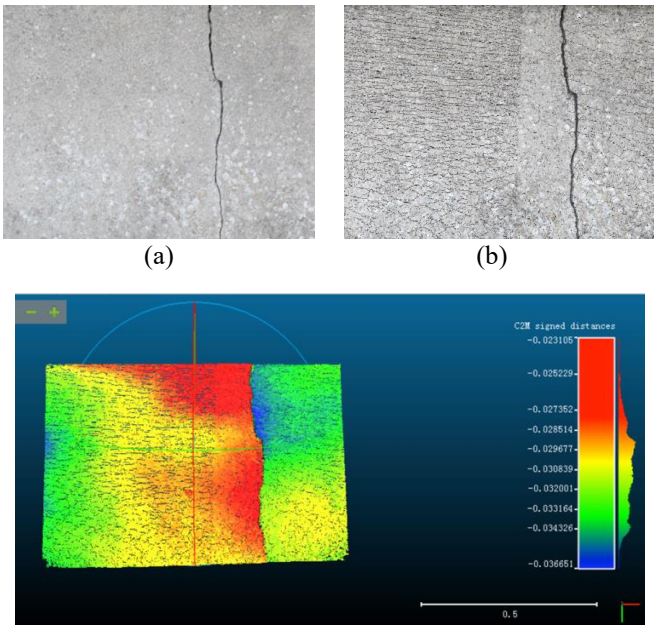

Figure 14. Damage detection on concrete surfaces: (a) Original image, (b) reconstructed point cloud, (c) digital elevation model (DEM) for damage identification.

A lab experiment is conducted to test damage also on masonry surfaces. In Figure 15, a brick wall with 1 cm wide cracks is used for 3D model reconstruction based on multiple images, as well as a laser scanner. The cracks could be automatically extracted from the background, which involve using normal vectors, texture information, statistical analysis and machine learning for detection and classification.

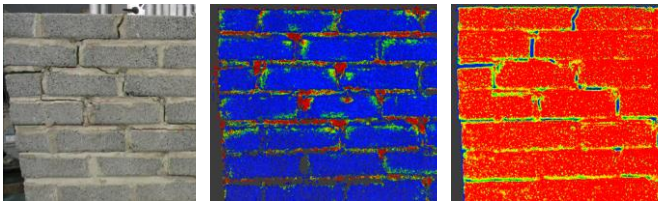

(a) (b) (c)

Figure 15. Damage detection on masonry surfaces: (a) Original image, (b) damage detection on image-based point cloud, (c) damages detection on laser scanner-based point cloud.

To evaluate the bridge pavement condition, Figure 16 illustrates the processing steps that are developed to trace the surface changes and locate the damages [33]. First, the UAV-based SFM method is applied to generate the point cloud (Figure 16(a)). Then, the pavement is extracted from the point cloud by K-mean segmentation (Figure 16(b)). After that, the polynomial surface fitting method and region growing methods are applied to visualize the surface damages and locate cracks.

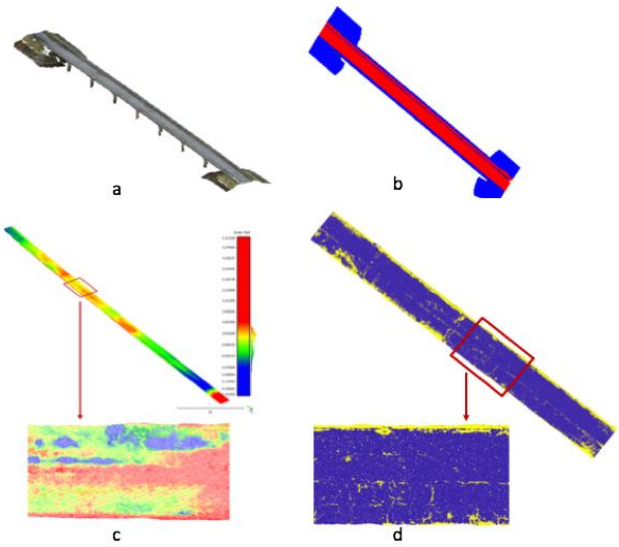

Figure 16. Bridge pavement evaluation.

4 CONCLUSIONS AND FUTURE WORK

This work has explored the potential of utilizing low-cost UAV images for 3D infrastructure inspection. The whole workflow has included UAV design, flight path planning, image data acquisition, and 3D reconstruction, with strong focus on evaluation of data post-processing. For the research purposes of this project, there has been two main challenges: resolving the outlier noise and achieving a robust damage detection scheme. In order to find an effective solution to resolve the outlier noise problem, caused by the water reflection and shadows, two commonly used noise filter and various parameter settings have been tested. To achieve a robust damage detection scheme, a two-step data extraction method has been developed for pavement extraction and damage extraction. Furthermore, a series of data quality evaluation metrics have been introduced, as well as the impact of various parameters, for example, the flight attitude, light condition, and image overlapping rate.

Currently, using a UAV-based digital camera, different surface faults can be successfully detected and measured. Future research aims to use multiple sensors as detectors, such as a thermal camera and multispectral camera, to identify the damages beneath the objects' outer surface.

ACKNOWLEDGMENTS

This project has received funding from the European Union's Horizon 2020 research and innovation programme under the Marie Skłodowska-Curie grant agreement No. 642453.

REFERENCES

[1] E.D. McCormack, *The use of small unmanned aircraft by the Washington State Department of Transportation*, Washington State Transportation. Commission. U.S. Department of Transportation, June, 1-27, 2008.

[2] Z. Yin, C. Seto, and Y. Mao, *Develop a UAV platform for automated bridge inspection*, Report 25-1121-0003-295, 1-26, 2015.

[3] Plasencia, G.N.M., Rodríguez, M.T., Rivera, S.C. and López, Á.H. (2012), 'Modelling and analysis of vibrations in a UAV helicopter with a vision system', *International Journal of Advanced Robotic Systems*, 9(5), 220.

[4] Caroti, G., Martínez-Espejo Zaragoza, I. and Piemonte, A. (2015), 'Accuracy assessment in structure from motion 3D reconstruction from UAV-born images: The influence of the data processing methods', *International Society for Photogrammetry and Remote Sensing*, ISPRS XL-1/W4, 103-109.

[5] Ullman, S. (1979), 'The Interpretation of Structure from Motion', *Proceedings of the Royal Society of London. Series B, Biological Sciences*, 203(1153), 405-426.

[6] Hallermann, N., Morgenthal, G. and Rodehorst, V. (2014), 'Vision-based deformation monitoring of large scale structures using unmanned aerial systems', *Proceedings of 37th IABSE Symposium*, Madrid, Spain, 102(8), 2852-2859.

[7] Hallermann, N., Morgenthal, G. and Rodehorst, V. (2015), 'Vision-based monitoring of heritage monuments - Unmanned Aerial Systems (UAS) for detailed inspection and high-accurate survey of structures', *Proceedings of 14th International Conference on Studies, Repairs and Maintenance of Heritage Architecture (STREMAH)*, A Coruna, Spain, 621-632.

[8] Hallermann, N. and Morgenthal, G. (2014), 'Visual inspection strategies for large bridges using Unmanned Aerial Vehicles (UAV)', *Proceedings of 7th International Conference on Bridge Maintenance, Safety and Management (IABMAS)*, Shanghai, China, 661-667.

[9] Wu, C. (2014),'Critical configurations for radial distortion self-calibration', *Proceedings of the IEEE Conference on Computer Vision and Pattern Recognition*, Columbus, Ohio, US, 25-32.

[10] Schall, O., Belyaev, A. and Seidel, H.-P. (2005), Robust filtering of noisy scattered point data, '*Proceedings of SPBG'05 Second Eurographics / IEEE VGTC conference on Point-Based Graphics*', New York, US, 71-77.

[11] Alexa, M., Behr, J., Cohen-or, D., Levin, D. and Silva, C.T. (2003), 'Computing and Rendering Point Set Surfaces', *IEEE Transactions on Visualization and Computer Graphics*, 9(1), 3-15.

[12] Shen, C., Brien, J.F.O. and Shewchuk, J.R. (2004), 'Interpolating and approximating implicit surfaces from polygon soup', *Computer Graphics Proceedings, Annual Conference Series (ACM SIGGRAPH 2004)*, Los Angeles, California, US, 1-9, 2004.

[13] Yingjie, Z. and Liling, G. (2011), 'Improved moving least squares algorithm for directed projecting onto point clouds', *Measurement*, 44(10), 2008-2019.

[14] M. Berger, P. Alliez, A. Tagliasacchi, L. M. Seversky, C. T. Silva, J. A. Levine, and A. Sharf, *State of the art in surface reconstruction from point clouds*, Eurographics 2014 - State of the Art reports, April, Strasbourg, France, 1(1), 161-185, 2014.

[15] Nurunnabi, A., West, G. and Belton, D. (2015), 'Outlier detection and robust normal-curvature estimation in mobile laser scanning 3D point cloud data', *Pattern Recognition*, 48(4), 1404-1419.

[16] Zaman, F., Wong, Y.P. and Ng, B.Y. (2016), 'Density-based denoising

of point cloud', *Proceedings of the 9th International Conference on Robotic, Vision, Signal Processing and Power Applications (ROVISP 2016)*, Penang, Malaysia, 287-295.

[17] Wolff, K., Kim, C., Zimmer, H., Schroers, C., Botsch, M. and Alexander, O.S. (2016), 'Point cloud noise and outlier removal for image-based 3D reconstruction', *Proceedings of the 2016 Fourth International Conference on 3D Vision Point*, California, US, 118-127.

[18] Sui, H., Tu, J., Song, Z., Chen, G. and Li, Q. (2014), 'A novel 3D building damage detection method using multiple overlapping UAV images', *International Society for Photogrammetry and Remote Sensing*, ISPRS XL-7, October, 173-179.

[19] Lucieer, A., de Jong, S.M. and Turner, D. (2014), 'Mapping landslide displacements using Structure from Motion (SfM) and image correlation of multi-temporal UAV photography', *Progress in Physical Geography*, 38(1), 97-116.

[20] B. Guldur and J. Hajjar, *Laser-based structural sensing and surface damage detection*, Report no. NEU-CEE-2014-03, Department of Civil and Environmental Engineering, Northeastern University, Boston, US, 2014.

[21] Verma, V., Kumar, R. and Hsu, S. (2006), '3D building detection and modeling from aerial LIDAR data', *Proceedings of the IEEE Computer Society Conference on Computer Vision and Pattern Recognition*, 2, 2213-2220.

[22] Vo, A.V., Truong-Hong, L. and Laefer, D.F. (2015), 'Aerial laser scanning and imagery data fusion for road detection in city scale', *Proceedings of the IEEE GRSS Data Fusion Contest (IGARSS 2015)*, Milan, Italy, 4177-4180.

[23] Chen, S., Laefer, D.F. and Mangina, E. (2016), 'State of Technology Review of Civilian UAVs', *Recent Patents on Engineering*, 10(3) 201, 160-174.

[24] Spica, R., Giordano, P.R., Ryll, M., Bülthoff, H.H. and Franchi, A. (2013), 'An open-source hardware/software architecture for quadrotor UAVs', *Proceedings of 2nd Workshop on Research, Education and Development of Unmanned Aerial System*, 2, Part 1, Compiegne, France, 198-205.

[25] Ziegler, J.G. and Nichols, N.B. (1995), 'Optimum settings for automatic controllers', *InTech*, 42(6), 94-100.

[26] Nex, F. and Remondino, F. (2014), 'UAV for 3D mapping applications: A review', *Applied Geomatics*, 6(1), 1-15.

[27] Chen, S., Laefer, D.F., Byrne, J. and Natanzi, A.S. (2017), 'The effect of angles and distance on image-based, three-dimensional re-constructions', *Safety and Reliability - Theory and Applications, Proceedings of 27th annual European Safety and Reliability Conference (ESREL 2017)*, Portoroz, Slovenia, 2757-2761.

[28] CloudCompare (2017), *CloudCompare Stereo, V2.9, Open Source Project*, 2017, accessed 10 December 2018, <http://www.danielgm.net/cc/>.

[29] Rusu, R.B. and Cousins, S. (2011), '3D is here : Point Cloud Library (PCL)', *Proceedings of the IEEE International Conference on Robotics and Automation (ICRA2011)*, Shanghai, China, 1-4.

[30] PCL-SOR, Statistical Outlier Removal filter -PCL, 2018, accessed 10 December 2018, <http://pointclouds.org/documentation/tutorials/statistical_outlier.php>.

[31] CloudCompare-SOR, *CloudCompare-SOR*, 2015, accessed 10 December 2018, <http://www.cloudcompare.org/doc/wiki/index.php?title=SOR_filter>.

[32] CloudCompare-Noise filter, *CloudCompare-Noise filter*, 1-2, 2015, accessed 10 December 2018, <http://www.cloudcompare.org/doc/wiki/index.php?title=Noise_filter>.

[33] Chen, S., Truong-hong, L., Laefer, D.F. and Mangina, E. (2018), 'Automated bridge deck evaluation through UAV derived point cloud', *Proceedings of 2018 Civil Engineering Research in Ireland conference (CERI)*, Dublin, Ireland, 735-740.

The TRUSS project (www.trussitn.eu) has received funding from the European Union's Horizon 2020 research and innovation programme under the Marie Skłodowska-Curie grant agreement No. 642453